TECHNISCHE UNIVERSITÄT WIEN

DIPLOMARBEIT

Optimization and Qualification of the Process Quality Control for the Silicon Sensor Production of the CMS Phase-2 Upgrade

zur Erlangung des akademischen Grades

Diplom-Ingenieur/in

im Rahmen des Studiums

Masterstudium Technische Physik

eingereicht von

Maximilian Babeluk
Matrikelnummer 01609369

ausgeführt am Institut für Hochenergiephysik
der Österreichischen Akademie der Wissenschaften
und am Atominstitut
der Technischen Universität Wien

Betreuung
Betreuer/in: Privatdoz. Dipl.-Ing. Dr.techn. Christoph Schwanda
Mitwirkung: Univ.Lektor Dipl.-Ing. Dr.techn. Thomas Bergauer

Wien, 14.07.2021

(Unterschrift Verfasser/in) (Unterschrift Betreuer/in)

Acknowledgments

This thesis has been created during the Covid-19 pandemic. Despite the conditions, I really enjoyed working at HEPHY. Many people directly or indirectly contributed to the work described in this thesis, both from HEPHY and the CMS Collaboration. Although most of the interaction was via the internet, the atmosphere in the meetings was always very friendly and professional.

First of all, I want to thank Thomas Bergauer for the guidance through my whole time at HEPHY. Although we did not meet that often in person, I have to thank him for the many hours of calls and steady and prompt support for all kinds of problems. Furthermore, the finalized version of this thesis is owed to him, providing expertise and proof-reading.

Special thanks to Marko Dragicevic, who was also always available for discussions and advice. Although we personally met only towards the end of my thesis, working together online with you was always fruitful.

I also owe thanks to thank Andreas Bauer and Margit Oberegger for conducting most of the measurements in this thesis, and for the close collaboration to develop and optimize all the procedures for a fluid measurement process.

Furthermore, I want to thank Bernhard Arnold, who develops and maintains the PQC software. The discussions with him were always very productive. Together we worked out many new features of the software, and he always expertly implemented them.

Thanks also to Wolfgang Brandner, who keeps everything running in the cleanroom.

Finally, I want to thank my family for all the support throughout my whole time as student. I could not have studied in that pace without their backing.

Abstract

The Large Hadron Collider (LHC), operated by CERN is currently the largest particle collider in the world with a diameter of 8.5 km. The Compact Muon Solenoid (CMS) is one of the four experiments of the LHC. For the next years, an update from the LHC to the so-called High Luminosity LHC (HL-LHC) is planned, increasing luminosity enabling the study of rare decay channels.

However, the increase in luminosity also raises the radiation stress on the detectors. Therefore, the so-called CMS phase 2 upgrade is scheduled for the same time as the HL-LHC integration. It includes a full replacement of the silicon tracking system and upgrades for the calorimeters. The replacement is necessary as the detector performance degrades due to the high levels of irradiation caused by current operation. In the most radiation stressed parts of the calorimeter in the endcap, the scintillators are replaced by silicon detectors. This new design called High Granularity Calorimeter (HGCal) allows not only a higher radiation hardness, but also has a high spatial resolution required to handle the increased pile-up and allow particle flow analysis. The total number of silicon detectors for this upgrade is in the order a few ten-thousands, requiring about three years for production.

During the sensor development, the optimal layout as well as the process parameters such as doping concentrations are evaluated via extensive tests, both on the sensors itself and via dedicated test structures. The prototyping phase also included irradiation with X-rays and neutrons, followed by electrical characterizations to evaluate the remaining performance.

During the production period, a fast and reliable way of testing is required to ensure quality and detecting possible long time drifts in parameters. This is done via the Process Quality Control (PQC), which consists of dedicated test structures together with an associated test setup. To simplify the handling, a fixed contact layout has been defined to make it possible to connect multiple contacts at once with a probe-card. Various test structures are connected to those contacts to extract silicon properties such as layer thicknesses and doping concentrations in a reproducible and non destructive way via electronic measurements. As the whole PQC test structure set requires only a very small fraction of the wafer space, it can be located directly on the production masks, on the segments remaining from the square or hexagonal sensor in the round wafer.

The PQC structures as well as the setup have been developed already, however, the exact measurement procedures are not yet fully defined for optimal results. This has been developed in the course of this thesis and also required hardware modifications to the setup. To allow faster characterization, the measurement routines have been optimized for maximum throughput. Furthermore the parameter extraction algorithms were not automatized and required manual verification to ensure successful parameter extraction. This procedure is now automatized to reduce the required manpower and achieve the high throughput planned for the production phase.

Zusammenfassung

Der Large Hadron Collider (LHC), ist mit einem Durchmesser von 8,5 km der derzeit größte Teilchenbeschleuniger der Welt. Das Compact Muon Solenoid (CMS) ist eines der vier Experimente des LHC. Für die nächsten Jahre ist ein Update des LHC zum sogenannten High Luminosity LHC (HL-LHC) geplant, der durch eine Erhöhung der Luminosität die Untersuchung seltener Zerfallskanäle ermöglicht.

Mit der Erhöhung der Luminosität steigt jedoch auch die Strahlungsbelastung für die Detektoren. Daher ist zeitgleich mit der HL-LHC-Integration das sogenannte CMS Phase 2 Upgrade geplant. Es umfasst den Austausch des Silizium-Trackersystems und Upgrades für die Calorimeter. In den am stärksten strahlungsbelasteten Teilen des Calorimeters in der Endkappe werden die Szintillatoren durch Siliziumdetektoren ersetzt. Dieses neue Design (High Granularity Calorimeter) ermöglicht nicht nur eine höhere Strahlungshärte, sondern auch eine hohe räumliche Auflösung. Dies ist notwendig um die erhöhte Pileup-rate zu bewältigen und Particle-Flow Analyse zu ermöglichen. Die Zahl der Siliziumdetektoren liegt in der Größenordnung von einigen Zehntausend, drei Jahre sind für die Produktion geplant.

Während der Sensorentwicklung werden das optimale Layout sowie die Prozessparameter durch umfangreiche Tests evaluiert, sowohl an den Sensoren selbst als auch über spezielle Teststrukturen. Die Prototyping-Phase beinhaltet auch die Bestrahlung mit Röntgen- und Neutronenstrahlen.

Während des Produktionszeitraums ist eine schnelle und zuverlässige Art der Prüfung erforderlich, um die Qualität zu sichern und mögliche Langzeitdrifts der Parameter zu erkennen. Dies geschieht über die Process Quality Control (PQC), die aus dedizierten Teststrukturen und einem zugehörigen Testsetup besteht. Um die Handhabung zu vereinfachen, wurde ein fixes Kontaktlayout definiert. Dieses ermöglicht mehrere Kontakte auf einmal mit einer Probe-Card anzuschließen. An diese Kontakte werden verschiedene Teststrukturen angeschlossen, um Siliziumeigenschaften wie Schichtdicken und Dotierungskonzentrationen reproduzierbar und zerstörungsfrei über elektronische Messungen zu extrahieren. Da der gesamte PQC Teststruktursatz nur einen sehr kleinen Teil der Waferfläche benötigt, kann er direkt auf den Produktionsmasken auf den vom quadratischen oder sechseckigen Sensor übrig gebliebenen Segmenten des runden Wafer platziert werden.

Die PQC-Strukturen sowie der Aufbau sind bereits entwickelt, die genauen Messverfahren sind jedoch noch nicht vollständig für optimale Ergebnisse definiert. Dies wurde im Rahmen dieser Arbeit erarbeitet und erforderte auch Hardwaremodifikationen am Setup. Um eine schnellere Charakterisierung zu ermöglichen, wurden die Messprozeduren auf maximalen Durchsatz optimiert. Außerdem waren die Algorithmen zur Parameterextraktion nicht automatisiert und erforderten eine manuelle Überprüfung, um eine erfolgreiche Parameterextraktion sicherzustellen. Diese Prozedur ist nun automatisiert, um den erforderlichen Personalaufwand zu reduzieren und den für die Produktionsphase geplanten hohen Durchsatz zu erreichen.

Contents

Chapter 1

The LHC and the CMS experiment

1.1 Overview

The European Organisazion for Nuclear Research (CERN) operates the world's largest particle collider, the LHC (Larger Hadron Collider). The beam tunnel ring is located 100 m below the surface between the Jura Mountains and Lake Geneva and has a diameter of 8.5 km.

During operation, bunches of protons or heavy ions are accelerated to target energy and stored in the ring. At four dedicated interaction points, the bunches are brought into collision and the resulting particle showers are recorded in huge detector systems, referred to as experiments. Two of those experiments are designed for specific purposes: The Large Hadron Collider beauty (LHCb) experiment is dedicated to precise measurements of the properties of the bottom quark and violation of the CP-Symmetry. A Large Ion Collider Experiment (ALICE) focuses on collisions of heavy ions to analyze the quark-gluon plasma. The other two are general purpose experiments, A Toroidal LHC ApparatuS (ATLAS) and the Compact Muon Solenoid (CMS). They have a general setup and aim to take data for most particle types to answer a variety of questions, probe the standard model and search for new physics beyond the standard model.

From the start of the LHC in 2009, the center of mass energy was gradually increased to 13.5 TeV and is planned to reach up to 14 TeV. [1]

Luminosity $\mathcal{L}$ is another important property of particle detectors. It characterizes the rate dN_p/dt of a given process with cross-section σ_p that is achievable with the accelerator via:

$$\frac{dN_p}{dt} = \sigma_p \mathcal{L}. \tag{1.1}$$

Integrating equation 1.1 over the time the accelerator is running gives the expected total number of events of that kind on the left side. On the right side, the so called integrated luminosity appears, with an unit of inverse area, typically inverse femtobarn (fb^{-1}). To achieve a good distinction between real results and quantum noise of other processes, it is important to have as many reactions of the desired kind as possible. For processes with small cross-sections, this requires a high luminosity. [2]

1.2 CMS phase-2 upgrade and HL-LHC

LHC operation is organized in time periods, so called runs. Between the runs, the accelerator is shut down for maintenance and upgrades. The major upgrades are implemented in long shutdowns (LS) as shown in figure 1.1. For LS3, the CMS phase-2 upgrade is scheduled with major upgrades, refurbishments or replacements for the detector systems.

Figure 1.1: LHC and HL-LHC schedule from [3]. The CMS phase-2 denoted as HL upgrade

1.3 The CMS detector

The CMS experiment consists of a variety of detectors for different kinds of particles, arranged in a cylindrically onion-shaped way. The innermost part is the Tracker, detecting tracks of charged particles. In the whole inner region is a magnetic field of 3.8 T is maintained, so that the track curvature directly gives insight to the particle momentum and charge polarity over the Lorentz force. The next detectors are the electromagnetic and Hadron calorimeters.

The next shell is the superconducting magnet, followed by the magnetic return yokes. The outermost detector are the muon-chambers. A 3D drawing of the CMS detector system is shown in figure 1.2.

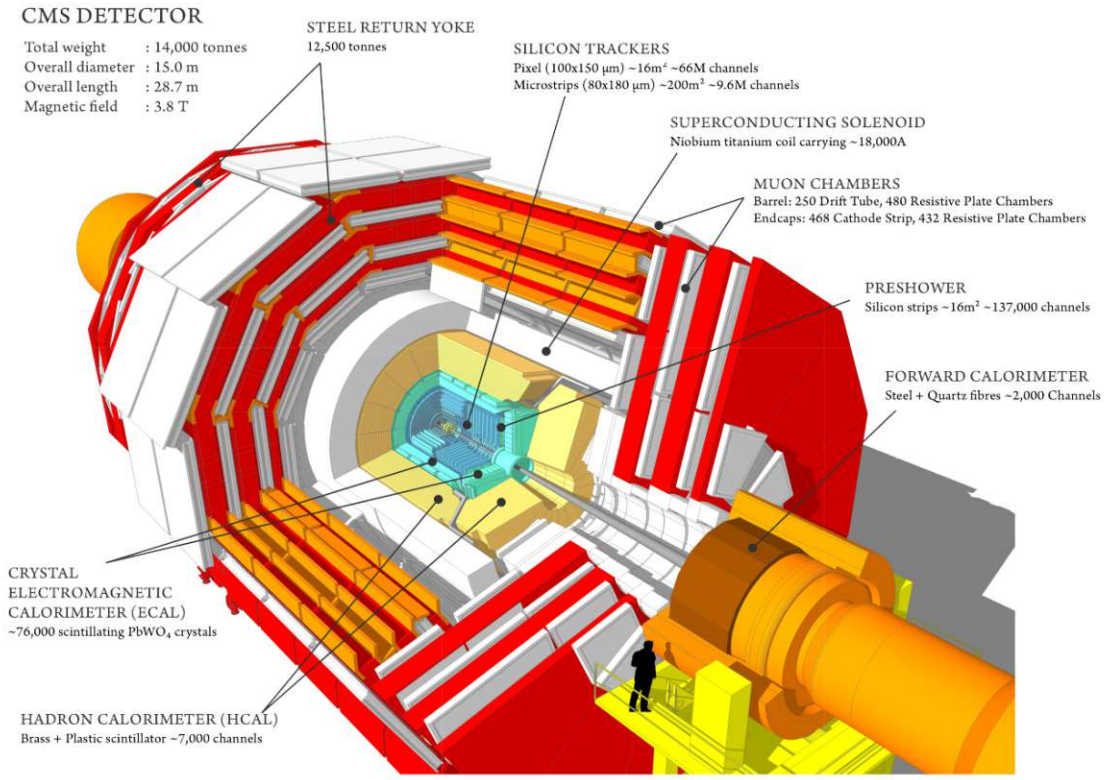

Figure 1.2: CMS detector system, image from [4]

1.4 Tracker

The CMS tracker consists of silicon strip and pixel sensors. The pixel detector is used for extracting particle trajectories separating primary from secondary vertices. With the strip detectors, the curvature of the trajectories can be measured, allowing the calculation of the momentum of charged particles in the magnetic field.

In the CMS phase-2 upgrade, the whole silicon tracking system will be replaced for higher radiation hardness, higher granularity and faster readout. Furthermore, information about the transverse momentum of particles will be supplied to the first trigger stage (L1 trigger). In the present, this information is available only for the second trigger stage (high level trigger). The L1 trigger is a lot faster in the decision of keeping interesting or discarding uninteresting events. This allows to keep the trigger data rate at a manageable level for the increased luminosity without loosing relevant events.

The phase-2 tracker is divided into an inner tracker section (IT) with silicon pixel sensors and an outer tracker section (OT) with silicon strip and macro-pixel sensors. This thesis treats the production for the outer tracker sensors.

The outer tracker consists of silicon detector modules arranged in cylinders and disks. A schematic of the arrangement is given in figure 1.3. Two types of modules exist for the outer tracker: 2-S and PS. The 2-S modules consist of two strip sensors of the same type (2-S) spaced by 1.8 or 4 mm. The PS modules consist of one strip sensor (PSs) and one macro-pixel sensor (PS-p) for additional resolution in polar angle. The module assembly for both types of modules is shown in figure 1.5.

More detailed information about the CMS tracker can be found at [5].

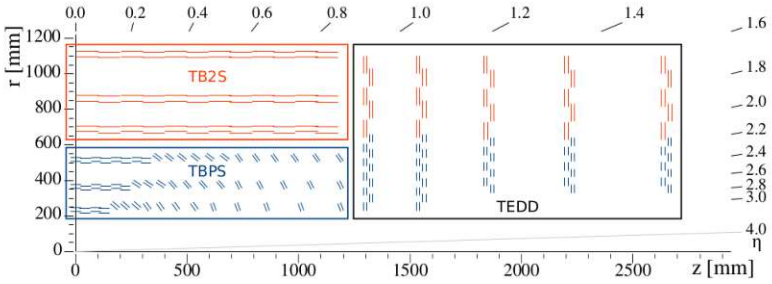

Figure 1.3: One quarter of the CMS Phase-2 Outer Tracker module assembly with 2-S modules in red, PS modules in blue, from [5]

Figure 1.4: OT TBPS detector arrangements, in the central section, modules are mounted side by side on a flat bease (left), the tilted regions are mounted on rings (right), the lower left shows a side view with the overlap region of the module on either side, from [5]

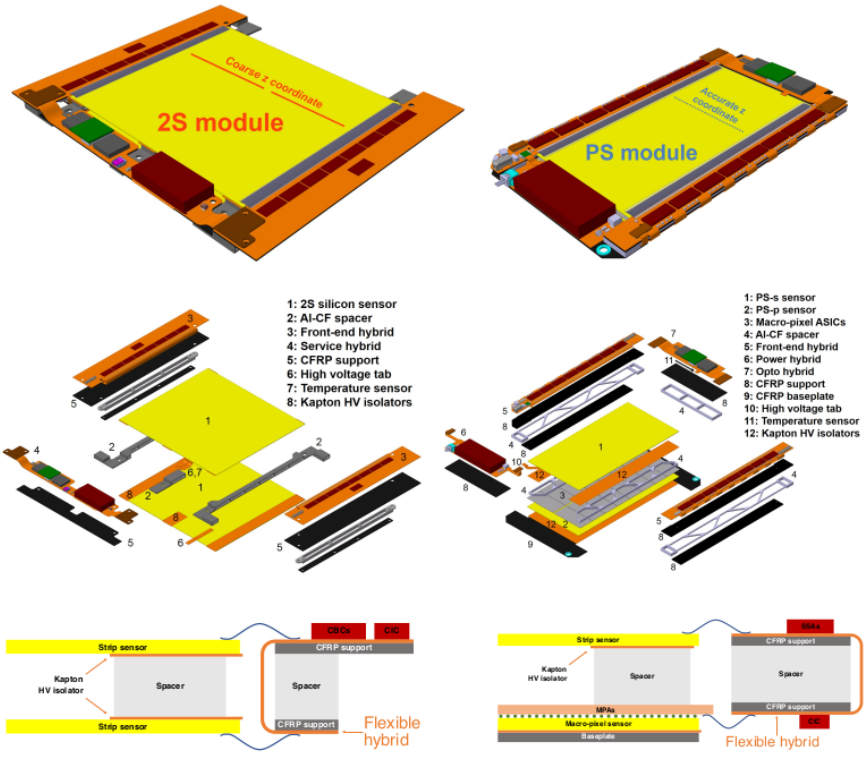

Figure 1.5: 2-S and PS modules in an exploded- and side-view, from [5]

1.5 Calorimeter and HGCal

The increased luminosity of the HL-LHC requires a new design of the endcap calorimeter. Typical sampling calorimeters use layers of scintillators as active elements. This is a cost-effective solution, but the spatial resolution is limited by the size of the scintillator crystals and the optical readout system.

However, due to the high number of pileup events expected, a high granularity is required to effectively separate concurrent jets of different events. This can be achieved by the use of silicon pad detectors with sizes around $1\,\mathrm{cm}^2$.

Another advantage of such a design is the increased radiation hardness. Scintillators have a limited amount of dose and subsequently degrade with irradiation. Silicon sensors proved high radiation hardness in the tracker and therefore are a good alternative to scintillators.

On the other hand, the cost for silicon sensor production is considerably higher compared to scintillators. In addition, the readout infrastructure is more complicated as the number of channels is increased drastically with semiconductor detectors.

The new high-granularity-calorimeter (HGCal) design for the endcaps uses both, silicon sensors at the inner part with higher expected radiation levels and scintillators at the outer positions. The expected fluence distribution and detector types inside the HGCal is shown in figure 1.6. More detailed information about the CMS HGCal design can be found at [6].

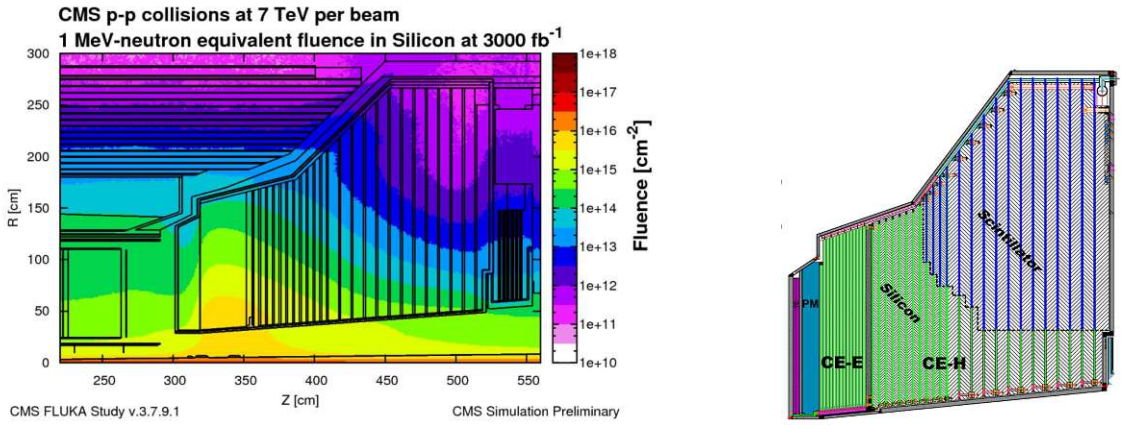

(a) (b)

Figure 1.6: Expected fluence in 1 MeV neutron equivalent (a) [6], areas of silicon (green) and scintillation detectors (blue) in the HGCal (b) [7].

Chapter 2

Silicon as particle detector material

2.1 Silicon as semiconductor

Today's electronic devices rely on integrated circuits (ICs), silicon is by far the most commonly used base material for ICs. As a group IV element, it has four valence electrons, that form covalent bonds when condensed into the typical diamond-like crystal lattice structure. The discrete energy states of the individual electrons merge together into a band structure typical for solids. Of special interest for semiconductor physics is the valence band and the conduction band. The energy difference of the highest position in the valence to the lowest in the conduction band is referred to as the band gap E_g. For silicon, the band gap is $E_g = 1.14\,\mathrm{eV}$ (300 K). [8]

At zero temperature, all electrons are fixed in their respective bonds and no free charge carriers are available. This means that the valence band is fully occupied and the conduction band is empty. The material behaves like an insulator.

For nonzero temperature however, bonds can break due to thermal excitation. This results on one hand in a freely movable electron, and on the other hand in a missing electron in the bond. The silicon ion of the missing bond acts now as a net positive charge and neighboring electrons may jump into the hole, leading to an effective movement of the positive charge. Therefore, holes can be viewed as positively charged particles, just as electrons. In the band model, breaking a bond means that one electron is lifted from the valence band into the conduction band, resulting in an excited electron-hole pair.

2.1.1 Doping

The properties of intrinsic semiconductors can be altered via the introduction of small amounts of impurities. This is referred to as doping, two main types can be distinguished: n-type and p-type doping. For n-type doping, group V elements are introduced into the silicon crystal, leading to one loosely bound extra electron per doping atom. Those elements are referred as donor, as very little energy is required to free those extra electrons into the conduction band leaving a fixed positive ion bound in the lattice and a mobile electron in the conduction band.

For p-type silicon, group III elements are used. Here, only three electrons are available to bond with silicon neighbors. In this case, little energy is required to lift an electron from the valence band to this so-called acceptor states, leaving a

movable hole and a fixed negative ion. At room-temperature, nearly all acceptor or donor states are excited thermally for typical dopants.

The resistivity of a material is proportional to the inverse of the charge carrier concentration times the mobility. For silicon, two types can coexist, leading to:

$$\rho = \frac{1}{q(\mu_n n + \mu_p p)}, \tag{2.1}$$

with n and p the concentration for electrons and holes respectively, and the μ_n and μ_p the corresponding mobilities.

For a doped part of silicon, the dopant is the main contribution for free charge carriers at room temperature, simplifying this to:

$$\rho = \frac{1}{q\mu_n N_n} \quad \text{or} \quad \rho = \frac{1}{q\mu_p N_p}, \tag{2.2}$$

assuming total excitation and with dopant concentration of N_n or N_p.

2.1.2 The pn-junction

A pn-junction is created when p and n-type silicon are brought together. In the contact region, charge carriers diffuse to the opposite side. When an electron meets a hole, they annihilate, forming a charge carrier depleted region. This leads to a charge density, as only the fixed dopant ions remain. This region is therefore known as space-charge or depletion region. On the p-side, an excess negative charge and on the n-side excess positive charge remains. The created potential difference suppresses further diffusion, leading to a finite width in equilibrium. This is equivalent of an equal Fermi level on both regions for the band model. The potential difference or built-in voltage V_{bi} created is therefore proportional to the difference in the Fermi levels of the two materials:

$$V_{bi} = \frac{E_{Fn} - E_{Fp}}{q}. \tag{2.3}$$

2.2 Production process

The silicon sensors for the CMS project are produced by specialized companies, in this case Hamamatsu Photonics K.K. (HPK). The same equipment and similar processes as in the chip industy are used. Wafers are cut from High purity single crystal silicon ingots as base material. These wafers undergo many processing steps, including thermal treatment, photo-lithography, etching, sputtering. Finally, the sensors are cut out from the wafers. Since the sensors are either rectangular (tracker) or hexagonal (HGCal), cutoffs have circular-segment shapes. Because of the circular shape of the cutoffs, they are referred to as half-moons. The half-moons are used for different test-structures, such as the PQC structures.

2.2.1 Substrate preparation

Crystal growth for ingot production is typically facilitated using the Czochralski process. For this, a container with melted silicon is kept close to the melting point. A seed crystal is brought into contact with the liquid surface and slowly withdrawn and rotated around the velocity axis. With the pulling velocity and speed of rotation,

the desired diameter of the ingot can be controlled. Typically a basic doping of the wafers is desired, which can be added to the melt before ingot production.

If higher purity is required, a subsequent purification is necessary. This can be acived using the float zone technique. For that, a small cross-sectional portion is melted using an RF-heater. The heater is slowly moved along the ingot, and the melted region moves with the heater. Impurities are dragged along in the floating region until the end of the ingot is reached. The end region of the ingot is then discarded together with the in this region accumulated impurities.

The thickness of the wafers used for detectors is typically 200 to 300 µm. This is already on the lower side of the easily possible, as the chip industry uses thicker wafers. For very high radiation environments, even lower active thicknesses such as 120 µm are desired. This can be achieved using epitaxial growth, depositing silicon directly on a base wafer that is only used for mechanical stability. Typical processes for this are chemical-vapor deposition and molecular-beam epitaxy. In both processes, dopants can be introduced into the growing layer. [9, 10]

2.2.2 Wafer processing

The wafer undergoes a lot of steps during production to create the necessary shapes of different materials and implants.

For the implants, an oxide layer is grown first via thermal oxidation. Subsequently, a light-sensitive paint, the photoresist is applied on the oxide. The layout is projected via masks on the photoresist layer. After exposure, the photoresist is developed, where depending on the type used, either the exposed or non-exposed portions dissolve in the developing solution.

In the following etching step, the oxide layer is etched away in the regions without photresist, leaving the bare silicon in these regions. When the dopant is applied, the molecules can diffuse into the wafer only in those regions, forming the desired pattern.

These steps are repeated for all implants and slightly modified for the metallisazion and polysilicon layer.

A final thick oxidation layer, the passivation is commonly applied to prevent damage to the sensor structures and isolate it from the environment. Only where contacts to external circuitry are located, the passivation has openings.

2.2.3 Fixed oxide charges and p-stop

During oxide creation, positive charges are bound inside the developing oxide. For n-type bulk material, this poses no problem. However, for a p-type substrate, these fixed positive charges repel holes and attract electrons. This can result in an inverted region at the surface between oxide and bulk material, where the charge carriers are electrons.

This inversion layer effectively forms a conductive connection between neighboring n-implants. Since a low coupling between the channels of a silicon detector are desired, actions have to be taken to prevent this phenomenon.

On one hand, the fixed oxide charges have to be minimized during the production process. For this reason, different variations of the process and process-parameters have been produced for the HGCal prototypes. Those variations are referred to as process splits in this document.

The typical means to quantify the oxide charge is via the flatband voltage, measured from a MOS Capacitor. A more detailed description of the measurement can be found in section 4.1, the analysis of the HGCal oxide process splits is subject of section 5.5.1.

Reducing the oxide charge alone does not solve the problem of inversion. To that end, an extra implant is necessary, the so called p-stop implant. The higher hole concentration in this region counters the inversion, forming a barrier. It is therefore necessary to surround each n-implant with a p-stop ring to isolate it from the neighbors, as shown in figure 2.1.

Two different layout options for the routing are available: A so called individual p-stop with an individual ring around each pad, and a common p-stop with one common net of implant that branches at three-pad corners. Thus, for an individual p-stop, each implant gap has effectively two lines of p-stop implant, whereas for the common-type, there is only one.

In the tracker, the individual layout is used, however, the final decision for the HGCal has not been made yet. Therefore, for all HGCal wafers, there exist both types of p-stop layout.

Since these layout options relate only to the sensors, and the test-structures for PQC do not differ between the two types, no analysis comparing these two types can be made from PQC data. The doubled number of samples is however beneficial for the statistics of all other results.

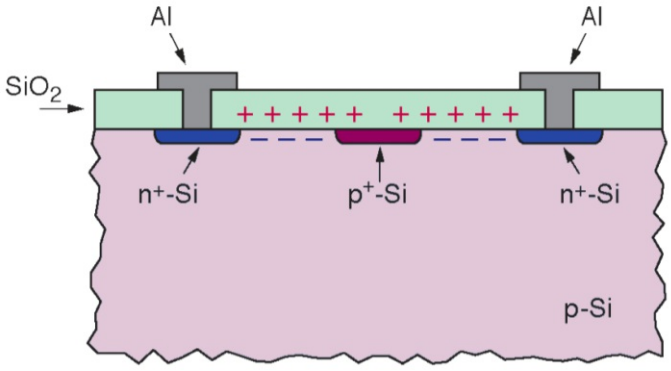

Figure 2.1: Cross section over a wafer with (common) p-stop implant, slightly modified from [11]

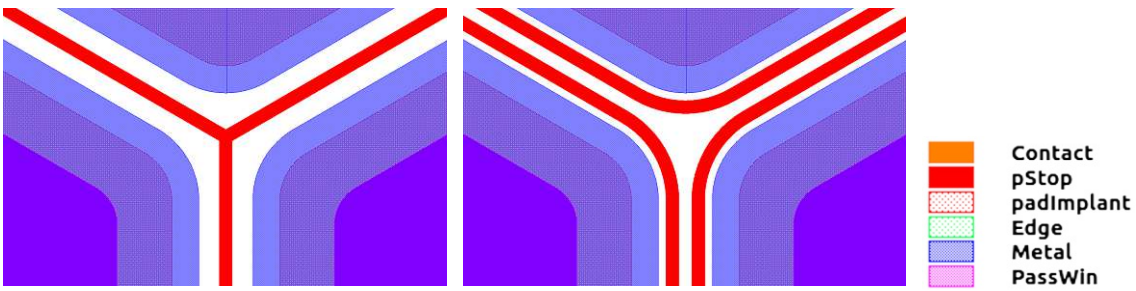

(a) (b)

Figure 2.2: HGCal p-stop layout options: common (a) and individual (b)

2.3 Quality assurance

The quality assurance system described in this chapter focuses on the tracker sensors, as the production is already running at the time of writing. For HGCal, a similar process is planned, but the project is currently in the prototyping phase.

As silicon sensor production is a highly elaborated multi stage process, an effective quality assurance (QA) system is mandatory to control and monitor sensor performance. Three types of quality assessment procedures are part of the QA system, described in the following sections. A schematic of the process is shown in figure 2.3.

The production is taking place in batches, one batch contains around 40 wafers. After a batch is qualified, it is shipped to the module assembly sites for module integration.

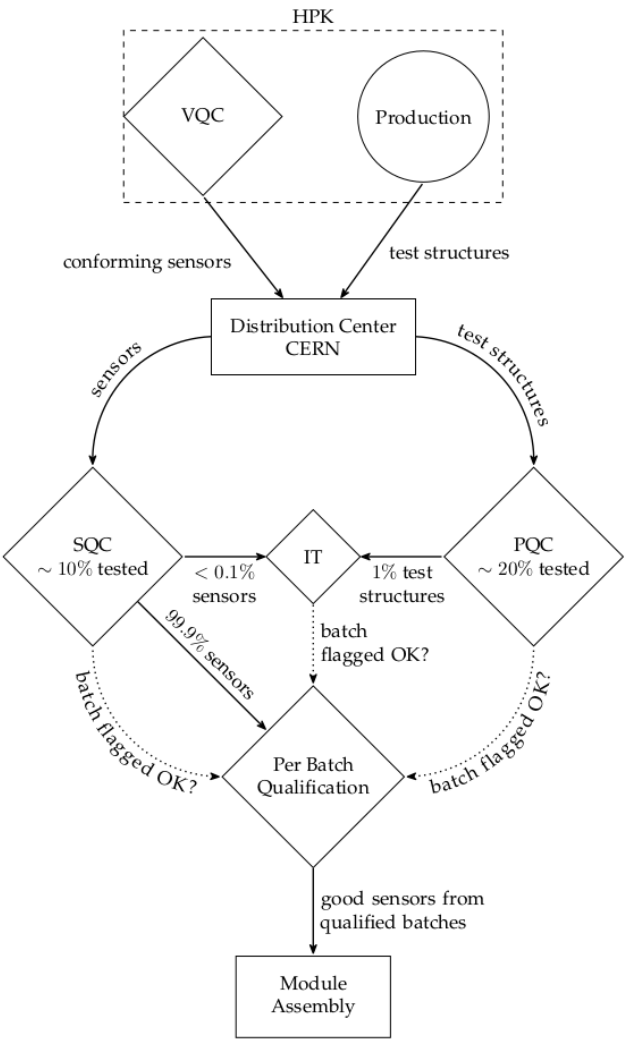

Figure 2.3: QA process flow for the outer tracker, taken from [12]

2.3.1 Vendor quality control (VQC)

The Vendor quality control (VQC) is taking place at the production site by the vendor. Each sensor shipped has to undergo this first stage of testing to ensure that only compliant sensors are delivered to CERN. The results from this electrical

characterization are supplied in plain text files and stored in the CMS construction database.

2.3.2 Sensor quality control (SQC)

Some of the sensors of every batch are shipped to sensor quality control (SQC) centers. These centers are scientific institutions of the CMS outer tracker and/or HGCal collaborations, capable of detailed sensor performance evaluation.

The sensor quality control (SQC) centers characterize the performance of the sensors, including single strip and inter-strip measurements across the whole sensor.

2.3.3 Process quality control (PQC)

The halfmoons cut from the wafers to produce the square shaped sensors are shipped to the process quality control (PQC) centers. They contain dedicated teststructures to electronically extract a wide variety of parameters. This allows quality assessment without touching the sensors, reducing the risk of damage during the sensor handling. Furthermore, more wafers can be tested compared with SQC, as the PQC measurements are faster and less involved than strip scans. The PQC is the topic of this thesis and treated extensively in chapter 3.

2.3.4 Irradiation tests (IT)

A very small fraction of the produced sensors are reserved for irradiation testing during production. This ensures that the radiation hardness is maintained. However, irradiated sensors cannot be used for the CMS experiment as their performance is degraded.

2.4 Wafer types and processes

The tracker and HGCal sensors use different processes for production. The tracker sensors are produced on 6 inch wafers. The 6 inch production process is well established and similar processes have been used for the sensors currently in use at the CMS tracker. At the time of writing, the tracker sensors are already in production.

The HGCal sensors use 8 inch wafers as hundreds of square meters of covered area are required. This process is new and at the time of writing still in the prototyping phase. Therefore, many different variants (so called process-splits) exist. Those process splits deviate is some parameters to find an optimum for the production phase.

2.4.1 Tracker

Three different types of sensors exist for the outer tracker. For the 2-S modules, two sensors of the same type are used. Those are therefore labeled 2-S sensors. The PS modules consist of one strip sensor (PSs) and one macro-pixel sensor (PSp). Both strip sensor types (2-S and PSs) use an AC coupled readout and are biased via polysilicon resistors. This is not possible for the macro-pixel sensors due to the smaller area of the pads. Therefore, the PSp pads are DC coupled. Due to the lack of a polysilicon layer for the DC production process variant, the bias voltage will be

applied through the pixel readout electronics for the final modules. However, the pixels can also be biased via punch-through structures for testing purposes when the sensor is tested before module assembly. The active area of the tracker wafers is 290 µm for all three types, the physical thickness is 320 µm. This comes from the field-stop region, a 30 µm backside-implant at the bottom of the wafer. This p-doped layer allows a defined end of the depletion region and prevents it, and therefore the electric field, from reaching the back surface of the sensor. This would cause avalanche breakdowns on non-ideal surfaces in case of over-depletion. [5, 12]

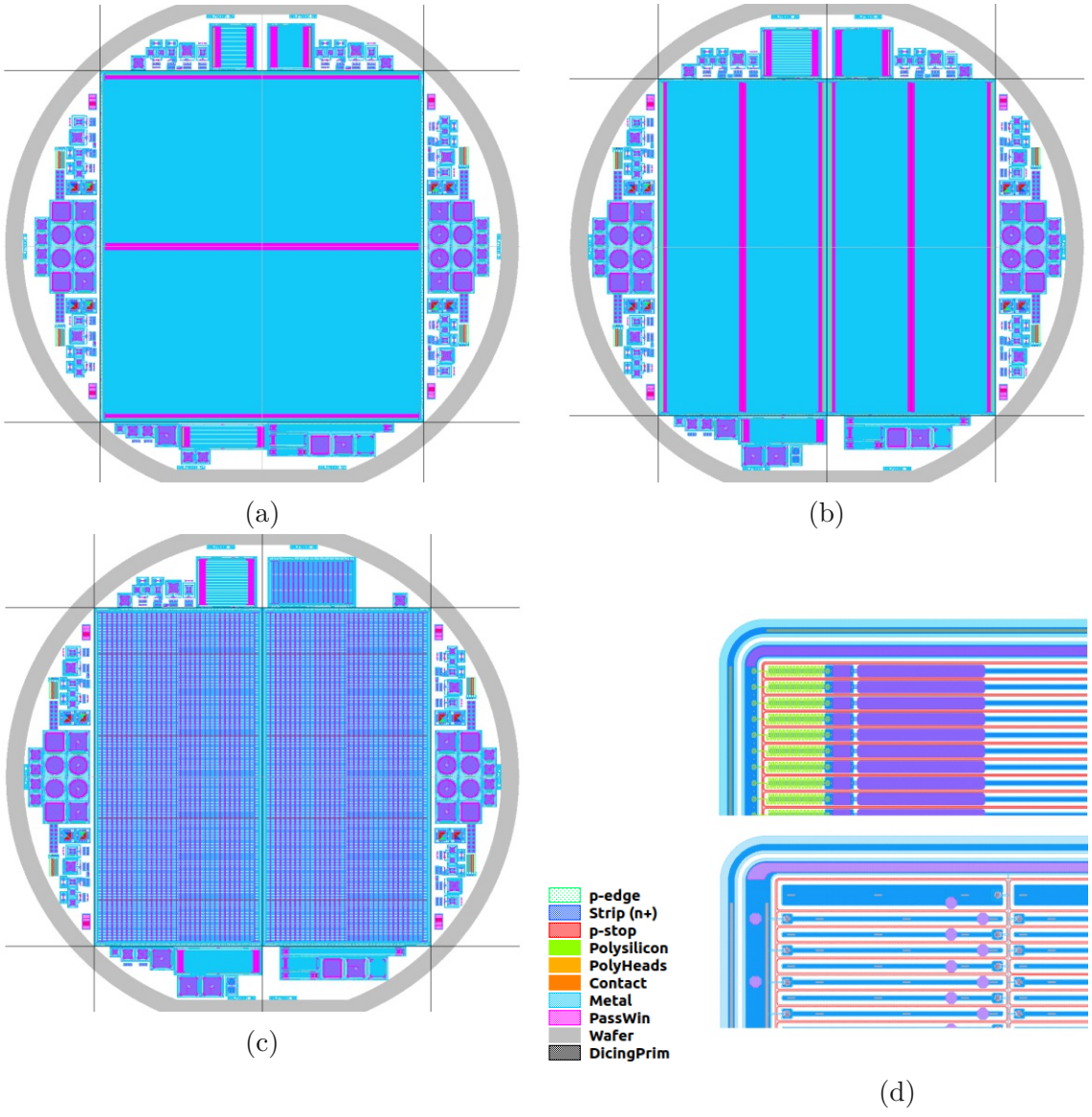

Figure 2.4: Layouts for the tree types of tracker sensors: 2S (a), PSs (b) and PSp (c), zoomed corners of PSs (d-top) and PSp (d-bottom) sensors.

2.4.2 HGCal

As the required area of detectors is in the range of hundreds of m^2 , the maximum of the wafer needs to be used as detector. This is achieved using hexagonal sensor modules on 8 inch wafers. The pads on the wafer itself are also hexagonal with areas of either $1.18\,cm^2$ or $0.52\,cm^2$. This hexagonal form allows a full coverage of the plane, however, at the corners of the sensor planes, partial sensors are required. The partial layout is shown in figure 2.5c, figure 2.6 shows one plane of the endcap calorimeter.

Three different sensor variants exist. Those are used at different locations inside the HGCal and therefore are designed for different irradiation resistances. Generally, a thick sensor is beneficial for the readout efficiency. The drawback of this is the required voltage to achieve full depletion. As irradiation increases the depletion voltage, this limits radiation hardness. Therefore, the thickness is a trade-off between signal strength and radiation hardness.

The two sensor types for lower radiation loaded parts in the HGCal have thicknesses of 200 µm and 300 µm. They share a common layout with 192 channels, designated as HGCal Low Denity (LD).

The third type has an active thickness of 120 µm. This is too thin to allow safe handling during production. Therefore, the active layer is deposited on a so called handling-wafer via epitaxial growth. The layout for this type is different and has 432 channels for higher spatial resolution. Therefore, this layout variant is called HGCal High Density (HD). [6]

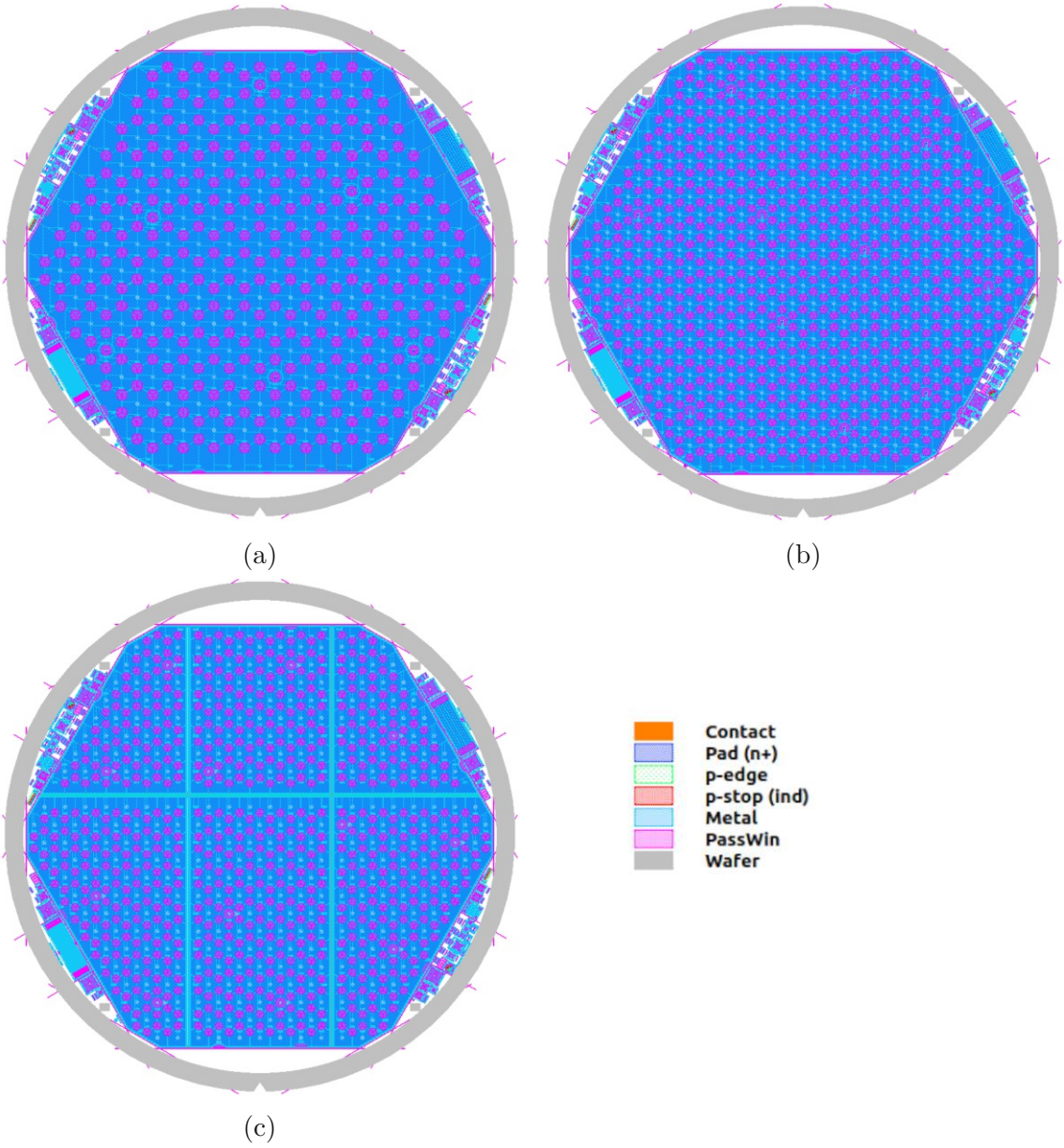

Figure 2.5: Layouts for the HGC LD (a), HGC HD (b) and HD partial (c) sensors.

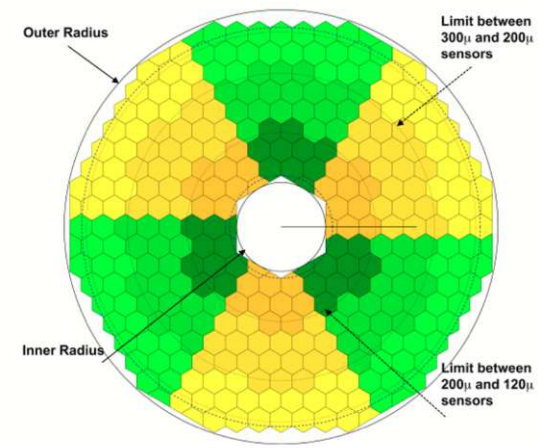

Figure 2.6: One layer of the HGCal CE-E part, the hexagons are the sensor modules built from 8 inch wafers, from [5]

Chapter 3

The Process Quality Control

With the Process Quality Control (PQC), a wide variety of parameters can be obtained from the samples via non-destructive, electrical measurements. On one hand, this requires a dedicated test-structure system on the wafers. On the other hand, a dedicated but flexibly configurable measurement setup is required.

For an efficient measurement sequence, multiple contacts can be connected at the same time. The contacts are organized in 2-by-10 arrangements, the so called flutes. To those flutes, the teststructures are connected on the wafer. One flute is shown in figure 3.1. Typically, the DUT (device under test) are so called halfmoons, circular segments cut from the periphery of the wafer. In the center, the real sensor is located, in the space inside the segments the teststructures are placed. One complete set of PQC teststructures includes 4 main flutes. Although other teststructures are also placed in a PQC-futeset, this thesis focuses only on the 4 main flutes. The additional flutes and teststructures are either legacy structures or were used for prototyping. On a regular basis, only the 4 main flutes are characterized now. Typically, one halfmoon contains two separate, independent PQC-sets.

For a measurement, all contacts of one flute can be connected at once via a special probe-card with matched geometry. All the contacts are connected to a switching matrix. This allows software configurable measurements, and a highly automated measurement process.

The PQC teststructures, together with the specific measurement configurations are described in chapter 4.

Figure 3.1: One flute (PQC main flute 1) with passivation openings for contacting shown in magenta.

3.1 Hardware setup

The measurement setup consists of several instruments connected to the rows of the switching matrix. The columns are connected to the needles of the probecard. Furthermore, manual positioners can be connected to the spare columns for measurements without the probecard. This can be necessary for finding loose contacts or for test structures with a deviating contact layout. A schematic is shown in figure 3.3.

Previously, the SMU used for the four-wire measurements (V source) was a Keithley 2657A. However, the lowest voltage range of this model is 200 V, and the accuracy for resistance measurements was not satisfying. Especially for structures with low resistance (metal VdP), this problem was evident. The V source was therefore replaced by a Keithley 2410.

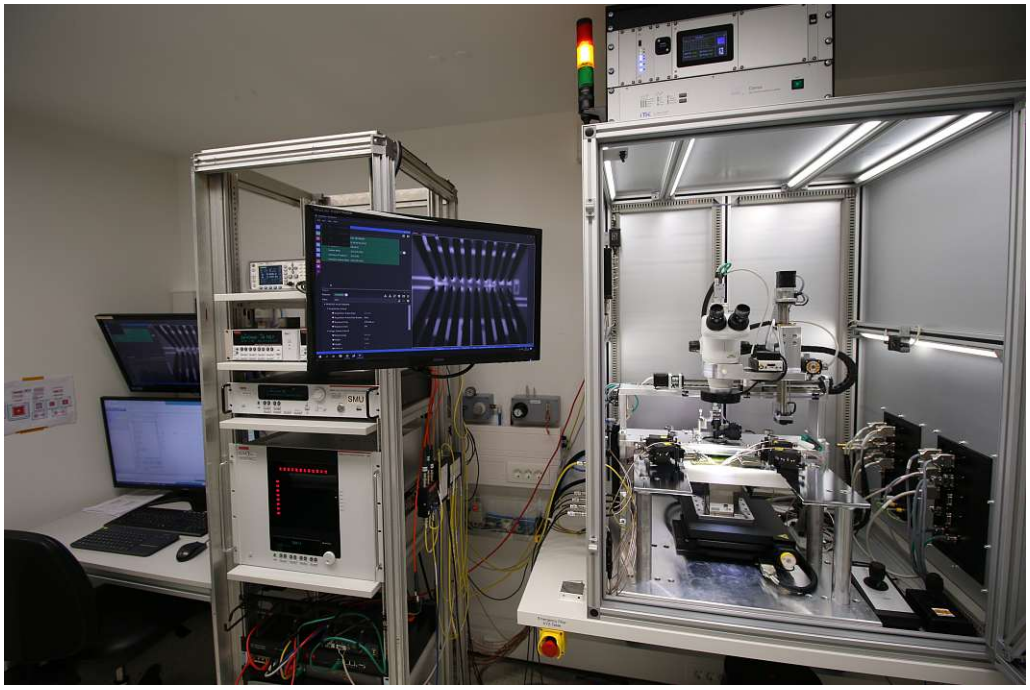

Figure 3.2: The PQC setup in at HEPHY in Vienna

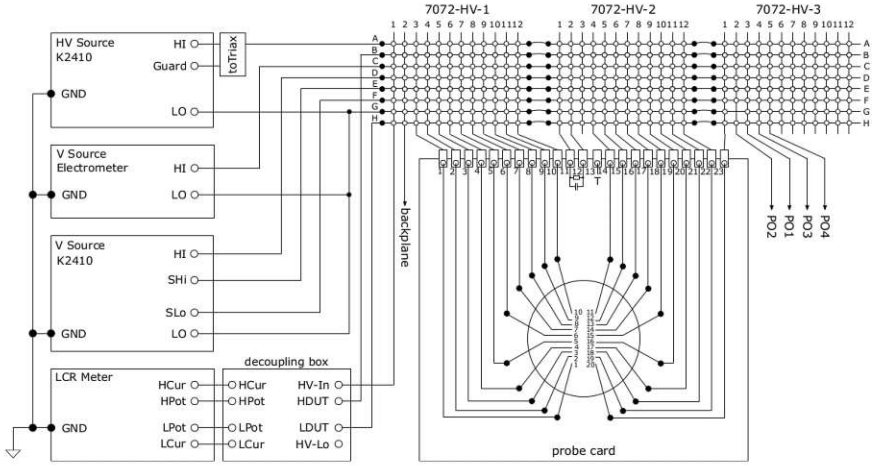

Figure 3.3: Schematic of the PQC setup, modified from [12]

3.2 Contacting procedure

Contacting the DUT via a probecard is a delicate procedure. The needles need some amount of pressure to the contact pads for electrical connection. On the other hand, moving too much into the sample can damage the sample, the probecard itself and appears to worsen the contact reliability.

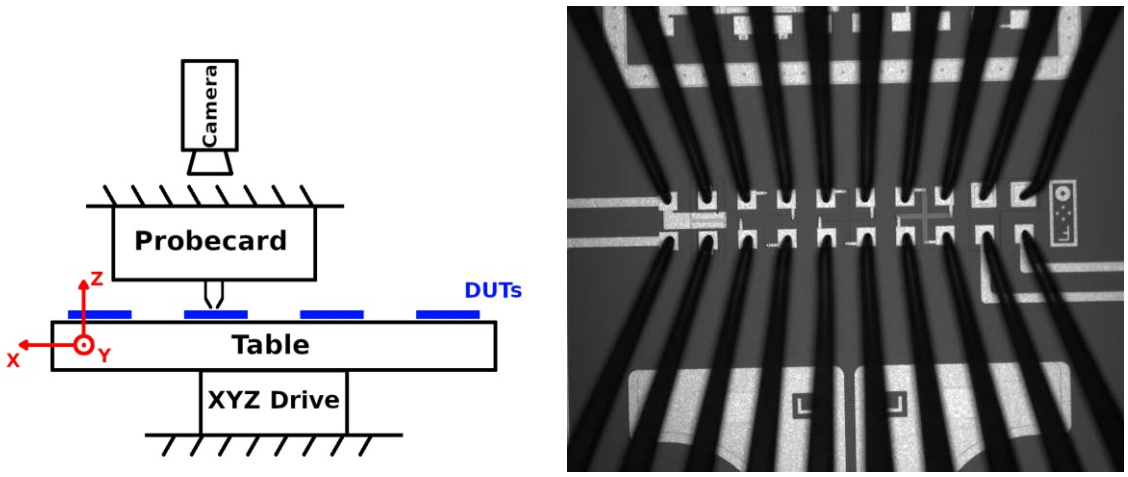

(a) (b)

Figure 3.4: Sketch of the table with the probecard, viewed from the front (a). The camera focuses the needles and DUT directly through a hole in the probecard chassis. The camera picture after contacting a flute 1 is shown in (b)

The coordinate system used by the software to control the table has the xy-plane parallel to the surface of the silicon sample. The positive z-direction points from the table with the DUT towards the needles.

When the table is moved in positive z-direction ("up"), the needles start to touch the surface at some point, this is called touchdown. The distance moved further into the DUT after touchdown is referred to as overdrive. A sketch is shown in figure 3.4a with the table coordinate system.

For the probecard used in the setup, the recommended overdrive is 50 µm, however, the maximum allowed overdrive is 70 µm. If more overdrive is applied permanent damage to the probecard can occur. It is therefore crucial for a reliable measurement to have a repeatable way of detecting the touchdown height.

In the past, the needles were observed via a microscope camera during stepping up in 10 µm steps. When the needles moved, the current z-height was declared as touchdown position. This procedure worked sometimes, but as the optical axis of the camera is parallel to the z-axis, only the very small movement of the needles in xy-direction could be observed due to bending. This caused missed or too early triggers, and required a lot of training and experience for the operators. Still, even for experienced users, around 50% of measurements failed due to bad contacts for some particularly sensitive types of test structures, especially VdP-structures.

The new contacting procedure uses the camera only for placement in the xy-plane, and electrical resistance measurement to determine the touchdown. This proved to be a very objective way to find the required position. This alignment procedure needs to be repeated for every teststructure to be measured. For one fluteset, it consists of following steps:

1. Move to saved position of corresponding flute-set (coarse)
2. Move up in positive z-direction in steps of 100 µm until around 100 µm before touchdown is expected (the camera image is sharper then)
3. Move in xy-plane until the needles are above the contacts of flute 1
4. Step up in 10 µm steps in positive z-direction, observing the LCR meter resistance reading.
5. When the resistance is below 1 MΩ, further stepping up of maximally 50 µm is allowed
6. When the resistance change is less than 50% per 10 µm step, the position is final
7. Save position for flute 1 to the control software
8. Move 500 µm down in negative z-direction, 13.5 mm in negative y-direction and 400 µm up again to go to flute 4
9. repeat steps 3 to 7 for the flute 4
10. Interpolate the positions for flutes 2 and 3 from flutes 1 and 4 via a button in the software

3.3 Measurement control software

The measurement control software (COMET) is developed at HEPHY for the purpose of measurement control and automation. Multiple measurements can be defined for different flutes via configuration files. A single measurement definition contains the settings for the switching matrix and all the instruments, including a source ramp (e.g voltage or current source, with start and stop value and step size), an optional static source for biasing and one or multiple measurements taken on each step of the ramp (e.g. current, voltage, capacitance).

For an efficient operation, a measurement plan can be created. The chuck can be loaded with up to 8 PQC flutesets, either 8 small pieces with only one PQC-fluteset or 4 half-moons with two flutesets each. The serial numbers can be entered together with the desired configuration files defining the measurements. Then, the operator can sequentially align the flutes and save the positions using the procedure from the previous chapter. Finally, the measurement can be started, and the software moves the table through all flutes on the samples and measures automatically.

Depending on the exact type, a measurement of all properties of one fluteset requires between 1 and 1.5 hours. Therefore, the measurement can be initialized in the afternoon and is finished next morning.

In the configuration, a preliminary analysis can be defined. This uses the same functions used in the final analysis run. For the resulting parameters and

measurement-quality measures, such as correlation coefficients, boundaries can be defined. If a particular measurement does not fulfill all those boundaries, it is directly repeated automatically when the last planned measurement of that flute is finished. The maximum number of those direct repetitions is defined globally. When it is reached, a re-contacting of the same flute is triggered and the measurement is repeated again with cleared direct repetition counter. For a reliable operation, a maximum direct repetition number of 2, and one recontacting showed good results in many cases. This leads to a maximum number of 4 repetitions in case of a faulty structure or very different measurement result than expected. Since all results are stored, further analysis can be made manually in such a case to investigate.

3.4 Automated analysis

From each measurement, only few result parameters are extracted, for most measurements only one or two. This includes, among others, the slope of a linear fits of all data-points for resistance-type measurements and more complex algorithms like intersection points for linear fits in different regions for the MOS-Cap. A detailed description of the algorithms can be found in chapter 4. For each sample, a sub-directory is created by the software where the results for each measurement is stored in a separate file. The analysis scripts developed in the course of this thesis iterate through each sub-directory and analyze all the measurements. When there are more than one repetitions for the same measurement, the most recent one is selected for analysis.

As a result, plots and tables are created. Templates can be enabled for different output formats of the tables. The formats include pure ASCII-, HTML- and LaTeX-tables. Custom templates can be added via Django2 templates, the iterable result-table object containing all the data can be accessed directly within the template.

With arguments to the program call, plots and histograms can be created. The plots are individual for each measurement and show all data-points, together with the result and some intermediate or diagnostic properties of the analysis functions such as fitted lines or correlation coefficients.

Histograms can be created for each result type that show the distribution of an individual result parameter for a whole batch. This allows to visually detect inhomogeneities and the distribution of process parameters within a batch.

The usage of the python analysis script is descibed in appendix B.

3.5 Statistical analysis

The histograms comparing the plots, as well as all plots in chapter 5 are created using the R language. This language is intended for statistics and very well suited to process data-tables with many numeric variables as well as non-numeric properties. R provides native support for such so called factor variables, such as the location on the wafer, which can be one of ”WL”, ”WR”, ”EL” or ”ER”. Appendix C contains a small example R code to create a simple plot from the PQC tables created by the python script. This R code can be used as basis for more complex analysis.

Chapter 4

The PQC test structures

The PQC teststructures are organized in flutesets. One PQC-fluteset contains all the teststructures connected to multiple flutes. There exist four main flutes that are measured by default. Multiple other teststructures are placed for reference, but for this document, only the four main flutes were used. Figure 4.1 shows the layout of one whole PQC-fluteset.

On a single wafer, more than one PQC-fluteset can be placed. The PQC-flutesets are placed in cutoff regions of the wafer around the sensor. Those circular segments are generally referred to as half-moons and assigned to cardinal directions.

As the tracker sensors are rectangular, four half-moons are cut off from each wafer. The West, North and East half-moons contain two PQC flutesets respectively. Routinely, only sets from East and West half-moons are measured. This results in four nearly equally spaced locations at the wafer, allowing to spot inhomogenities of any parameter. The tracker sensors are produced with two different processes, for the the AC coupled 2-S sensors, and the DC coupled PS-p sensors. [13]

The 8 inch HGCal wafers only contain two PQC flutesets, one each on two opposing half-moons.

For comparison, measurements were also taken from 2016 6-inch HGCal test-structures. Those contained an old PQC layout and was measured manually with needles. Only some structures have been measured for this type.

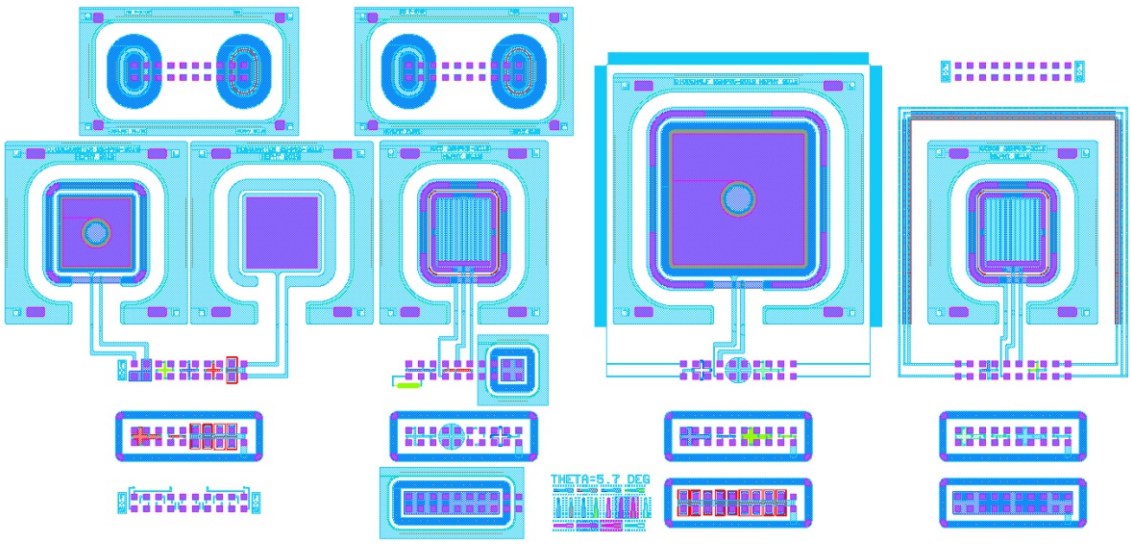

Figure 4.1: Layout of one full PQC-fluteset

4.1 Metal-oxide-semiconductor (MOS) capacitor

4.1.1 Theory

Metal-Oxide-Semiconductor Capacitors (MOS-Caps) are typical test-structures used in the semiconductor industry to access the properties of the silicon-oxide layer. Fixed oxide charges, flatband voltage and oxide thickness can be extracted from a single CV measurement.

A MOS capacitor consists of a planar metal electrode on top of a silicon-oxide layer. This layer is deposited on the silicon bulk. The whole arrangement can be surrounded by a guard-ring. The 4 PQC main flutes contain one square-shaped MOS-cap connected to flute 1 with a edge length of 1.29 mm.

The usual measurement for a MOS-cap is capacitance over a small bias voltage of a few volts. Depending on the bias voltage, three regions can be distinguished: accumulation, depletion and inversion.

In accumulation mode, positive charge carriers accumulate at the p-doped silicon bulk under the negatively charged metal electrode. This allows AC current to flow through the bulk, thus the effective thickness of the capacitor is only the thickness of the oxide. Therefore, in this region, the highest and fairly constant capacitance can be observed. Using the formula for a parallel plate capacitor, the thickness of the oxide t_{ox} can be directly calculated from the accumulation capacitance C_{acc} and the gate area A_G of the MOS-Cap and a dielectric constant of $\epsilon_r = 3.9$ for SiO_2:

$$t_{ox} = \epsilon_0 \epsilon_r \frac{A_G}{C_{acc}}. \tag{4.1}$$

When the bias voltage is decreased, the band bending decreases until the intrinsic Fermi-level of the bulk is at the same potential as the Fermi-level of the surface. This is called the flatband-condition and marks the transition to the second regime, the depletion mode. In depletion mode, a depleted region subsequently forms with increasing bias voltage. This increases the effective thickness of the capacitor as not only the oxide, but also the depletion region forms now a dielectric. Therefore, the measured capacitance decreases with the bias voltage in this region.

When the bias voltage is decreased further, the inversion mode is reached. In this regime, the now even more positively charged metal electrode not only repels holes like in the depletion region, but also attracts electrons, forming a zone of n-type like material just beneath the oxide. This layer shields the electric field from the gate, and the depletion layer stops growing with further bias voltage decrease.

The oxide charge concentration N_{ox} can be derived from the accumulation capacitance C_{acc} and flatband voltage V_{fb}:

$$N_{ox} = \frac{C_{acc}(\phi_{MS} - V_{fb})}{qA_G}. \tag{4.2}$$

Here, $\phi_{MS} = \phi_M - \phi_S$ is the difference between the work functions of the aluminum gate and the semiconductor. For the calculations in this thesis, a value of $\phi_{MS} = -0.69\,\mathrm{V}$ was used, corresponding to a p-type bulk doping of $5 \times 10^{12}\,\mathrm{cm}^{-3}$. [13, 14]

4.1.2 Measurement and analysis

For the analysis of a MOS-measurement, the first derivative is calculated via a cubic spline. Around the maximum derivative and the low-slope region at the depletion mode region, tangents are linearly fitted. For the low-slope fit, all data-points up to a certain slope are used.

The bias voltage at the intersection point of the accumulation- and the depletion-tangent is the flatband voltage result. For the accumulation capacitance, the mean in the accumulation region is used. An example plot for a mos measurement is shown in figure 4.2.

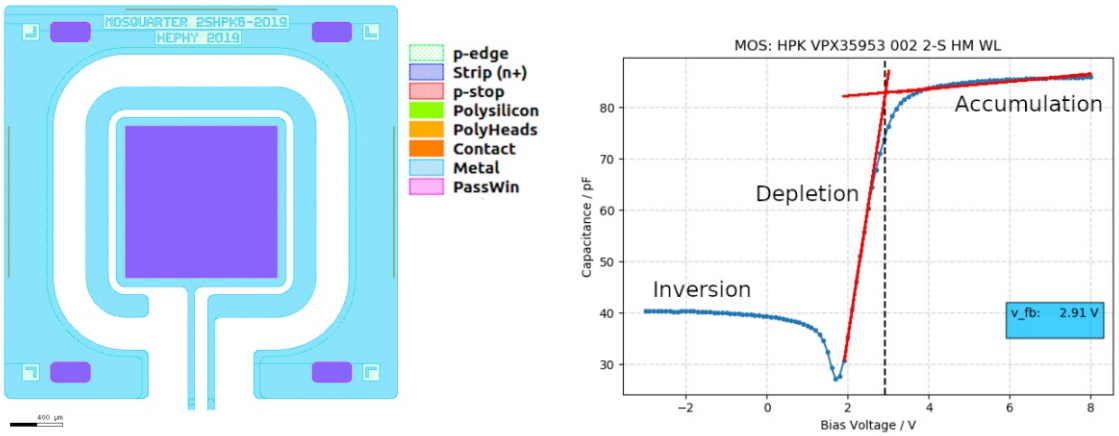

(a) (b)

Figure 4.2: MOS Capacitor layout (a) and corresponding measurement (b). Voltages are shown negative as the back-plane is used for biasing

4.1.3 Results

Figure 4.3 shows the distribution of the flatband voltage results, divided into categories of HGCal prototypes and batches. For the HGCal 5Vfb process, the flatband voltage is between 5 and 6 V. The HGCal 5Vfb and the HGC538 (New type C) types are distributed around 2.5 V.

For the tracker, the difference between the AC coupled 2-S sensors ($V_{fb} \approx 3\,\mathrm{V}$) and the DC coupled PS-p sensors ($V_{fb} \approx 5\,\mathrm{V}$) is clearly visible.

The oxide thickness is different for HGCal and tracker. Inside one of those families, it is distributed uniformly. The tracker oxide is about 100 nm thinner than the HGCal oxide.

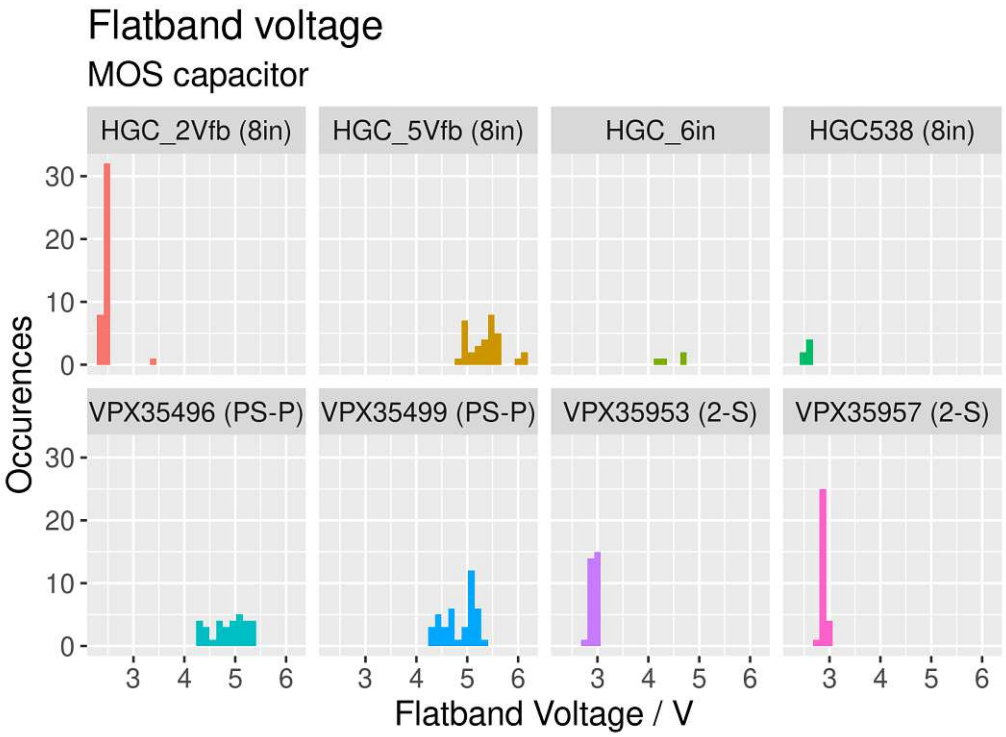

Figure 4.3: Histograms for the flatband voltage

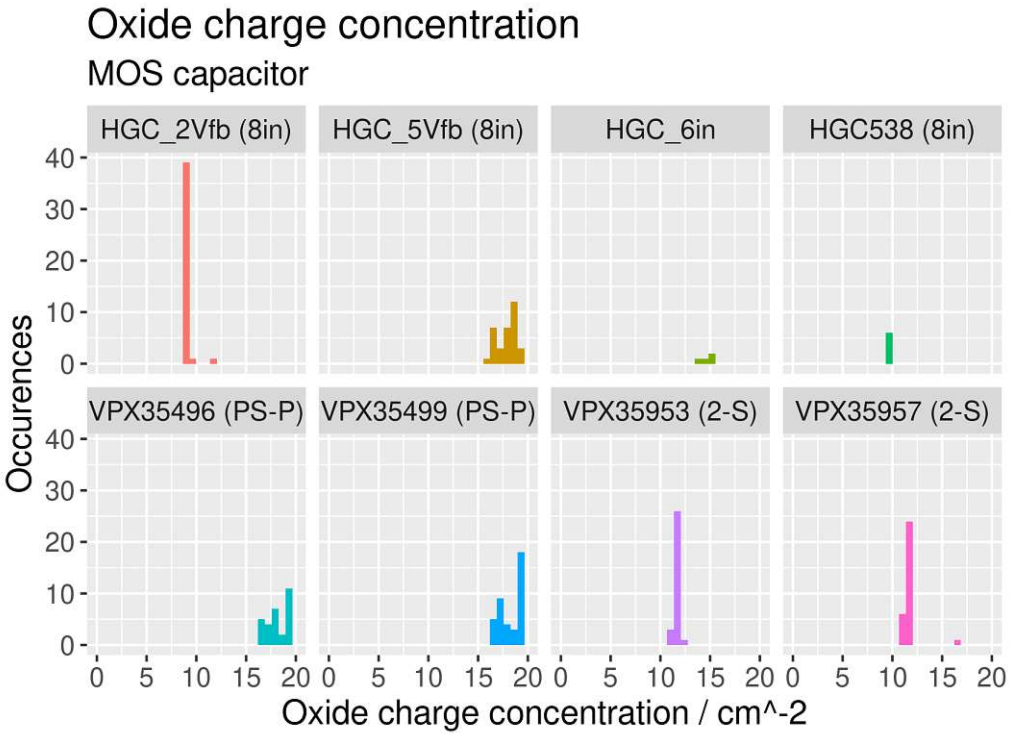

Figure 4.4: Histograms for the oxide charge concentration

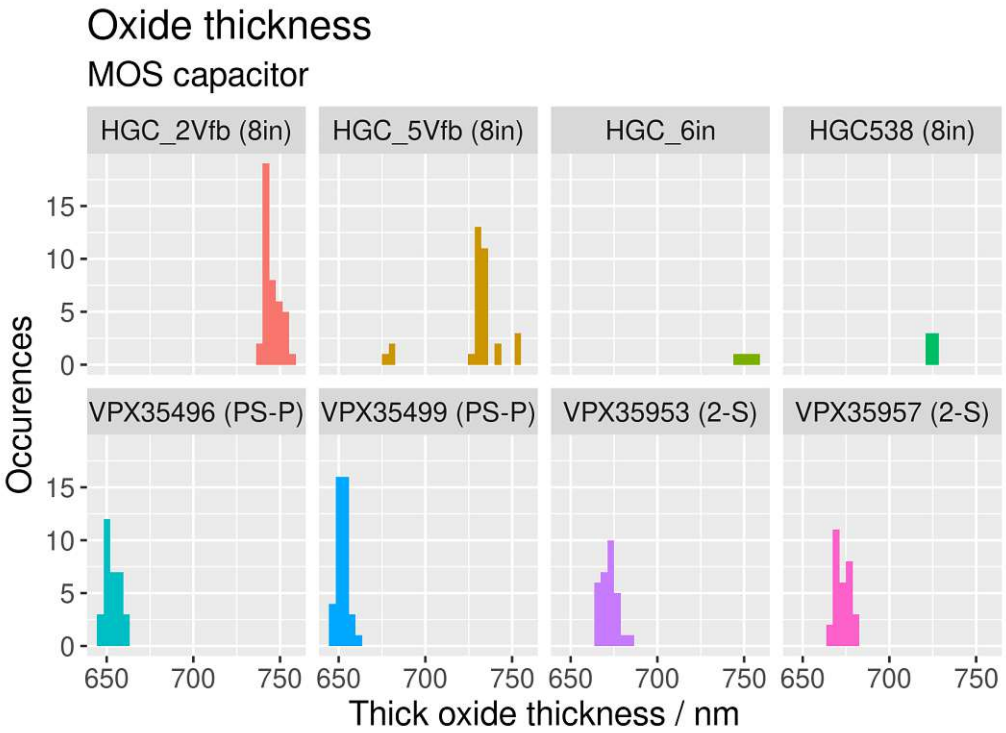

Figure 4.5: Histograms for the oxide thickness

4.2 Gate-controlled diode (GCD)

4.2.1 Theory

Gate-controlled diodes (GCDs) are test structures consisting of a comb-like pn-junction, interleaved with an oxide-isolated metal gate. It therefore combines the properties of a MOS capacitor with a pn-diode.

With GCDs it is possible to separate the surface current from the bulk current component. With these parameters, one can extract the surface generation velocity s_0 (sometimes denoted with s_g), a measure of the quality of the oxide-semiconductor interface, and the bulk generation lifetime τ_g.

To the 4 main flutes of the PQC test structure set for automated measurements, two different GCD layout variants are connected. The external dimensions are equal, but they feature a different gate width of 50 µm for "GCD" and 70 µm for "GCD05". Both have eleven gate strips and a pitch of 80 µm.

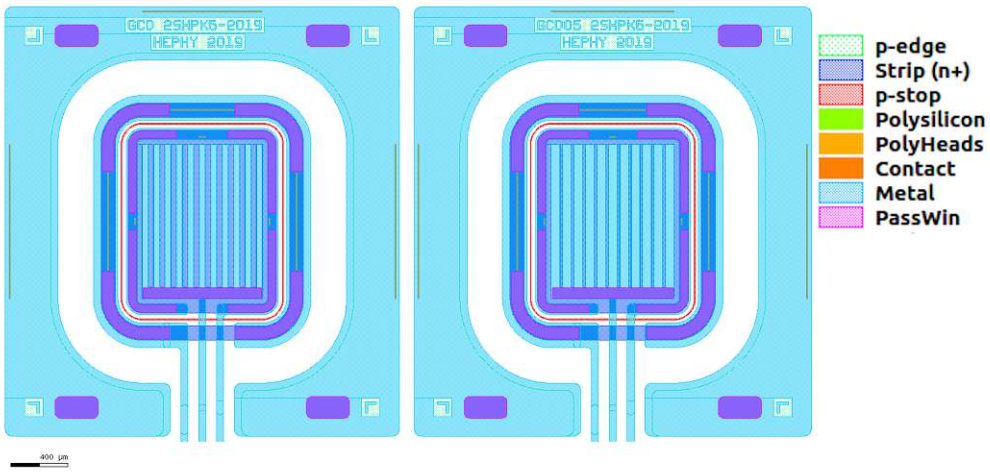

Figure 4.6: Layout for GCD (left) and GCD05 (right) in flute 2 and 4

The typical measurement procedure of a GCD is the diode leakage current in fixed reverse bias over a small varying gate voltage. The resulting waveform is shown in Figure 4.7 and features three characteristic regions. In those regions, different components contribute to the total leakage current of the diode-junction.

In accumulation mode, holes are attracted under the gate electrode. Therefore, only under the n-doped area a depletion region can form. The only contribution to the leakage current is the bulk leakage current $I_{acc} = I_{bulk}$ of the pn-junction.

When the gate voltage is increased, the leakage current jumps and depletion mode is reached. The bulk area under the gate now forms a depletion region as under the diode, increasing the magnitude of the total leakage current to $I_{dep} = I_{bulk} + I_g + I_{sg}$. The additional two components are the leakage current generated by spontaneous pair creation under the gate I_g and the surface contribution under the gate I_{surf}.

Further increasing of the gate voltage leads to inversion mode, forming a thin inverted layer above the gate. This layer prevents charge carrier creation at the surface, removing the corresponding contribution to the total leakage current: $I_{inv} = I_{bulk} + I_g$.

Therefore, the contributions can be extracted via:

$$I_{surf} = I_{dep} - I_{inv}, \tag{4.3}$$

$$I_{bulk} = I_{acc} - I_{inv}. \tag{4.4}$$

The bulk component has the opposed sign as expected for close to all measurements. This would indicate a negative bulk generation lifetime τ_g which is unphysical, so that this value cannot be used. This has been already reported in [12] for this process. However, the surface properties still show the expected behavior.

Surface generation velocity s_0

The surface generation velocity gives direct insight about the concentration of recombination centers (so called traps) at the silicon-oxide surface. It is therefore an important parameter to characterize the production-quality of the oxide-creation stage.

As the surface generation velocity is an intrinsic property of the material, it is independent from the geometry of the GCD test-structure used for measurement. This allows direct comparison of the the results of the two GCD structures on the 4 PQC main flutes. The surface generation velocity is directly proportional to the surface current I_{surf} and can be obtained via:

$$s_0 = \frac{I_{surf}}{q n_i A_G}, \tag{4.5}$$

where A_G is the gate area. For the intrinsic carrier density n_i, a value of $n_i = 7.01 \times 10^9\,\mathrm{cm}^{-3}$ is used corresponding to the lab room-temperature of 23°C. [15, 13]

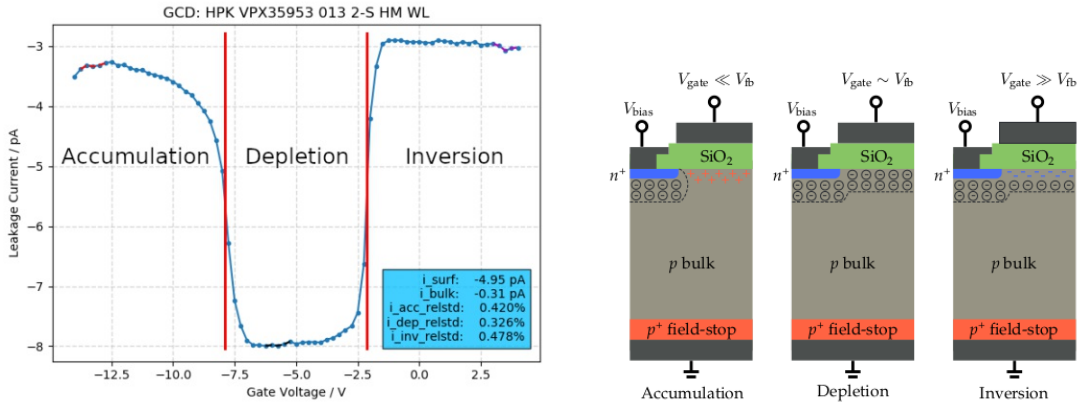

(a) (b)

Figure 4.7: Typical GDC measurement result (a), voltages are shown negative as the back-plane is used for biasing. Corresponding charge distributions from [12] (b)

4.2.2 Measurement and analysis

For the analysis, 5 data-points in the corresponding regions are averaged to determine the currents. For accumulation and inversion mode, the first and last data-point of the series is discarded. From the remaining series, the first and last 5 points are averaged to obtain I_{acc} and I_{inv}.

For the depletion region, the maximum (minimum for the shown plot) is used as central point for the 5 data points selected. Accordingly, the surface current is the difference between the leakage current between depletion and inversion. The surface generation velocity s_0 is subsequently calculated via formula 4.5.

4.2.3 Results

Histograms of all available measurements are shown in figure 4.8. For a more compact visualization, the results for the two available structures, GCD on flute 2 and GCD05 on flute 4 are both shown in the same subplot. To allow distinction, the GCD05 results are only shown as black frame, transparent inside. The agreement of both types is good despite the different dimensions of the two structures because s_0 is a general property of the sample.

Clearly visible is different distribution for the 2-S and the PS-p batches, however, the stability within one process family is good. For the HGCal, s_0 is generally higher and more spread.

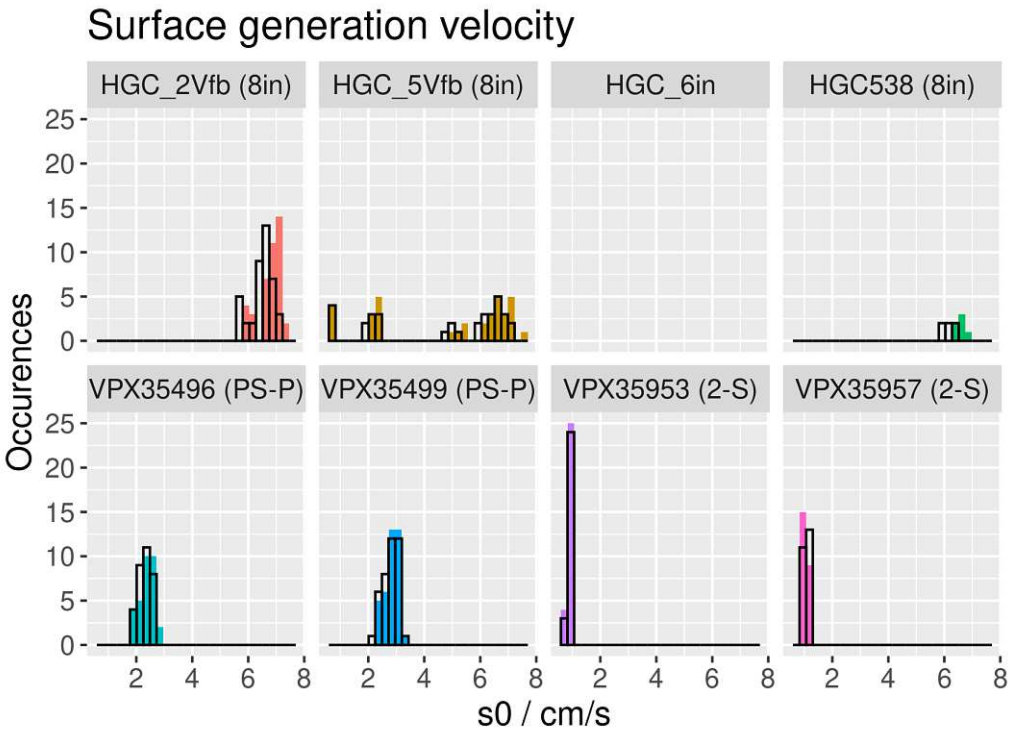

Figure 4.8: Histograms for the surface generation velocity results of the GCD (colored borderless bars) and GCD05 (transparent bars with black border) structures

4.3 Field effect transistor (FET)

4.3.1 Theory

Field effect transistors, especially MOSFETs (Metal-Oxide-Semiconductor FET) are a very well established structure in the semiconductor industry as they are the basis for integrated circuits. As a test-structure, they give insight to the inter-channel properties like interstrip-resistance via the p-stop performance.

The p-stop concentration can be directly determined via the corresponding VdP structure. However, the overall p-stop performance is also largely affected by the concentration depth profile. The FET teststructure uses the p-stop close to the actual application in the sensor. Therefore, it is sensitive to process variations affecting the p-stop implants, and allows to probe the real p-stop performance outside of the sensor.

The FET structure consists of two n+ doped regions with a certain distance. The connected terminals are called source (S) and drain (D). Both are surrounded by a p-stop ring. On top of the gap between the implants, there is an oxide isolated metal gate (G) electrode located. The layout is shown in figure 4.9a. [16, 14]

4.3.2 Measurement and analysis

The characteristic property of a FET is the threshold voltage V_{th}. To measure it, a small voltage V_{DS} (for PQC 100 mV) is applied between the source and drain terminals. Then the gate voltage in respect to source V_{GS} is varied from small negative to positive values. The drain current is measured and plotted over the gate voltage. A typical resulting curve is shown in Figure 4.9b.

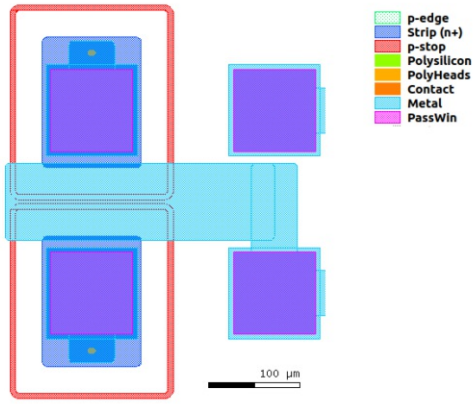

(a)

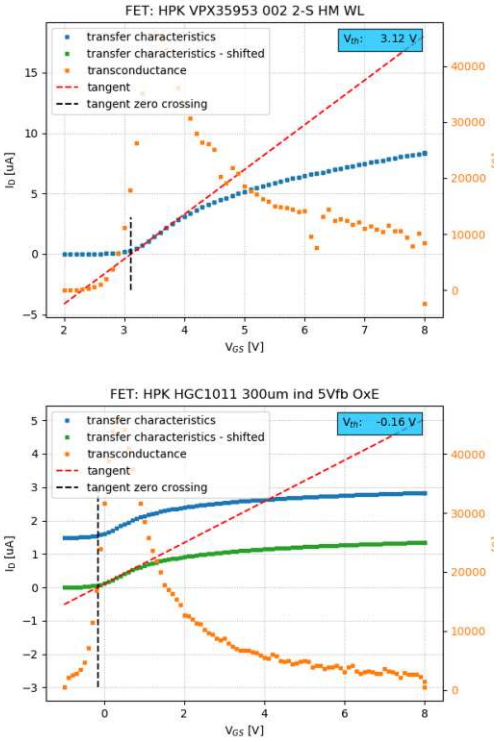

(b)

Figure 4.9: FET layout (a) and two measurements (b). The top measurement is typical for the FET structure, the bottom is one with high leakage current, that has been subtracted.

For low gate voltages, the FET is blocking, and very little current flows through the drain. When the gate voltage is increased over the threshold voltage V_{th}, the drain current increases with increasing gate voltage. The slope of the resulting curve, the trans-conductance, is highest close to V_{th}. This is the linear region. At higher gate voltage, the curve becomes nonlinear with decreased trans-conductance. To extract V_{th}, a tangent is fitted in the linear region and its crossing point with a horizontal line at blocking current level is evaluated.

4.3.3 Results

The measurement results are shown in a histogram in figure 4.10. For the tracker, the different threshold voltages for PS-p and 2-S are visible. The AC coupled 2-S sensors have a threshold voltage around 4 V, whereas the DC coupled process of the PSp sensors are around 2.5 V. Also visible is the inhomogeneity of batch *VPX35953 (2-S)* (purple). Two peaks are visible. A deeper analysis of this inhomogeneity is given in section 5.4.1.

The new type C *HGC538 (8in)* has results very similar to the PSp process. For the other HGC prototypes, variations can be seen. Also it is clearly visible that the 5Vfb structures have lower threshold voltage than the 2Vfb. This is understandable as the oxide charge also affects the threshold voltage. The smaller peaks in those two histograms relate to variations in the p-stop concentration for some samples.

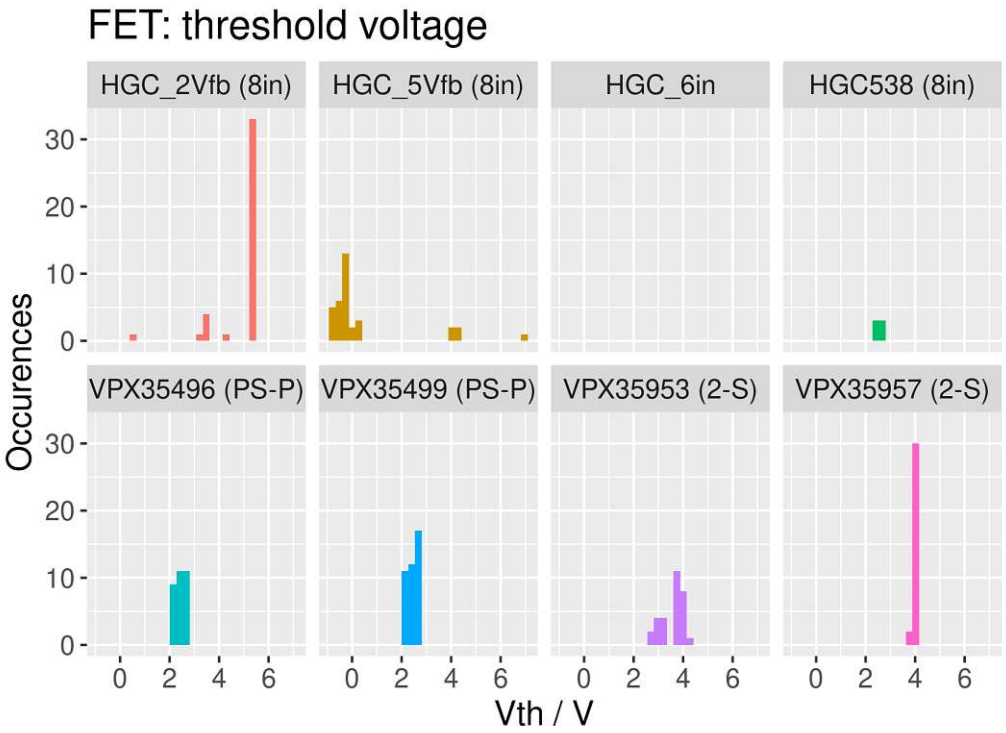

Figure 4.10: Histograms for the FET threshold voltage results. On the HGC 6in sensors, no comparable FET structure was available

4.4 Generic resistance measurement

There are many teststructures on the four main flutes that behave like a resistor. They reach from the polysilicon-meander that is actually used as bias-resistor in the sensors to Van-der-Pauw structures that give insight to the doping concentrations of the various implants.

4.4.1 Measurement and analysis

The measurement procedure for most of the resistive test-structures is very similar. A constant current is applied through the two force terminals of an SMU to the DUT. Two high impedance sensing wires measure the voltage drop between two points of the DUT. This is referred to as 4-wire measurement. Opposed to the 2-wire measurement, that connects the force and sensing wires inside the SMU, the 4-wire measurement is mostly independent from the contact resistance from the needles to the DUT. An additional voltage drop caused by this resistance does not affect the measurement, as it only increases the output voltage of the current source. As no current flows through the sensing wires, the contact resistance does not cause a voltage drop there. This is only true if the inner resistance of the sensing wires is big compared to the contact resistance. It has been observed for the SMUs used in the setup, that sensing wires tend to drift towards the corresponding force wires if left floating. This leads to a higher resistance reading than expected if there is a contact problem.

For a complete measurement, the current is varied between a negative and positive maximum. The resulting IV curve is fitted by linear regression, the slope corresponds to the resistance. Theoretically, one or two measurement points would

be sufficient to get a result, however the quality of the measurement cannot be determined then. For most of the the PQC measurements, 11 points are made equally spaced around the negative and positive maximum current. For the low-resistivity measurement of the metal-clover-leaf-VdP, more points are taken for better noise-immunity.

The only resistance measurement that does not follow this principle is the polysilicon meander. The resistance value of it is around 1.5 MΩ. For the measurement, different voltages are applied, and the flowing current is measured via the electrometer. This allows higher accuracy at lower voltages, as the electrometer current reading is more accurate compared to the SMU.

4.5 Van-der-Pauw (VdP) structures

4.5.1 Theory

Van-der-Pauw structures are a typical arrangement to measure the resistivity of thin sheets. They allow direct sheet resistance measurements without dependence on geometry.

Various implementations of VdP structures are available on the 4 main flutes to measure different layers.

The typical Greek cross shaped layout is implemented for the polysilicon layer, n+ and p-stop implants. A combined version with one elongated leg featuring two additional terminals for the line-width measurement is available for the p-edge implant.

Sheet resistance

For thin films, it is often useful to introduce the sheet resistance R_{sh}. It is defined as:

$$R_{sh} = \frac{\rho}{t}, \tag{4.6}$$

with resistivity ρ and sheet thickness t. The unit of R_{sh} is of resistance, commonly denoted as $Ohm/square$. The resistance R of a rectangular film resistor with length l and width w from the sheet resistance relates to:

$$R = R_{sh}\frac{l}{w} = \rho\frac{l}{wt}. \tag{4.7}$$

Van der Pauw showed that the sheet resistance of an arbitrarily shaped, uniform, flat sample with 4 contacts can be determined via two 4-wire resistance measurements, without knowing the current distribution or exact shape. The conditions for this to hold true is that the contacts are sufficiently small in size (point shaped) and at the circumference of the shape, and that the shape is simply connected. In that case, the sheet resistance is given by

$$R_{sh} = \frac{\pi}{ln(2)}\frac{R_{12,34} + R_{23,14}}{2}F_{(q)}, \qquad q = \frac{R_{12,34}}{R_{23,14}} \tag{4.8}$$

with

$$R_{12,34} = \frac{U_{34}}{I_{12}} \quad \text{and} \quad R_{23,14} = \frac{U_{14}}{I_{23}}. \tag{4.9}$$

Here, U_{ij} is the voltage measured across terminals i and j when a current I_{kl} is applied through the terminals k and l. The correction function $F(q)$ is only dependent on the quotient of the resistances q and is the solution to the transcendental equation:

$$\frac{q-1}{q+1} = \frac{F(q)}{ln(2)} arcosh\left(\frac{1}{2}e^{ln(2)/F(q)}\right). \tag{4.10}$$

For similar resistances, $F \approx 1$. This means that for a symmetrical teststructure, the sheet resistance is directly proportional to the mean of the two measured resistances to a good approximation. [17, 18]

Various copies of VdP structures are implemented for the PQC layout, shown in figure 4.11. These include all implant layers (n+, p-stop and p-edge), metal- and polysilicon layer and the bulk material.

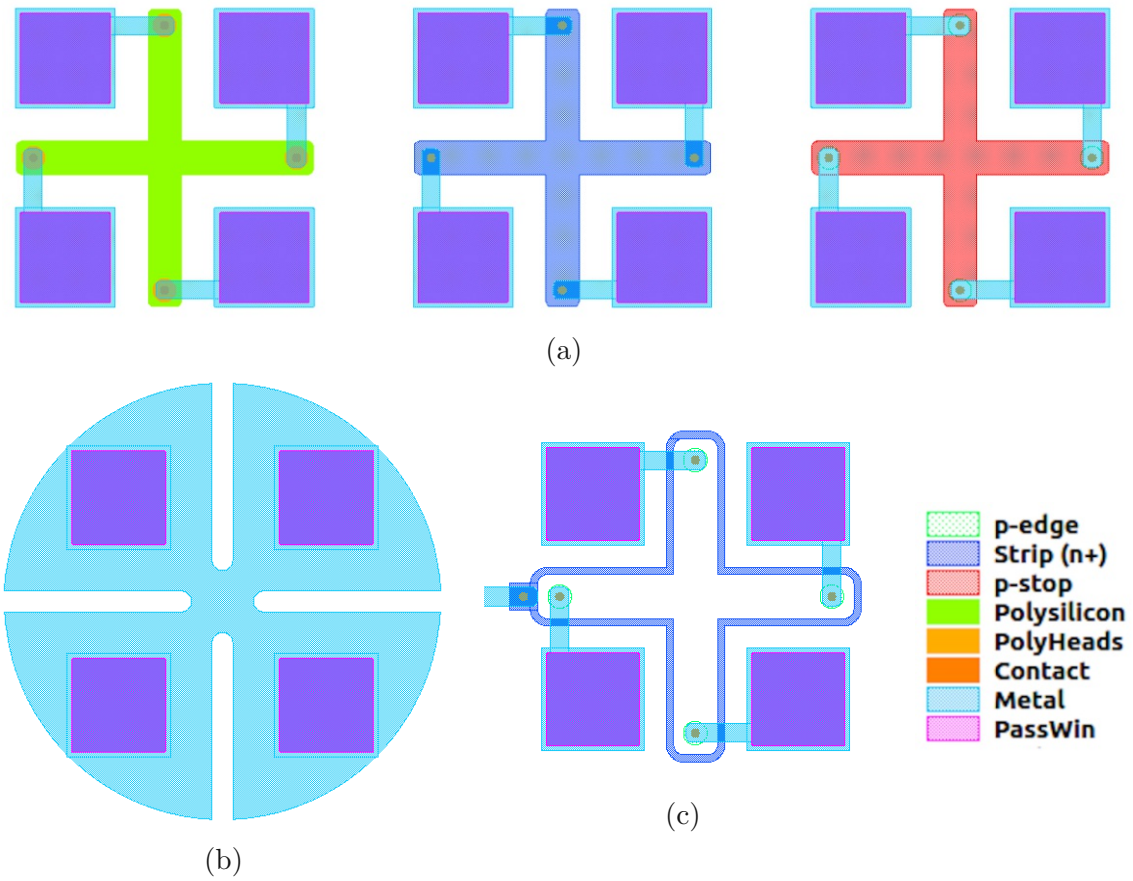

Figure 4.11: Different Van-der-Pauw structures: classical cross (a) metal clover leaf (b) and bulk (c). The p-edge VdP structure is shown in figure 4.19b and is combined with a line-width structure

4.5.2 Results

p-stop implant

Histograms of the Measurement results are shown in figure 4.12, tiled according to the variant.

For the *HGC 2Vfb* variant, two different nominal p-stop concentrations were measured, standard (STD) and half (STD*0.5). The two maxima are clearly visible in the histograms.

For the *HGC 5Vfb* variant, some samples with higher p-stop concentration were available (2.5 and 5 times higher than standard). This can also be seen in the corresponding histogram. A more detailed analysis of the different nominal p-stop concentration variants is available in section 5.5.2.

For the old *HGC 6in* variant, only four samples were available. The resistivity for the p-stop implant was lower by a factor of 10 compared to all other variants.

The *HGC538 (8in)* and the PS-p and 2-S batches all show very narrow sheet resistance distributions around 19 kΩ/sq. Only the *VPX35953 (2-S)* shows a broader tail on the higher resistance side. This is caused by a significant inhomogeneity in p-stop doing on some wafers. More about the inhomogeneity in section 5.4.1.

n+ (Strip) implant

Histograms for the n+ implants are shown in figure 4.13. The resistivity is slightly lower and with less variation for the tracker batches. The HGCal varieties show more spreading, especially the HGC 5Vfb types.

p-edge implant

The edge implant shows slightly different mean resistivities for each batch in the histograms of figure 4.14. Also for this implant, the spread in one variety is higher for the HGCal compared to the tracker. Another visible feature is the two-maxima distribution of batch VPX35496. This is caused by an inhomogeneity similar like observed at the p-stop implant (see chapter 5.4.1), but at much lower scale of a few percent.

Polysilicon

Only two batches with polysilicon layers were available. As visible in the histograms in figure 4.15, the two distributions are very similar.

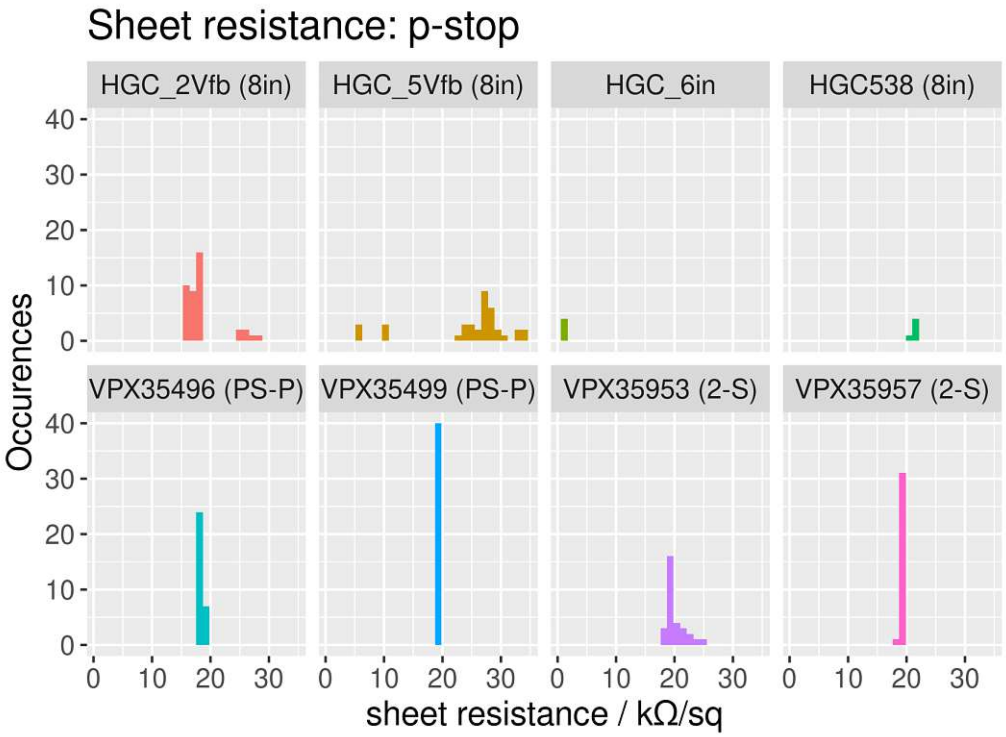

Figure 4.12: Histograms for the p-stop VdP results

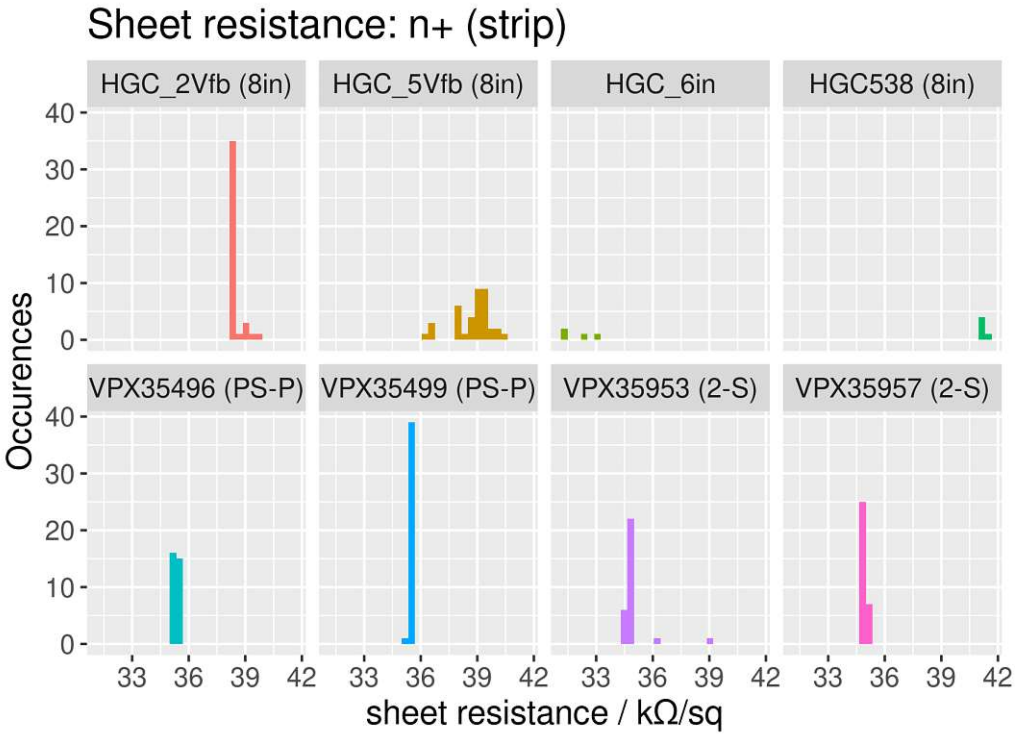

Figure 4.13: Histograms for the n+ (strip) VdP results

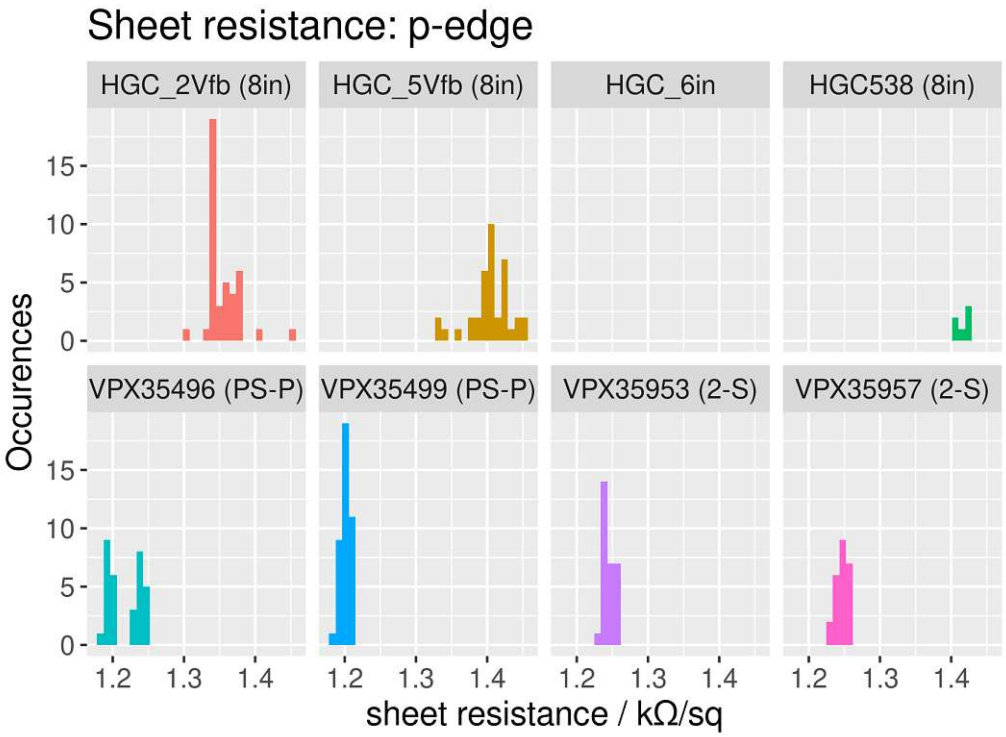

Figure 4.14: Histograms for the p-edge VdP results

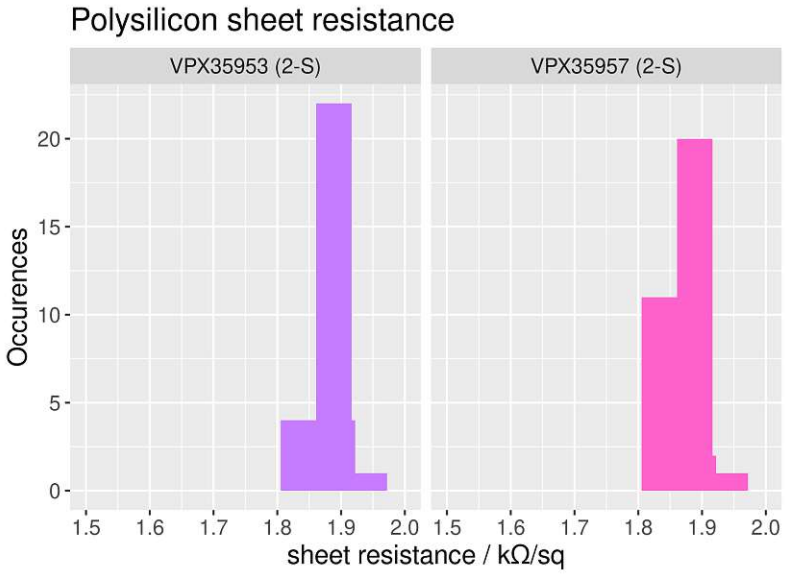

Figure 4.15: Histograms for the polysilicon VdP results

Metal clover leaf VdP

The metal clover leaf VdP has an expected sheet resistance of below 20 mΩ/sq. Therefore, the measurement for this structure is more difficult than the others. A higher current is required and the voltage drop is below the millivolt range. This required the exchange of the voltage source SMU to a K2410, as that device has a better low voltage resolution. However, the resulting measurement was still range dependent. This can be observed with a closer look to figure 4.16a. In the range of ±100 mA a small offset from the fit is visible. The slope really is different in

the region of ±10 mA. For the plot in figure 4.16b, only the points below a certain maximal absolute measurement current were selected, fitted and the resulting sheet resistance visualized over the maximal measurement current. On this basis, the default measurement current was selected to be 200 mA. The deviation for the result against the saturation value is below 3% for this current. A higher measurement current could increase the accuracy, however, for a small structure like the clover leaf, already 200 mA are a high current, and the risk of damage to the structure increases with the measurement current. This relationship was discovered during the measurements. Therefore, some structures were measured with 30 mA, others with 200 mA. For batch number VPX35496, some measurements were conducted with 100 mA, as that batch was currently measured when the current dependency was discovered.

The histogram of the measurements is shown in figure 4.17, the different peaks caused by current changes are clearly visible and annotated. Of course, only measurements with the same current can be compared to each other. Comparing tracker and HGCal structures, it is visible that the tracker structures have slightly lower metal resistances than the HGCal structures. This deviation is around 8% of the measured value.

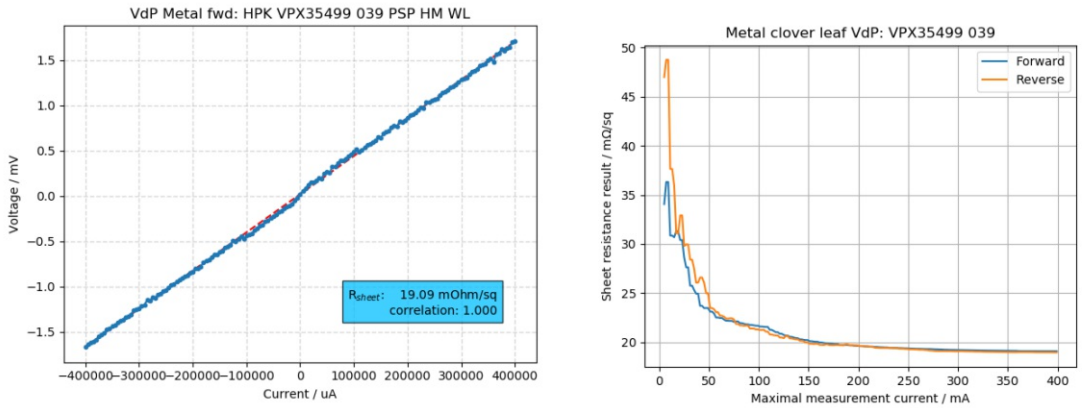

(a) (b)

Figure 4.16: Metal clover leaf VdP result: Raw result (a) and the resulting sheet resistance over different maximal currents (b)

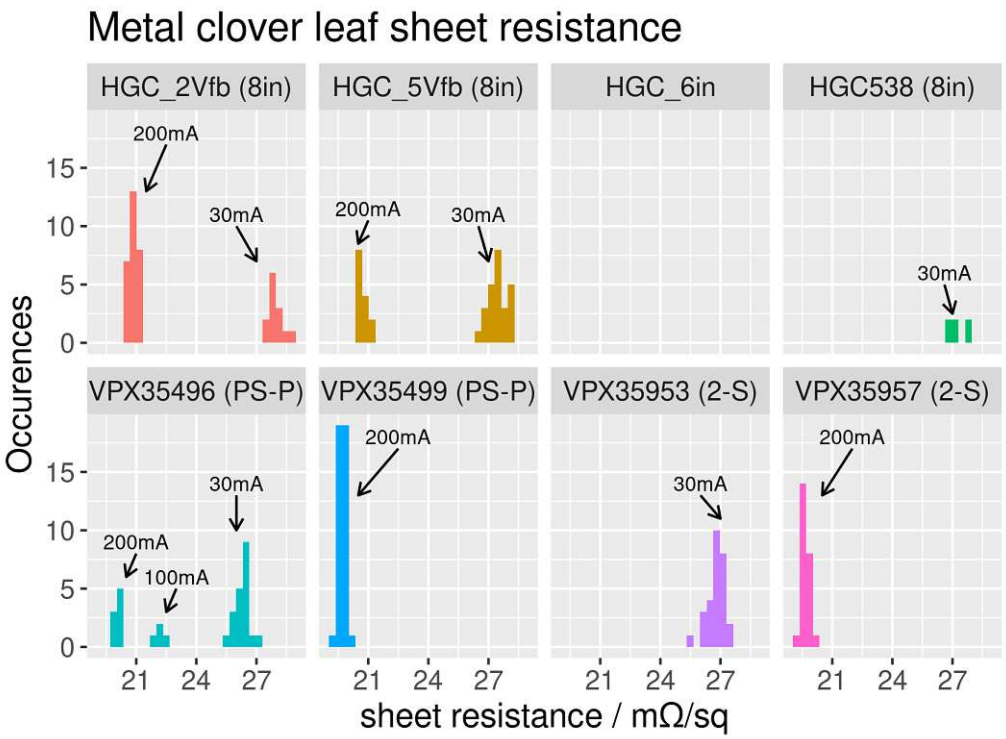

Figure 4.17: Histograms for the metal clover leaf VdP, the different measurement currents result in different peaks in the histogram

Bulk cross

The bulk resistivity was also measured using the VdP-cross-shaped structure. For isolation, the structure is surrounded by an n+ ring. For the measurement analysis, the typical thin film approximation is not valid. Still, the resistivity can be calculated for a thick sample using:

$$\rho_\infty = \frac{2\pi s}{2-\sqrt{2}} \frac{V}{I}, \tag{4.11}$$

with $s = 187\,\mu\text{m}$ the probe spacing. This result is valid if the thickness is large compared to the structure size. This is not true in this case, and a correction factor F needs to be applied to obtain $\rho = F\rho_\infty$. Calculations of two different models described in [13] lead to correction factors of $F_1 = 1.218$ and $F_2 = 1.081$. Comparisons with diode measurements have shown that F_2 is closer to the correct result. Therefore, the value of F_2 is used in this document. [19, 13, 12]

The histograms are shown in figure 4.18. The red dashed line marks the minimal target value of 3.5 kΩcm.

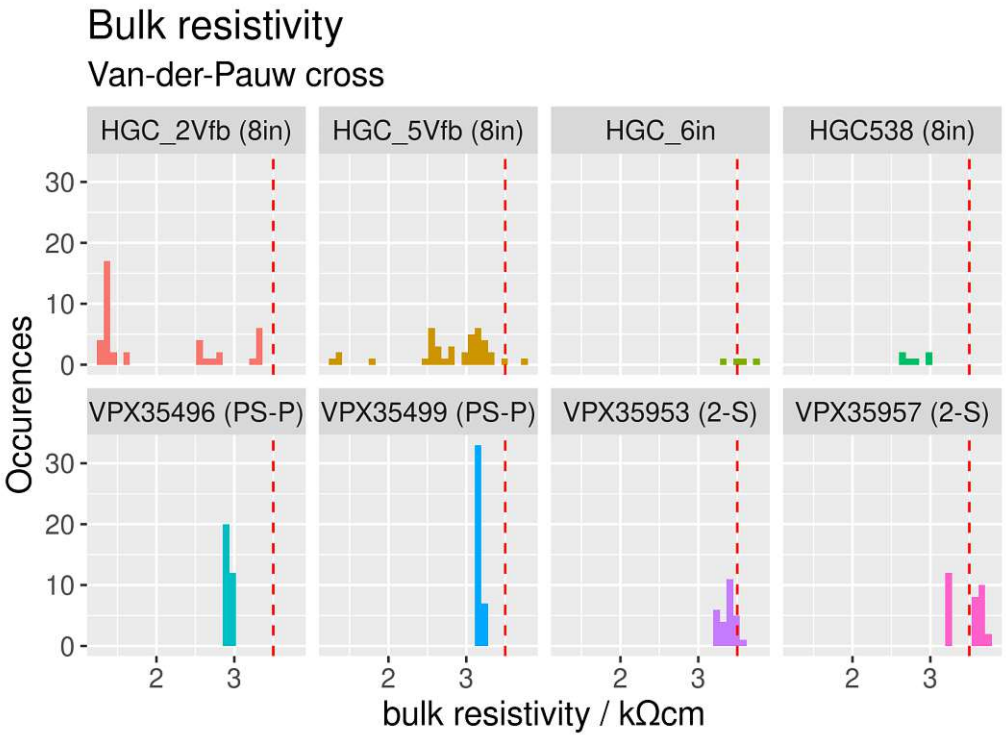

Figure 4.18: Histograms for the bulk-VdP results

4.6 Linewidth structures

4.6.1 Theory

The line width is the width of a strip-like layer on the plane of the wafer surface. Several test structures exist to electrically determine the line width of n+, p-stop and p-edge implants. A line width structure contains a strip of the implant of interest, connected at four positions along the strip. Optionally, the strip can be implemented as one arm of a VdP-cross structure to effectively save two contacts. The layout is shown in figure 4.19.

A current ramp is applied across the two outer contacts. The voltage between the inner two contacts is measured for each voltage step. Finally, a linear fit determines the slope corresponding to a resistance R_{lw} between the inner contacts of the line.

To obtain the line width W, the sheet resistance R_{sh} can be used together with the distance L between the two inner contacts [19, 12]:

$$W = \frac{R_{sh}}{R_{lw}} L. \tag{4.12}$$

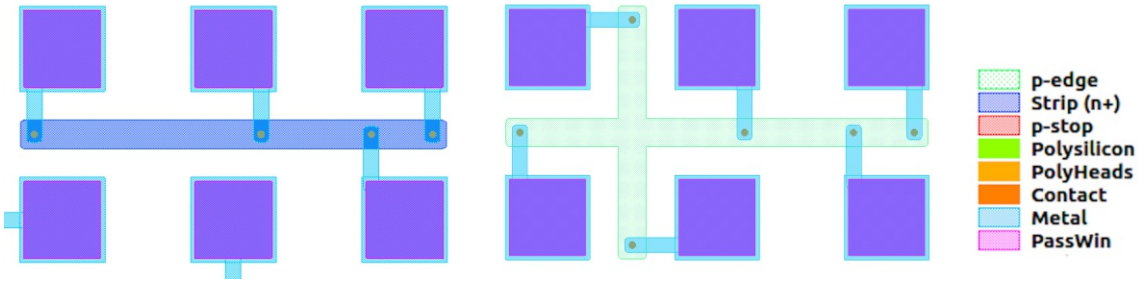

(a) (b)

Figure 4.19: Layout of linewidth-structures: classical (a) and combined with a VdP structure (b)

4.6.2 Results

The results of the line width measurements are shown in figures 4.20 to 4.22. The nominal width is 33 µm, for the n+ implant, the measured values are systematically higher but still close to the nominal value. For p-edge, the results for the tracker are distributed evenly around the nominal 33 µm. Very different are the results for the p-stop line width, which are different by a factor of two. This effect has been reported previously in [12].

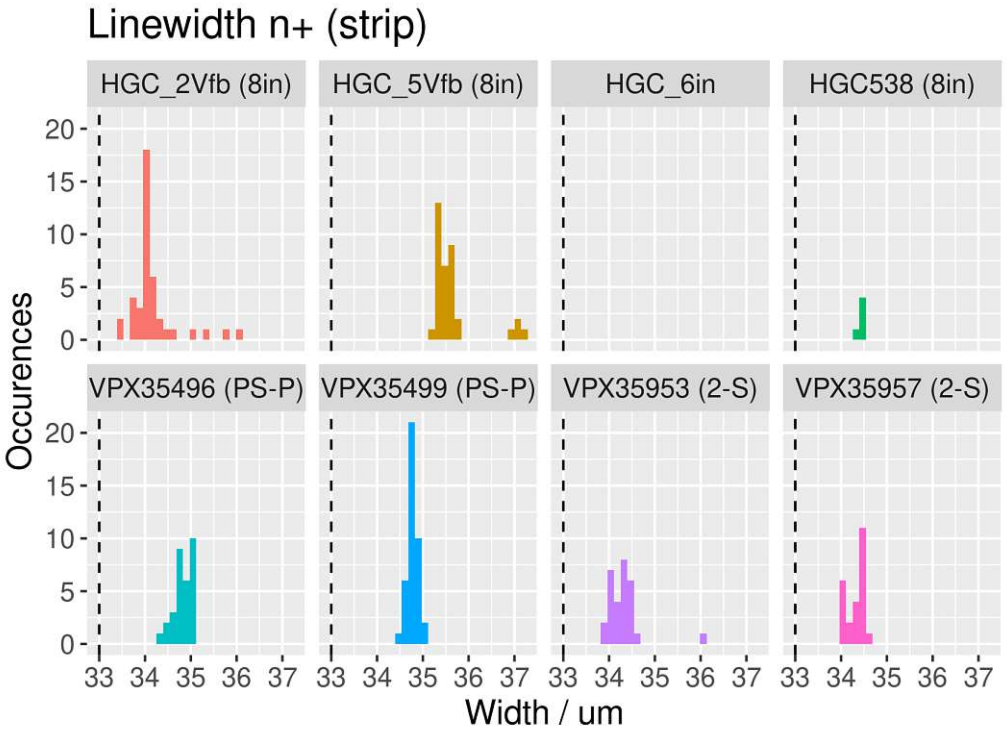

Figure 4.20: Histograms for the n+ line width results

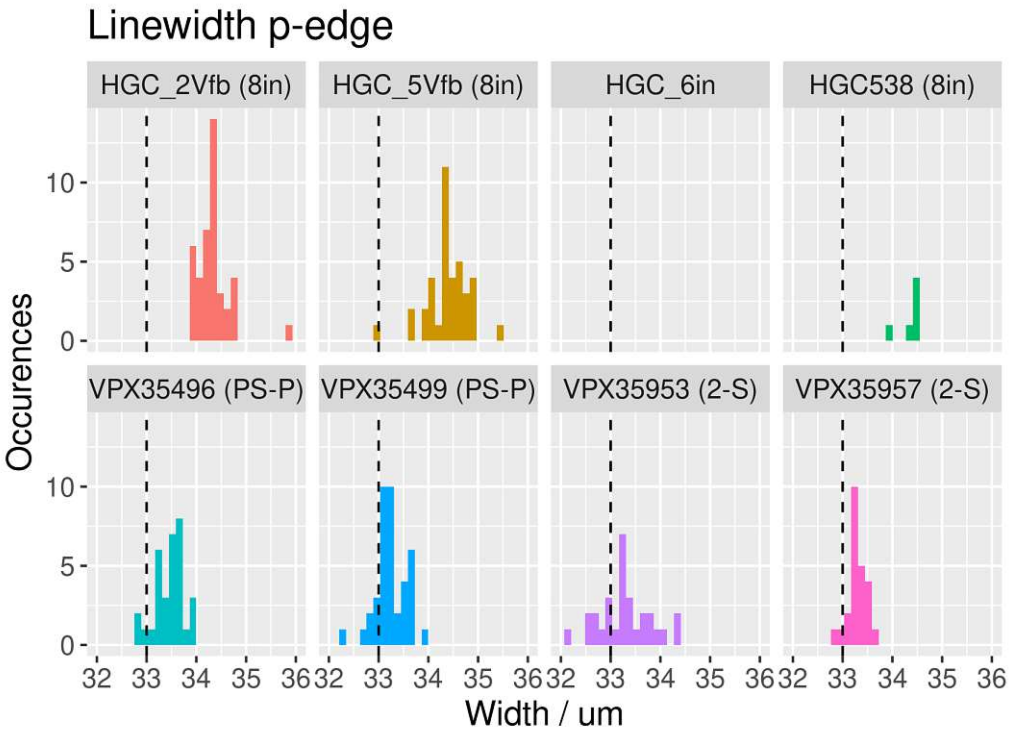

Figure 4.21: Histograms for the p-edge line width results

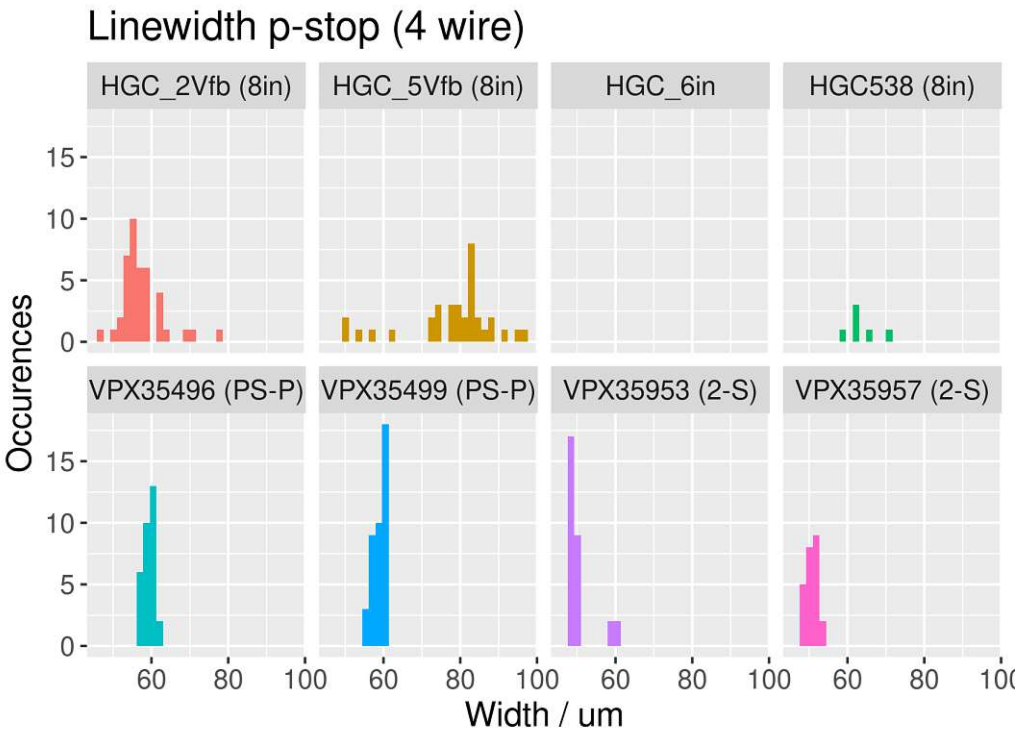

Figure 4.22: Histograms for the p-stop line width results

4.7 Cross-Bridge Kelvin Resistors

4.7.1 Theory

Cross-Bridge Kelvin Resistors (CBKRs) are teststructures to probe the specific contact resistance ρ_c of two materials. The shape is similar to the cross-VdP, but two different materials are used for two adjacent legs. In the center region, the two materials form a contact. A picture of the layout is shown in figure 4.23.

For measurement of a CBKR structure, a current is applied through two adjacent contacts of different material. The other two contacts are used to measure the voltage drop.

For the CMS Tracker sensors, two types of contacts are used: metal/strip and metal/polysilicon.

The specific contact resistance ρ_c relates to the actual resistance of a contact R_c via $\rho_c = R_c/A$ where A is the contact area. [20]

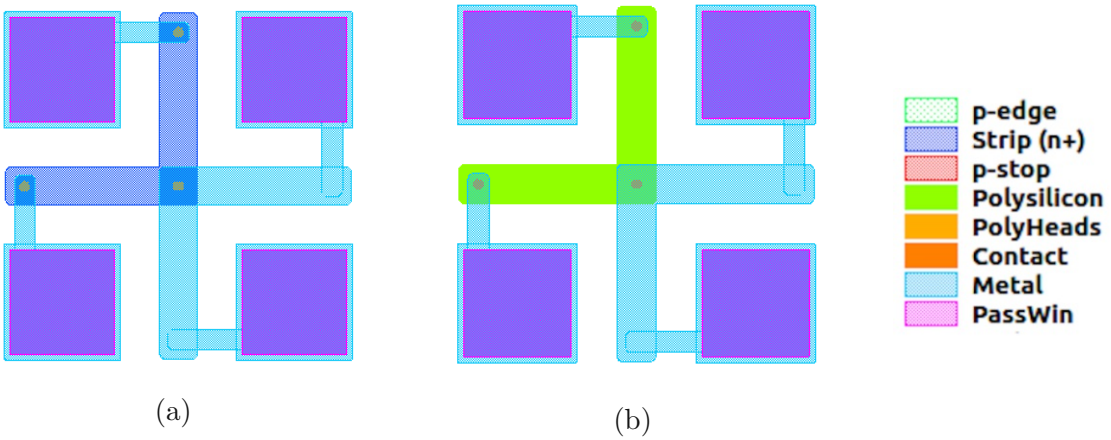

Figure 4.23: Layout of CBKR-structures: metal/n (a) and metal/polysilicon (b)

4.7.2 Results

Figure 4.24 shows the results for the n+/metal contact resistances. The distribution for the tracker is very narrow, the contact resistance for the HGC-prototypes is slightly higher. The polysilicon/metal contact results are shown in figure 4.32.

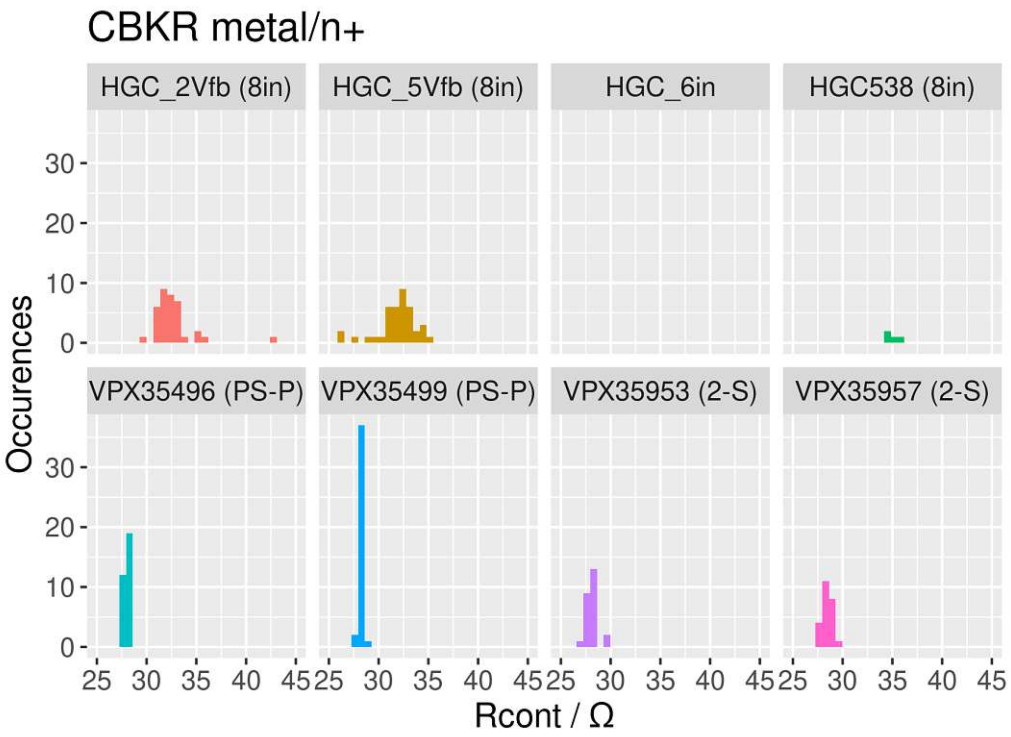

Figure 4.24: Histograms for n+ CBKR results

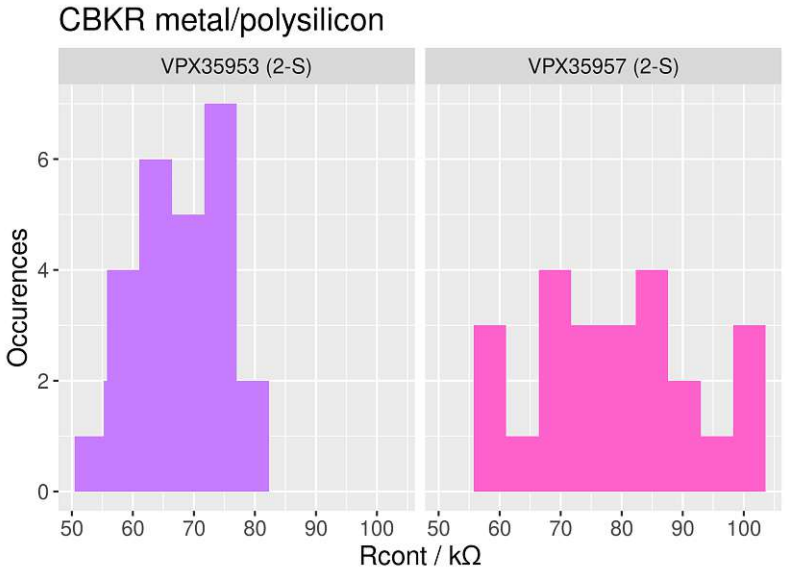

Figure 4.25: Histograms for polysilicon CBKR results

4.8 Capacitor test-structure

4.8.1 Theory and procedure

The capacitor test-structure consists of an n-doped first electrode, a dielectric of "thin oxide" and a metal second electrode. The "thin oxide" is the same as used for AC coupled strips to separate readout channel from the strip. Therefore it is important to monitor the thickness, which is easily possible through this structure. Also for DC coupled sensor it is of some interest as it is sensitive to process variations

that might affect also other parameters as well. With the capacitance, the thickness of the thin oxide can be calculated via the parallel plate capacitor formula:

$$C = \epsilon_0 \epsilon_r \frac{A}{d}. \tag{4.13}$$

The capacitor teststructure has dimensions of 130 µm × 130 µm and a nominal capacitance of 2.03 pF. [13]

The measurement of this structure is capacitance over a symmetric bias voltage ramp of a few volts. There are two capacitor teststructures with a common n-region and individual metal electrodes. They are designated as left and right capacitor structure. The layout is shown in figure 4.26a.

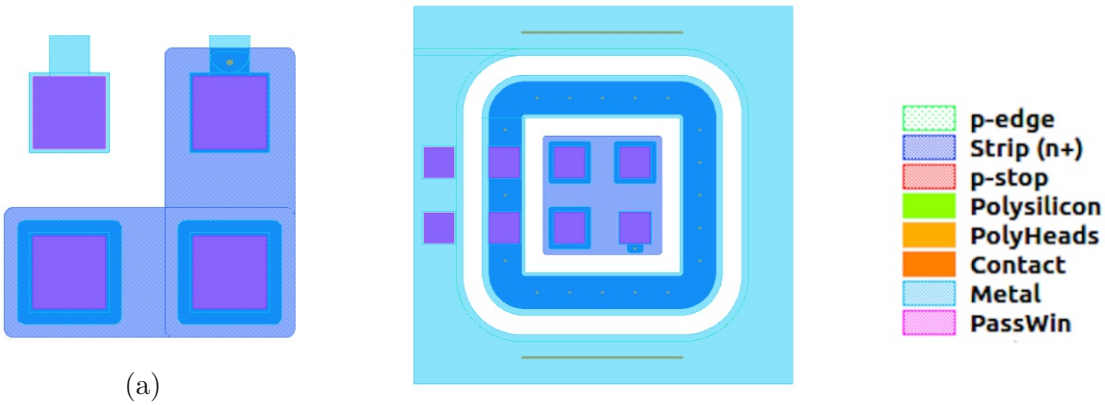

(a) (b)

Figure 4.26: Capacitor teststructure (a) and breakdown structure (b)

4.8.2 Results

The capacitance is generally in the range of 2 pF as expected. Good agreement is found between the left and right structure, however, the right structure always shows a capacitance slightly lower by 100 to 200 fF compared with the left.

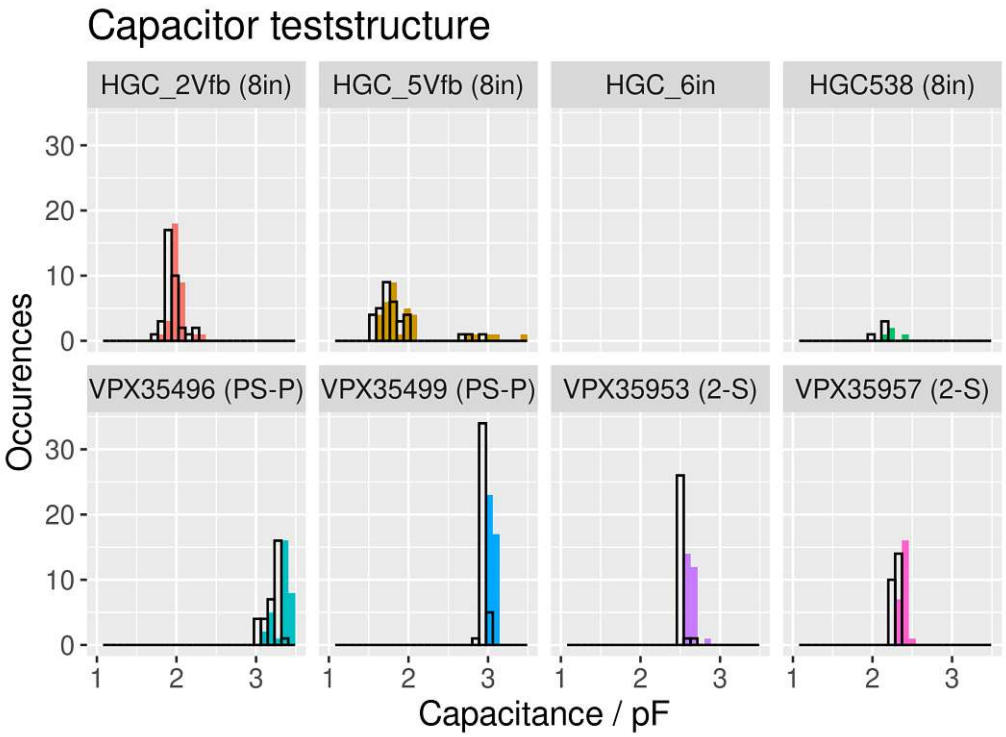

Figure 4.27: Histograms for the capacitor teststructure. The results of the left capacitor is plotted in colored bars, from the right capacitor in empty, black bars

4.9 Dielectric breakdown structure

The dielectric breakdown voltage of the thin oxide is also an important quality parameter of the production. It is important for the high voltage stability, as it separates the readout electronics from the high voltage bias.

It consists of similar capacitors as the capacitor test structure, but with a guard and edge ring for better separation from the other teststructures. The layout is shown in figure 4.26b.

To test the breakdown, a voltage ramp is applied to the capacitor. The SMU is set to a specific current compliance. When the current exceeds this value, the capacitor is considered as broken down. As the current compliance used is only 100 nA, this usually does not irreversibly destroy the structure. When a voltage of 200 V is reached, the measurement is aborted, as this is far beyond the specified minimum of 150 V. In this case, the breakdown voltage is treated as 200 V in the histograms.

As can be seen in figure 4.28, most structures reached 200 V. This means that the structure did not break down during the measurement. The two PSp batches break down earlier than the 2-S batch, however they still meet the specifications. As the PSp is a DC process, the thin oxide is not required as a dielectric.

An error was spotted in the configuration file of this test. Therefore, some of the measurements were unusable. Therefore, the number of tests is lower for this structure compared to the others.

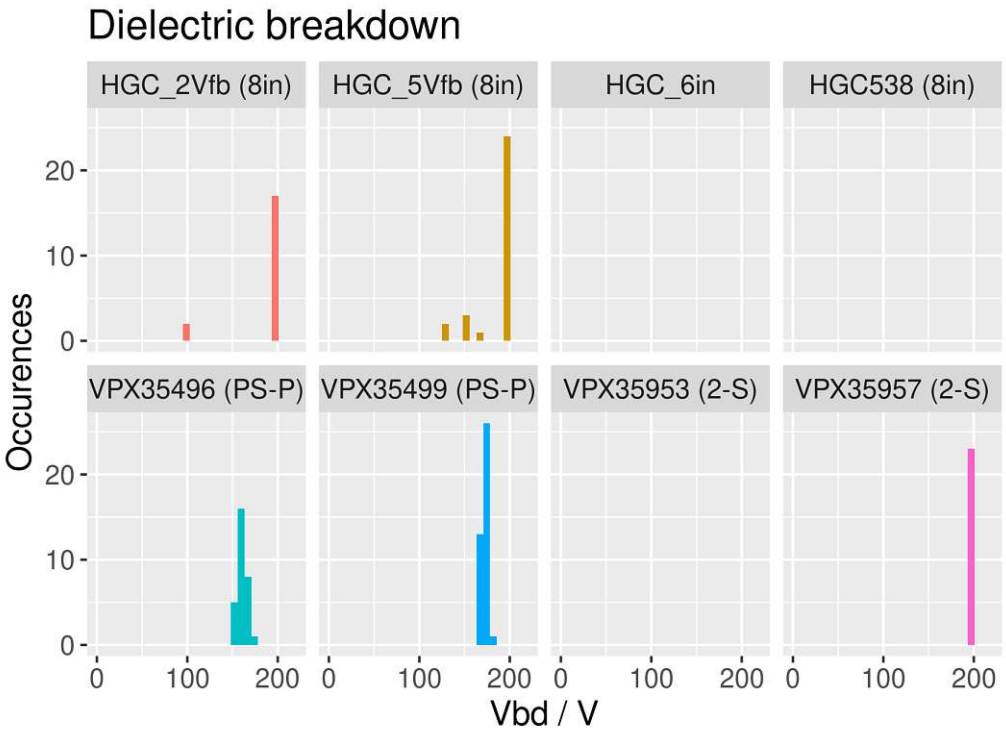

Figure 4.28: Histograms for breakdown measurement results

4.10 Contact chains

4.10.1 Theory and procedure

Contact chains are series of serially connected stubs of alternating material. Between each stub, a contact forms. This allows to measure the average contact resistance more easily as the total resistance is a multiple of a single contact. On the other hand, a single failing contact increases the resistance dramatically. Therefore, this structure is well suited for reliability analysis of the contact creation. There exist three different contact chain teststructures. For every type, one material is the metal layer. The second material for the three structures are polysilicon, p-edge and n-implant. A few chains of the layout are shown in figure 4.29a.

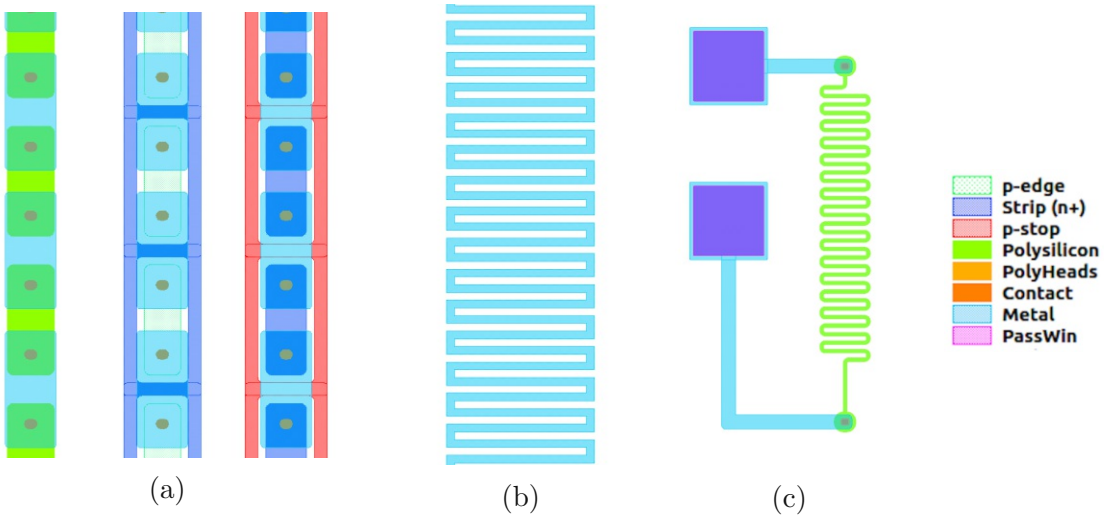

Figure 4.29: Selection of contact chains (a), selection of metal meander (c) and polysilicon meander (b)

4.10.2 Results

The results for the tracker contact chains show very uniform distributions around the same values. However, most of the the HGCal structures show a very high value with slightly nonlinear IV characteristic. Never the less it seems improbable to be caused by bad contacts as the values are also closely distributed. At a bad-contact rate of this magnitude, 2 or 3 bad contacts can also happen and would lead to an even higher resistance. Therefore another cause for this phenomenon is expected, but further investigation is required.

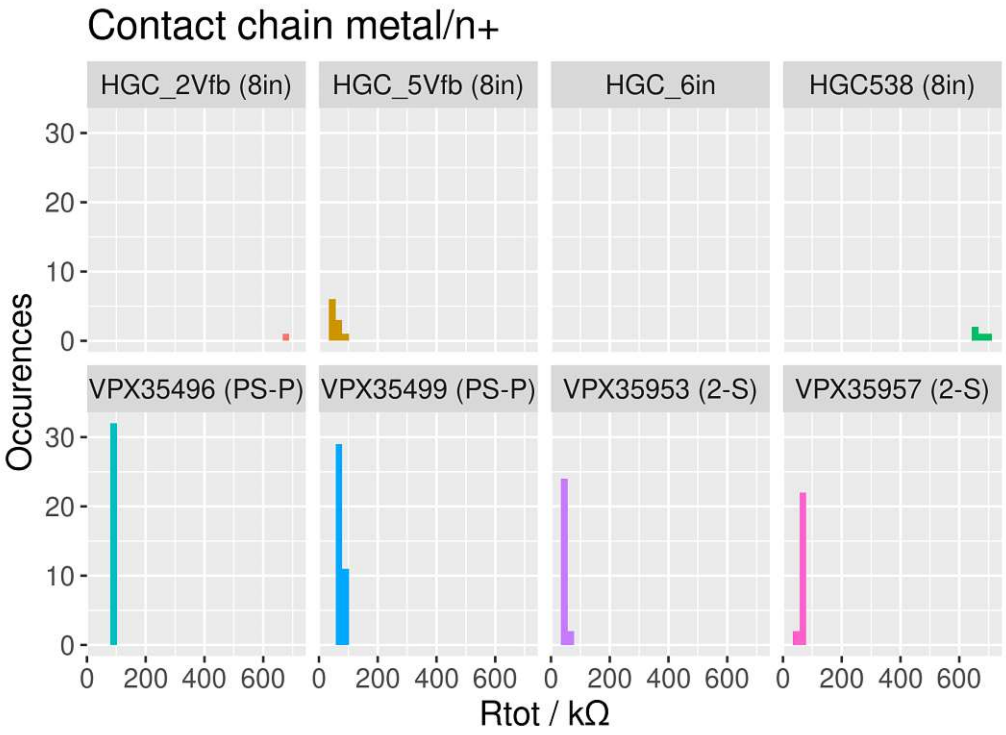

Figure 4.30: Histograms for n+ contact chain results

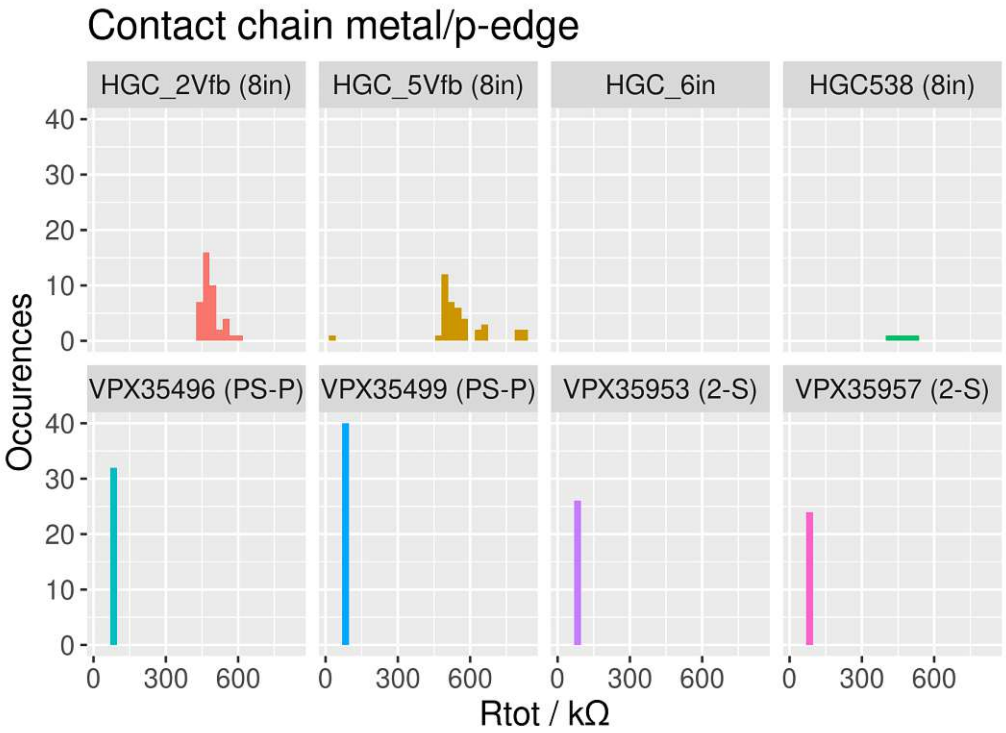

Figure 4.31: Histograms for p-edge contact chain results

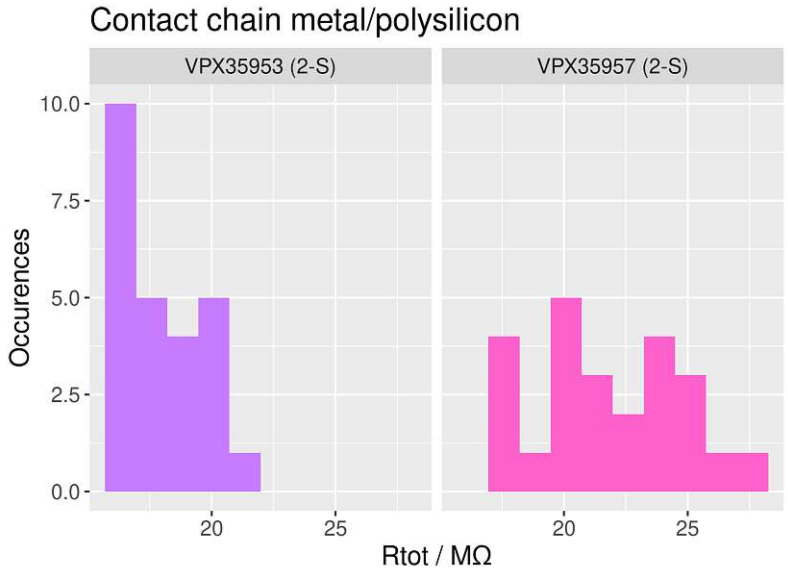

Figure 4.32: Histograms for polysilicon contact chain results

4.11 Meander teststructures

4.11.1 Theory and procedure

An alternative to the VdP structures are meanders. These structures consist of a thin strip of desired material, that is routed in meanders for a more compact format. This structure also allows to measure sheet resistance, however it is also dependent on the width of the line itself. Two different materials are used for the meanders, metal and polysilicon. The layouts are shown in figure 4.29b and 4.29c.

For the metal meander, the very long and thin line increases the absolute resistance of the structure. This makes the measurement easier as less current is required compared to the metal VdP structure.

For the polysilicon meander (or polysilicon resistor), the layout dimensions are exactly the same as used for the bias resistor of the tracker. Therefore it allows to directly access the resistance expected on those sensors.

4.11.2 Results

For the polysilicon meander, the results are slightly lower than the target value of 1.5 MΩ. The metal meander shows very similar resistances through all structures.

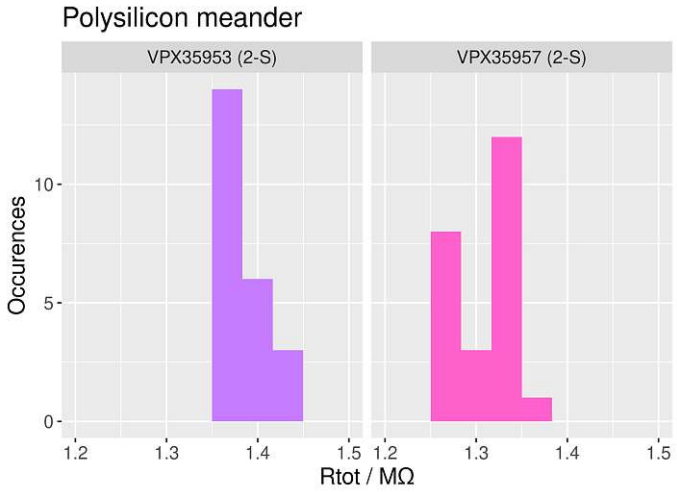

Figure 4.33: Histograms for polysilicon resistor results

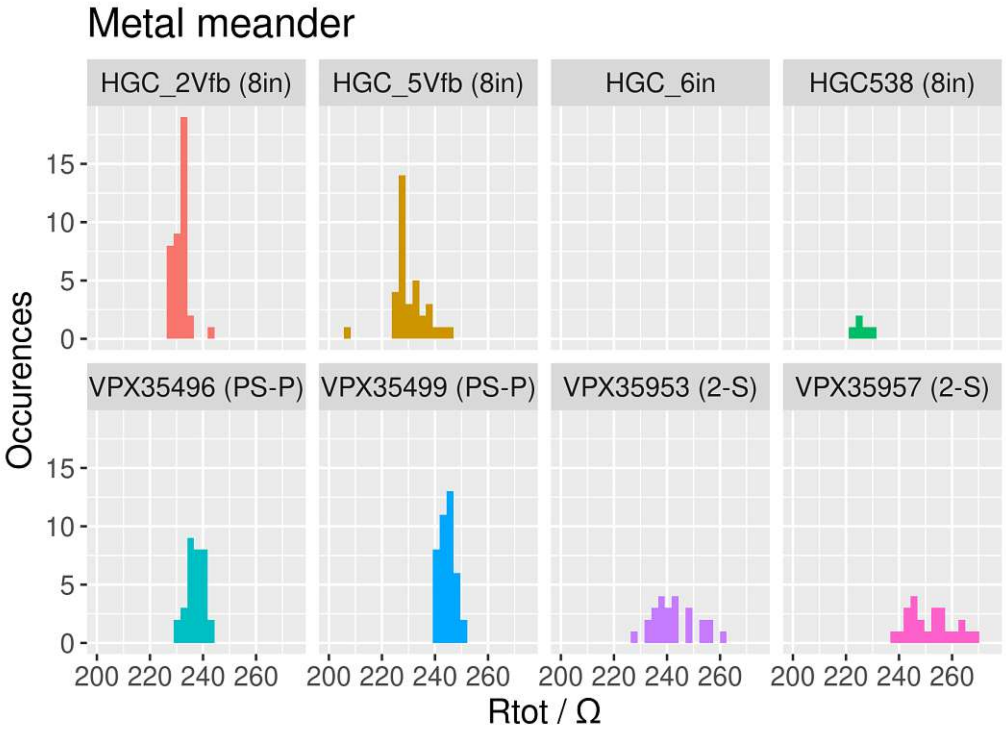

Figure 4.34: Histograms for metal meander results

Chapter 5

Statistical analysis

5.1 GCD and GCD05 comparison

Since the surface generation velocity is, unlike the surface current of a GCD structure, independent from the geometry of the teststructure, the results from GCD and GCD05 can be directly compared. This is shown in figure 5.1, the dotted line represents the identity. As visible, the agreement of the two results is within the statistical fluctuations for low values of s_0. For higher results, a systematic error of around less than 10% is visible with lower results from the GCD05 structure.

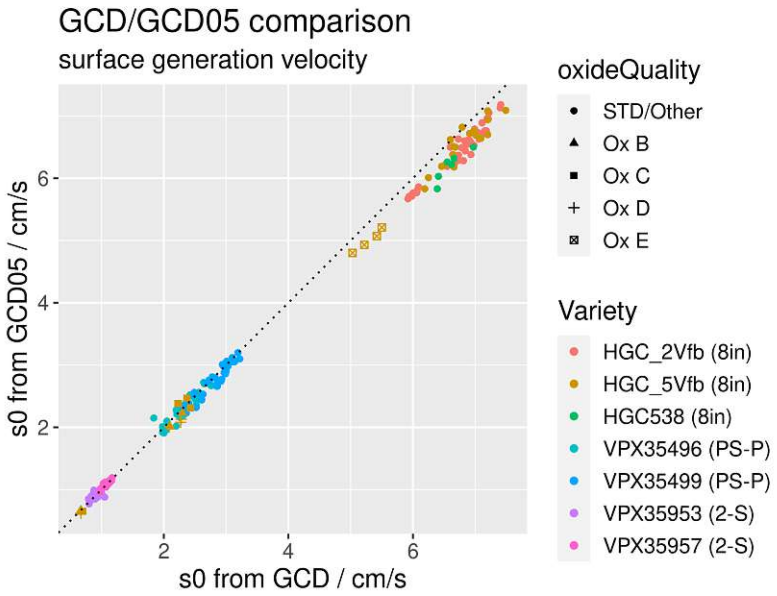

Figure 5.1: Comparison of the surface generation velocities obtained from the GCD and the GCD05 structures

5.2 Contact chains and CBKR comparison

Since contact chains and CBKR structures both measure contact resistance, a comparison of the two results is possible. The number of contacts in the contact chain is 225, the contact area is the same for the two structures.

Figure 5.3 shows correlation plots for the metal/strip and metal/polysilicon contacts. The distribution of the results for the metal/strip contacts is very narrow. No

correlation is visible, so the spreading of the values appears to be measurement noise instead of real variation in contact resistance. For the metal/polysilicon contacts however, a correlation is visible. The slope of the fitting curve is with 217 close to the expected 225 that arises from the number of contacts. The nonzero intercept is also expected. With the CBKR structure, the contact resistance is measured directly. For the contact chains, the contacts are connected via the polysilicon layer. The intercept can be interpreted as the resistance of all polysilicon connection stubs.

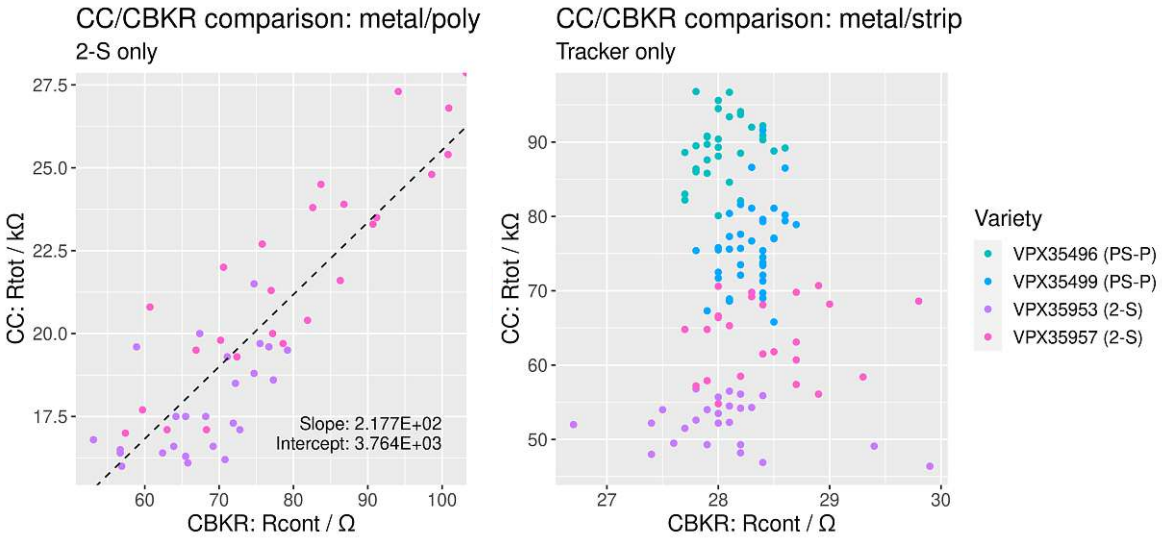

Figure 5.2: Comparison of the results for contact chains and CBKR structures.

5.3 Meander and VdP comparison

The resistance of the meander teststructures should also be proportional to the corresponding sheet resistances. Correlation plots are shown in figure 5.3 for the polysilicon and the metal layer. The metal layer shows no visible correlation, and the distribution is very narrow. Most of the spreading appears to be measurement error. For the polysilicon, a correlation is visible, however, there is also a lot of noise.

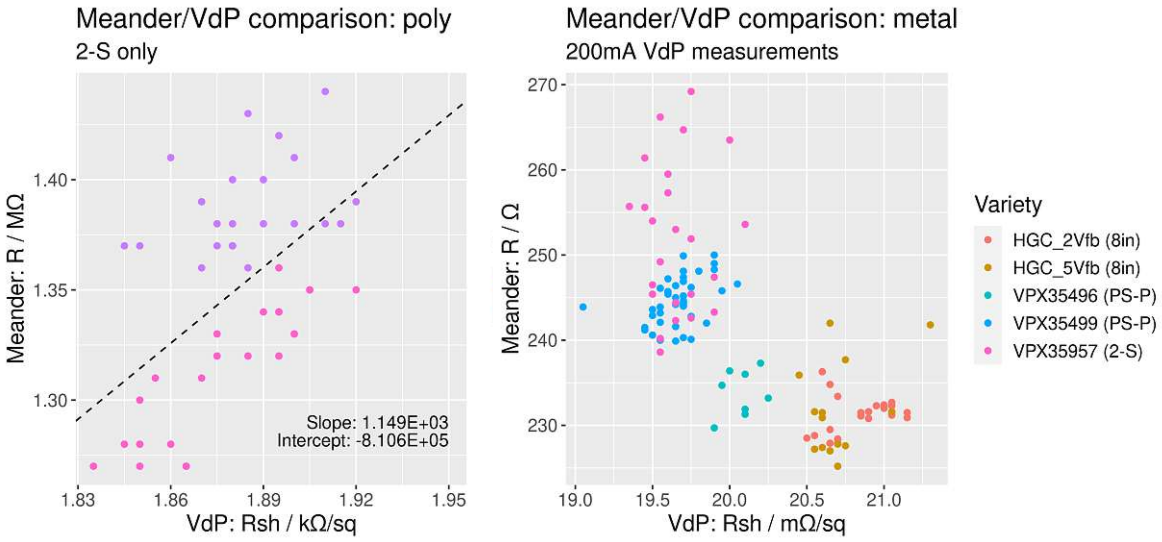

Figure 5.3: Comparison of the results for meander and VdP structures.

5.4 Tracker

5.4.1 p-stop inhomogeneity

For one of the batches *(VPX35953)*, an inhomogeneity in the p-stop concentration has been observed on some wafers. This means, that the results at the four different positions differ by around 10 to 30%. The histograms in figure 5.4 show the p-stop VdP and FET for the two 2-S batches for comparison. The four subplots correspond to the physical positions on the wafer.

The x-axis is normalized to the median of the results for all four positions of this particular batch, the deviation from it is given in percent.

In the first plot, the top row (WR and EL) shows a narrow distribution around the median, which is the expected behavior. However, for the bottom row (WL and ER), a broad spread of values can be observed, that is asymmetrically placed on the higher resistivity side. For the FET, a similar plot is shown, but mirrored along the y-axis because of the negative correlation between p-stop resistivity and threshold voltage of the FET.

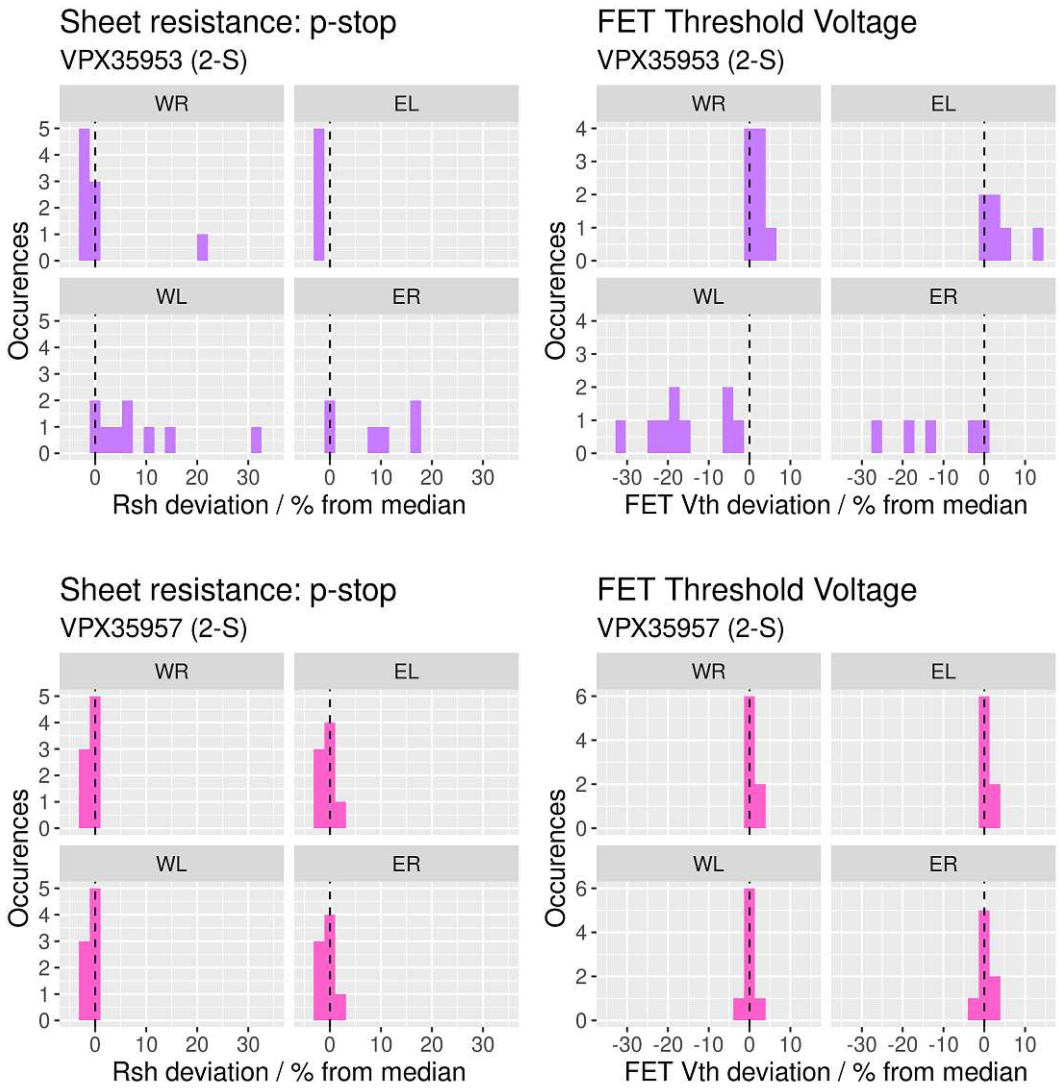

Figure 5.4: Comparison of the two 2-S batches, position resolved

5.5 HGCal process splits

As the HGCal silicon sensors are still in a prototyping phase, there are many different process splits available. These have to be evaluated to determine which is best suited for the production.

Generally, the HGCal has two kinds of sensors: low density (LD) and high density (HD). The HD sensors have an active thickness of 120 µm that are grown via chemical vapor deposition on a handling wafer for mechanical stability. The LD wafers are produced in two different thicknesses: 200 µm and 300 µm. All three are needed at different locations in the HGCal dependent on the expected radiation level.

The other process splits are used for evaluation of the final design, table 5.1 shows an overview of the available structures. All wafers come in two different p-stop layouts: common and individual. The PQC structures do not differ between those types, so the increased number of samples only is beneficial for the statistics. Furthermore there exist a *HGC 5Vfb* and a *HGC 2Vfb* process. These labels represent the nominal flatband voltage of the structures. Additional variations include

different p-stop concentrations (nominal) and different oxide qualities.

Split	Variety	120 µm		200 µm		300 µm	
		ind	com	ind	com	ind	com
Standard (STD)	5Vfb	2	2	2	2	2	2
Standard (STD)	2Vfb	10	10	3	5	3	4
New type C	HGC538			2	2	1	1
Oxide quality A-E	5Vfb			5	5	5	5
p-stop conc. 2.5 STD and 5 STD	5Vfb			2	2	2	2
p-stop conc. 0.5 STD	2Vfb	3	3				

Table 5.1: number of samples for the HGC process splits of the 8 inch wafer prototypes

In the following section, the different process splits are investigated more thoroughly, each type of split at a time.

5.5.1 Oxide qualities

There are different process variants regarding the silicon oxide growth available from the manufacturer. Not much information about the differences is disclosed, the different variants are identified via capital letters from A to E. The relevant measurement results are shown in figure 5.5.

As visible in the first plot, the flatband voltages of the *HGC 2Vfb* and *HGC538 (New type C)* are very narrowly distributed around 2.5 V. The *HGC 5Vfb* variants show a flatband voltage between 5 and 6 V, regardless of the oxide quality type. Only for the oxide quality A, no reliable measurement was possible and a value of over 8 V is suspected.

For the oxide thickness, types B to D are very similar around 730 nm, only the type E is thinner with 680 nm. Also the new type C is slightly lower compared to the initial type C. The standard oxide quality has a stronger variation in oxide thickness.

For the FET threshold voltage, the value for the *HGC538 (New type C)* is about in the middle between the *HGC 2Vfb* and *HGC 5Vfb* (similar across oxide qualities).

The results of the surface generation velocity show an interesting pattern. For the oxide qualities B, C and D, the resulting value is lower for one (C, D) or two (B) of the available 4 wafers. The 4 wafers included 200 µm and 300 µm crossed with individual and common p-stop layout. But for each of those 4 categories, one of those outliers exists. This suggests that the manufacturer also experimented with the processes. The results specific to this observation are shown in table 5.2.

Notably is the higher s_0 for the *HGC538 (New type C)*, comparable to the *HGC 2Vfb* and *HGC 5Vfb* STD results.

Type	s0 from GCD in cm/s				s0 from GCD05 in cm/s			
	200 µm		300 µm		200 µm		300 µm	
	ind	com	ind	com	ind	com	ind	com
Oxide B	2.10	0.67	2.30	0.65	2.01	0.67	2.23	0.64
Oxide C	2.23	2.43	0.70	2.37	2.38	2.31	0.65	2.47
Oxide D	0.67	2.27	2.09	2.28	0.62	2.08	2.01	2.13

Table 5.2: Results for s0 from GCD and GCD05 for HGC Oxide qualities B, C and D. Cells with lower value are colored gray.

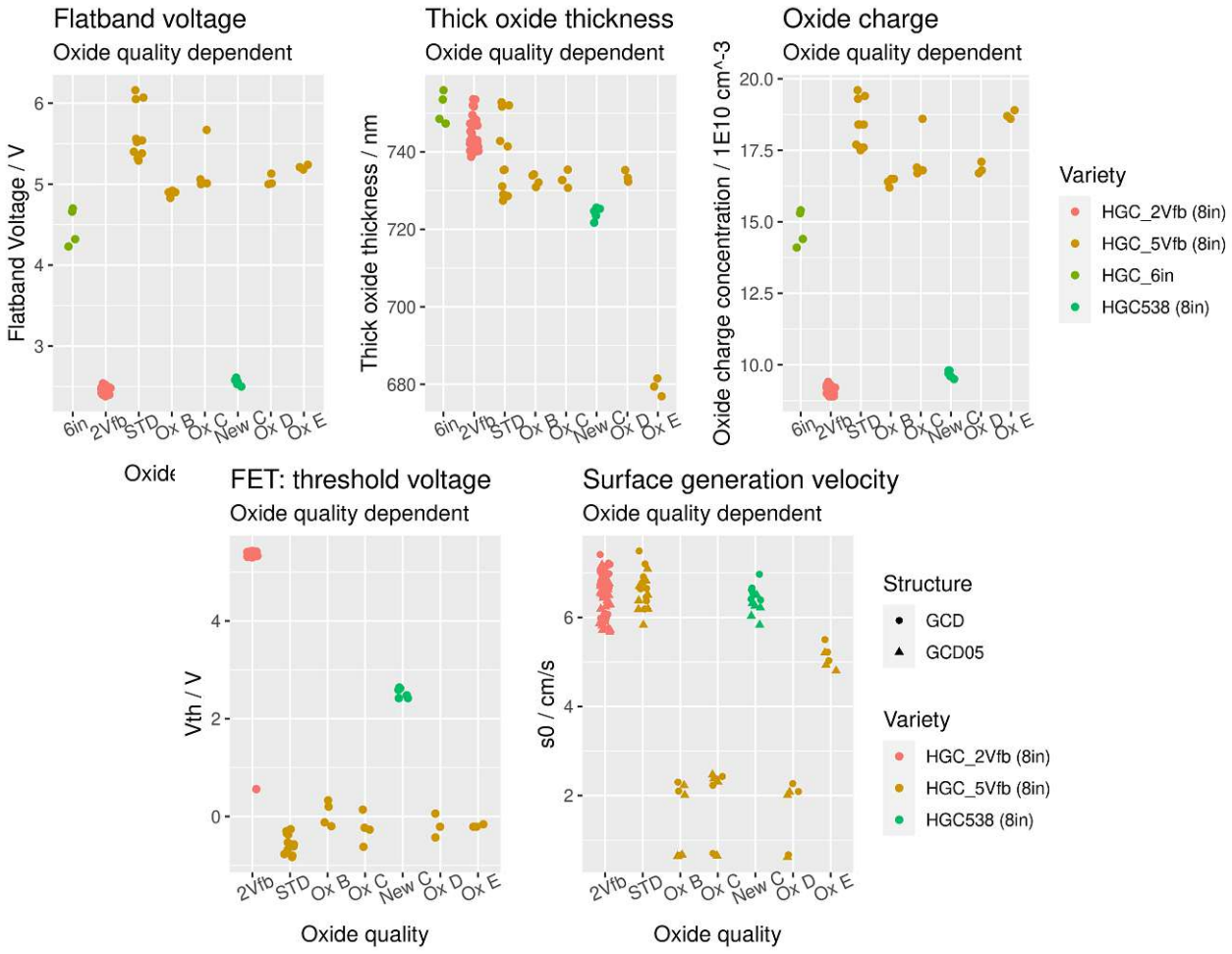

Figure 5.5: Results for HGCal structures (standard p-stop concentration only), separated by oxide qualities. A small jitter was added in x-direction to allow better distinction of the individual datapoints.

Swapped samples

For the plots, two pairs of samples were suspicious. This was on one hand the structures 2006/2007 (STD5/OxA, 200 µm) and 3004/3005 (5Vfb/2Vfb STD0.5, 120 µm). According to all PQC parameters that vary between those process splits, those two pairs have been swapped. Therefore, it was assumed that an error happened during labeling and the according data-points were altered in the graphs. For the 2006/2007 samples, this has been observed on other teststructures already at [21], suggesting a confusion in an early stage of packaging or even at the manufacturer.

5.5.2 p-stop concentration

Process splits with different nominal p-stop concentrations were manufactured. For the *HGC 2Vfb* variety, samples with half of the standard concentration were available. For the *HGC 5Vfb* variety, multiples of 2.5 and 5 of the standard concentration were manufactured.

Summarized results are shown in table 5.3. As clearly visible from the sheet resistance, different standard (STD) p-stop concentrations are used for the two types of flatband voltage. The factor relative to the standard concentration is shown as inverse relative sheet resistance in respect to the standard types. This shows that the *STDx0.5 HGC 2Vfb* type has a similar p-stop concentration compared to the *HGC 5Vfb* types. Also, the factors for the different *HGC 5Vfb* types are close to the target values.

In the XY plot of figure 5.6, the anti-correlation inside one variety family is clearly visible. As the FET is not only influenced by the p-stop concentration, but also from the oxide charge, the results are shifted in between the varieties.

Variety	nominal p-stop conc.	p-stop VdP R_{sh} kΩ/sq	p-stop VdP inverse rel. to STD 5Vfb	p-stop VdP inverse rel. to STD 2Vfb	FET Vth V
HGC 5Vfb (8in)	STD	27.55	1.00	0.61	-0.27
HGC 5Vfb (8in)	x2.5	10.25	2.69	1.63	4.26
HGC 5Vfb (8in)	x5	5.25	5.25	3.19	6.94
HGC 2Vfb (8in)	STD	16.75	1.64	1.00	5.38
HGC 2Vfb (8in)	x0.5	26.25	1.05	0.64	3.57

Table 5.3: Median values in groups of p-stop concentration. For the sheet resistance, the inverse relative deviation in respect to the two STD types is also shown.

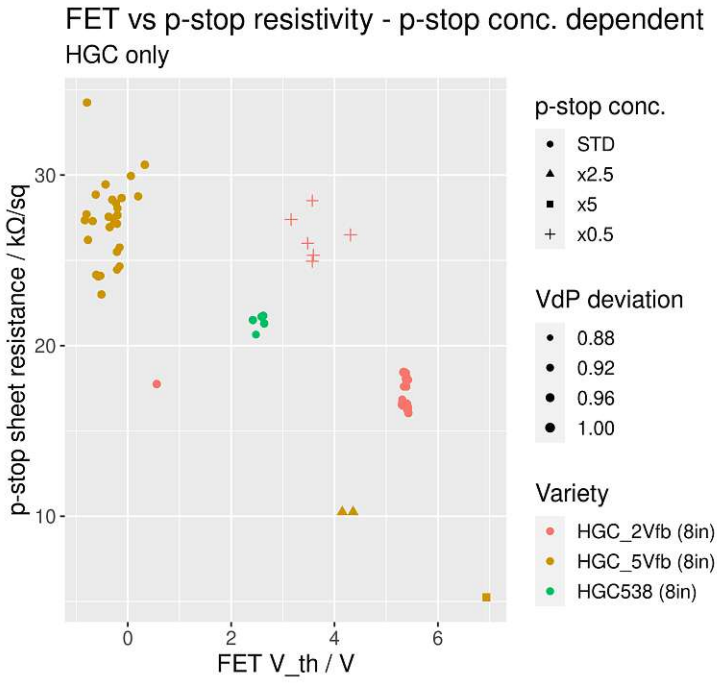

Figure 5.6: FET Vth versus p-stop sheet resistance for HGCal structures (standard oxide quality only), separated by nominal p-stop concentration.

Chapter 6

Conclusion

Since the start of LHC operation in 2009, steady improvements increased luminosity up to a level higher than initially designed. The detector systems degrade under the high radiation environment of the LHC, making a full replacement of the CMS tracker necessary at the next long shutdown (LS3: CMS phase-2 upgrade). The upgrade is also necessary for the even further increased luminosity due to the High Luminosity LHC (HL-LHC) installation scheduled for LS3.

Additionally, a more radiation tolerant, higher resolution endcap calorimeter design has been presented, the HGCal. It consists of mixed semiconductor and scintillation detectors, allowing jet separation necessary for the high number of pile-up events expected from HL-LHC.

For silicon sensor production, a high throughput, multi-value, non-destructive electrical characterization tool has been developed, the Process Quality Control (PQC). For this system, special teststructures are placed on the wafers and a dedicated measurement setup is used for characterization. Both projects, the tracker as well as the HGCal collaboration implemented the PQC teststructures, which also allows direct comparison between the two.

The teststructures and core of the setup had been developed already, however the exact measurement procedures, fine-tuning of the setup and general workflow development had not been carried out. This thesis summarizes the first PQC data taken on the first tracker production wafers, as well as on prototypes of HGCal wafers. Additionally, the problems arising from first production measurements have been solved, and the exact operating procedures for optimal results have been developed and established.

6.1 PQC Setup

The SMU used as V-Src of type Keithley 2657 showed too low accuracy in the millivolt range. It has been replaced by a Keithley 2410. This significantly improved the accuracy for the VdP measurements. For satisfactory results of the metal VdP, the current had to be increased to 200 mA after the SMU exchange.

A batch-wise analysis tool with automatic reliability check has been developed in python to process the high number of measurements performed with the PQC. As an output of this program, tables in multiple formats (plain text, HTML, LaTeX) and histograms of the results can be created. Additionally, one graph for every measurement containing the raw data is created for diagnostic purposes. Furthermore, the measurement quality of each individual measurement is determined to detect

failed measurements early. Previously, each measurement had to be checked individually by hand. Now, unexpected measurement results trigger re-measurements automatically. If the behavior of this particular structure persists, it is marked and further investigations can be initiated. This greatly reduces the required work for analysis, as the majority of the structures behave as expected.

6.2 Tracker

Generally, the tracker process is very stable. However, some batches show an instability on the p-stop layer. This results in wafers with a variation in sheet resistance of up to 30% on the wafer itself depending on location. The SQC has reported, that sensors from such batches indeed show degraded performance in the strip isolation. The problem has been communicated to the manufacturer and appears to be solved now. Similar inhomogeneities have been found on the p-edge implant, but on a much smaller scale of only 3% deviation. This is only visible as the measurement works very reliable and this value is extremely uniform for the other batches.

Slight variations in the resistivity of the polysilicon layer are found as expected. This allows correlation between the results for the meander-teststructure and the VdP structure that both depend on the polysilicon resistance. Additionally, the contact chain and CBKR-structure results for the polysilicon/metal contacts have been correlated successfully and show the expected behavior.

On the other hand, the results for the metal meander and the metal VdP show no correlation, however, the distribution is very uniform. This means that the variation between resistivity is smaller than the achievable measurement accuracy. The same is true for the n+/metal contacts, which have been measured using contact chains and CBKR-structures.

The two GCD structures on the main flute with different dimensions have been correlated successfully, and the agreement for the surface generation velocity is good.

It has been discovered that the flatband voltage is different for the AC and DC coupled sensors. The DC coupled PSp sensors have a flatband voltage around 4 V compared to the AC coupled sensors (2-S and PSs) with 2.5 V.

6.3 HGCal

The extensive survey across the HGCal prototypes show the convergence of the HGCal- towards the tracker process. The progress is particularly visible for the ”new type C” structures from the latest iteration. The results are very similar to the tracker strip sensors in most of the measured parameters.

The only difference is the different surface generation velocity. The upcoming variant scheduled for fall 2021 introduces a ”new type D” as a mixture of ”new type C” and ”type B” that addresses that difference.

Furthermore, two diodes are connected to the 4 PQC main flutes. However, the results from those structures are not fully usable yet. The leakage current is very high which causes problems during measurements. Most probably this is due to an opening in the p-edge implant where the metal wires cross to connect the teststructure with the contact pads. This has been reworked for the next HGCal prototypes scheduled for fall 2021.

After this second round of prototypes, the pre-series production is scheduled for winter 2021/22 followed by pre-production in 2022.

6.4 Final words

The PQC proved to be a very versatile tool in semiconductor characterization. On one hand, it is essential to control and monitor the quality of silicon device production. On the other hand, it is helpful for prototyping and validating performance of the prototypes.

During the next three years, the PQC setup will be heavily used for the production batch validation and for the upcoming prototypes of HGCal. The versatility and performance of the setup even inspired HEPHY to build another setup for general use similar to the PQC setup.

Bibliography

[1] LHC Guide Brochure. *https://cds.cern.ch/record/2255762/files/CERN-Brochure-2017-002-Eng.pdf.*

[2] HL-LHC project website. *https://project-hl-lhc-industry.web.cern.ch/content/project-schedule.*

[3] HL-LHC Project Schedule Plan. *https://hilumilhc.web.cern.ch/sites/hilumilhc.web.cern.ch/files/images/HL-LHC-plan-2021-1.pdf.*

[4] CMS collaboration public webpage. *http://cms.web.cern.ch/.*

[5] The Phase-2 Upgrade of the CMS Tracker. Technical report, CERN-LHCC-2017-009, CMS-TDR-014, Jun 2017.

[6] The Phase-2 Upgrade of the CMS Endcap Calorimeter. Technical report, CERN-LHCC-2017-023, CMS-TDR-019, Nov 2017.

[7] E. Pree. *Development of Large Area Silicon Sensors for the High Granularity Calorimeter at CMS.* September 09, 2018, Dissertation.

[8] R. Sauer. *Halbleiterphysik: Lehrbuch für Physiker und Ingenieure.* Oldenbourg, 2009.

[9] H. Theurer. *Method of processing semiconductive materials.* Patent, US 3,060,123, 1962.

[10] S. Sze. *SEMICONDUCTOR DEVICES, Physics and Technology.* John Wiley and Sons, Inc., 2002.

[11] A. Peisert. Silicon microstrip detectors. *DELPHI 92-143 MVX 2, CERN, 1992.*

[12] V. Hinger. *Silicon Sensor Process Quality Control for the CMS Phase-2 Upgrade.* 05.02.2021, Dissertation.

[13] PQC Specification Document: Version 1.6, June 15, 2021.

[14] S. M. Sze and K. K. Ng. *Physics of Semiconductor Devices, 3rd ed.* John Wiley and Sons, Inc., 2007.

[15] K. Misiakos and D. Tsamakis. *Accurate measurements of the silicon intrinsic carrier density from 78 to 340 K.* Journal of Applied Physics 74.5 (1993), pp. 3293–3297.

[16] U. Tieze, C. Schenk, E. Gamm. *Halbleiter-Schaltungstechnik.* Springer Verlag, 2000.

[17] A. Robert. *Van der pauw structure to measure the resistivity of a doped area under diffusion areas and gate structures.* Patent, US 6,144,040, 2000.

[18] E. Hesse. *Meßverfahren zur Bestimmung des spezifischen Widerstands dünner Schichten.* Patent, DE 27 26 982, 1977.

[19] L. van der Pauw. *A METHOD OF MEASURING SPECIFIC RESISTIVITY AND HALL EFFECT OF DISCS OF ARBITRARY SHAPE.* Philips Res. Repts 13, 1958.

[20] D. Schroder. *Semiconductor Material and Device Characterisazion.* John Wiley and Sons, Inc., 2005.

[21] M. Babeluk. *Interstrip properties of HGCal Ministrip teststructures.* December 12, 2020, Projektarbeit.

Appendix A

Full result tables

A.1 HGC 5Vfb and 2Vfb

Flute 1

	FET	MOS Quarter				Polysilicon VdP		n+ VdP		p-stop VdP		Capacitor	
	fet	v_fb	c_acc	t_ox	n_ox	vdp-Poly	vdp-Poly_r	vdpN	vdpN_r	vdpP-stp	vdpP-stp_r	cap_l	cap_r
	V	V	pF	nm	1E10cm^-2	kOhm/sq	kOhm/sq	Ohm/sq	Ohm/sq	kOhm/sq	kOhm/sq	pF	pF
HPK_HGC1003_300um_ind_2Vfb	5.38	2.48	77.5	741.3	9.2	—	—	38.3	38.2	18.5	18.3	0.56	0.46
HPK_HGC1004_300um_ind_5Vfb	-0.68	5.54	78.8	729.0	18.4	—	—	39.2	39.1	27.4	27.2	2.03	1.93
HPK_HGC1005_300um_ind_5Vfb_STD2_5	4.36	5.44	78.2	734.2	18.0	—	—	39.4	39.0	10.3	10.2	2.05	1.94
HPK_HGC1006_300um_ind_5Vfb_STD5	6.94	5.48	78.7	730.2	18.2	—	—	39.2	39.2	5.2	5.3	0.68	1.94
HPK_HGC1007_300um_ind_5Vfb_OxA	-0.79	-1.38	32.0	1797.3	-0.8	—	—	39.9	40.0	34.2	34.3	1.96	1.85
HPK_HGC1008_300um_ind_5Vfb_OxB	-0.12	4.90	78.3	733.9	16.4	—	—	38.0	38.1	28.7	28.6	1.85	1.75
HPK_HGC1009_300um_ind_5Vfb_OxC	0.14	5.01	78.6	730.7	16.8	—	—	36.6	36.8	failed	32.2	1.76	1.66
HPK_HGC1010_300um_ind_5Vfb_OxD	-0.43	5.13	78.3	733.3	17.1	—	—	38.4	38.1	29.4	29.5	1.63	1.79
HPK_HGC1011_300um_ind_5Vfb_OxE	-0.16	5.18	84.3	681.5	18.6	—	—	38.7	38.6	25.9	25.6	3.00	2.91
HPK_HGC1012_300um_ind_2Vfb	5.42	2.41	77.4	741.8	9.0	—	—	38.2	38.2	18.1	17.9	0.22	0.21
HPK_HGC1013_300um_ind_2Vfb	5.39	2.38	77.5	741.3	8.9	—	—	38.2	38.4	18.6	17.9	2.05	1.97
HPK_HGC1014_300um_ind_5Vfb_MCZ	-0.37	5.32	78.1	735.3	17.6	—	—	39.1	39.0	27.5	27.6	0.22	0.20
HPK_HGC1101_300um_com_5Vfb	-0.30	5.40	77.3	742.8	17.7	—	—	39.0	39.1	28.5	28.6	1.78	1.69
HPK_HGC1102_300um_com_2Vfb	5.33	2.54	77.3	742.8	9.4	—	—	38.4	38.4	18.5	18.4	2.00	1.90
HPK_HGC1103_300um_com_2Vfb	5.33	2.52	77.3	742.8	9.3	—	—	38.2	38.6	18.0	18.8	1.95	1.87
HPK_HGC1104_300um_com_2Vfb	5.35	2.44	77.4	742.5	9.1	—	—	38.2	38.4	18.5	18.4	2.02	1.92
HPK_HGC1105_300um_com_5Vfb	-0.80	5.54	78.8	728.6	18.4	—	—	39.1	39.2	27.8	27.6	1.84	1.75
HPK_HGC1106_300um_com_5Vfb_STD2_5	4.15	5.57	78.8	729.1	18.5	—	—	39.4	39.1	10.3	10.2	1.94	1.82
HPK_HGC1107_300um_com_5Vfb_STD5	failed	5.52	78.7	729.9	18.3	—	—	39.3	39.2	failed	failed	1.90	1.78
HPK_HGC1108_300um_com_5Vfb_OxA	failed	-1.39	28.1	2041.9	-0.7	—	—	39.8	40.0	33.5	33.8	1.67	1.58
HPK_HGC1109_300um_com_5Vfb_OxB	0.33	4.83	78.2	734.2	16.2	—	—	36.5	36.2	30.6	30.6	1.69	1.58
HPK_HGC1110_300um_com_5Vfb_OxC	-0.23	5.06	78.4	732.7	16.9	—	—	38.1	38.1	28.1	28.6	1.81	1.81
HPK_HGC1111_300um_com_5Vfb_OxD	-0.20	failed	78.3	failed	failed	—	—	38.0	38.0	28.3	27.8	1.80	1.72
HPK_HGC1112_300um_com_5Vfb_OxE	-0.21	5.21	84.5	679.4	18.7	—	—	38.7	38.7	25.4	25.6	2.78	2.71
HPK_HGC1113_300um_com_2Vfb	5.38	2.40	77.3	743.0	8.9	—	—	38.4	38.4	18.6	18.1	2.06	1.98
HPK_HGC2003_200um_ind_2Vfb	5.39	2.43	77.7	739.4	9.1	—	—	38.3	38.2	17.7	17.5	2.22	2.24
HPK_HGC2004_200um_ind_5Vfb	-0.77	5.56	78.6	731.1	18.4	—	—	39.1	39.0	26.1	26.3	1.99	1.89
HPK_HGC2005_200um_ind_5Vfb_STD2_5	4.37	5.42	78.4	732.4	18.0	—	—	39.3	39.1	failed	10.1	2.04	1.96
HPK_HGC2006_200um_ind_5Vfb_STD5	failed	5.41	78.5	731.6	18.0	—	—	39.2	39.3	5.2	5.3	2.08	1.97
HPK_HGC2007_200um_ind_5Vfb_OxA	-6.49	-1.10	26.4	2173.2	-0.4	—	—	39.9	39.8	33.0	33.3	1.94	1.86
HPK_HGC2008_200um_ind_5Vfb_OxB	-0.20	4.92	78.6	730.9	16.5	—	—	38.0	38.1	27.7	27.6	0.22	0.20
HPK_HGC2009_200um_ind_5Vfb_OxC	-0.62	5.67	78.1	735.4	18.6	—	—	47.9	38.3	28.7	29.0	0.59	1.73
HPK_HGC2010_200um_ind_5Vfb_OxD	0.06	5.01	78.4	732.3	16.8	—	—	36.8	36.6	30.1	29.8	0.22	0.20
HPK_HGC2011_200um_ind_5Vfb_OxE	-0.21	5.24	84.8	676.9	18.9	—	—	38.9	38.5	24.7	24.2	3.12	0.44
HPK_HGC2012_200um_ind_2Vfb	5.38	2.40	77.8	738.7	9.0	—	—	38.1	38.4	18.0	18.1	0.22	0.20
HPK_HGC2013_200um_ind_2Vfb	5.41	2.39	77.6	740.0	9.0	—	—	38.3	38.4	17.0	19.9	0.47	0.40
HPK_HGC2014_200um_ind_5Vfb_MCZ	-0.35	5.29	78.1	735.4	17.5	—	—	42.0	39.2	26.9	27.0	0.21	0.19
HPK_HGC2101_200um_com_5Vfb	-0.26	5.38	77.5	741.4	17.6	—	—	38.9	39.3	27.2	27.3	1.80	1.72
HPK_HGC2102_200um_com_2Vfb	0.56	2.46	77.6	740.1	9.2	—	—	37.9	38.5	17.7	17.8	2.03	1.94
HPK_HGC2103_200um_com_2Vfb	failed	2.48	77.5	741.2	9.2	—	—	38.4	38.1	17.9	17.4	1.97	1.89
HPK_HGC2104_200um_com_2Vfb	5.34	2.44	77.5	740.8	9.1	—	—	38.2	38.2	17.4	17.8	2.04	1.94
HPK_HGC2105_200um_com_5Vfb	-0.83	5.52	79.0	727.4	18.4	—	—	39.2	39.4	27.4	27.3	1.84	1.75
HPK_HGC2106_200um_ind_5Vfb_STD2_5	4.15	5.52	78.8	729.2	18.4	—	—	39.5	39.3	10.2	10.3	1.85	1.76
HPK_HGC2107_200um_ind_5Vfb_STD5	failed	5.51	78.6	730.4	18.3	—	—	39.2	39.5	5.2	5.4	1.95	1.83
HPK_HGC2108_200um_com_5Vfb_OxA	failed	failed	26.9	failed	failed	—	—	40.0	40.2	32.0	32.8	3.46	- 411.46
HPK_HGC2109_200um_com_5Vfb_OxB	0.20	4.90	78.5	732.1	16.5	—	—	36.7	36.6	28.6	28.9	1.60	1.51
HPK_HGC2110_200um_com_5Vfb_OxC	-0.27	5.00	78.4	732.7	16.7	—	—	38.0	38.0	27.2	27.7	1.69	1.61
HPK_HGC2111_200um_com_5Vfb_OxD	-0.21	5.00	78.1	735.3	16.7	—	—	38.0	37.9	27.2	27.1	1.69	1.62
HPK_HGC2112_200um_com_5Vfb_OxE	-0.16	failed	84.8	failed	failed	—	—	38.6	38.8	24.4	24.9	2.87	2.79
HPK_HGC2113_200um_com_2Vfb	5.38	2.40	77.4	741.9	9.0	—	—	38.5	38.6	17.3	18.5	2.06	1.98
HPK_HGC2114_200um_com_2Vfb	5.38	2.40	77.4	742.3	9.0	—	—	38.4	38.3	18.5	17.6	2.07	1.99
HPK_HGC3001_120um_ind_5Vfb	-0.51	failed	77.5	failed	failed	—	—	39.2	39.3	22.9	23.1	1.74	1.66
HPK_HGC3002_120um_ind_2Vfb_STD0_5	3.16	3.41	76.0	755.6	11.7	—	—	39.4	38.4	27.3	27.5	1.85	1.75
HPK_HGC3003_120um_ind_2Vfb	5.41	2.42	76.4	752.0	8.9	—	—	38.8	37.9	16.5	16.3	1.95	1.86
HPK_HGC3004_120um_ind_5Vfb	-0.61	6.07	76.4	752.0	19.4	—	—	58.4	39.1	24.2	24.1	1.82	1.73
HPK_HGC3005_120um_ind_2Vfb_STD0_5	3.57	2.45	76.5	750.6	9.0	—	—	40.7	38.2	29.0	28.0	0.22	2.12
HPK_HGC3006_120um_ind_2Vfb_STD0_5	4.31	2.54	76.4	752.1	9.3	—	—	38.6	37.9	26.5	26.5	0.22	0.20
HPK_HGC3007_120um_ind_2Vfb	5.42	2.42	76.4	751.7	8.9	—	—	38.4	38.3	19.7	16.6	0.58	2.05
HPK_HGC3008_120um_ind_2Vfb	5.40	2.44	76.2	753.6	9.0	—	—	38.7	38.0	16.6	16.2	1.93	1.85
HPK_HGC3009_120um_ind_2Vfb	5.40	2.42	76.2	753.5	8.9	—	—	38.7	38.1	16.6	16.6	1.92	1.83
HPK_HGC3010_120um_ind_2Vfb	5.41	2.42	77.1	745.3	9.0	—	—	39.9	38.0	16.3	16.2	1.97	1.87
HPK_HGC3011_120um_ind_2Vfb	5.41	2.42	76.9	747.3	9.0	—	—	38.9	38.0	16.4	16.6	2.02	1.94
HPK_HGC3013_120um_ind_2Vfb	5.30	2.48	76.8	747.4	9.1	—	—	38.6	38.2	16.1	16.9	1.96	1.89
HPK_HGC3014_120um_ind_2Vfb	5.31	2.49	76.7	748.6	9.2	—	—	41.0	38.2	16.5	16.9	2.37	2.26
HPK_HGC3015_120um_ind_2Vfb	5.32	2.47	76.8	748.2	9.1	—	—	38.4	38.3	16.6	16.7	failed	2.08
HPK_HGC3016_120um_ind_2Vfb	5.31	2.47	77.4	742.1	9.2	—	—	38.6	38.3	16.6	16.6	2.05	1.96
HPK_HGC3023_120um_ind_2Vfb	5.31	2.49	76.9	746.8	9.2	—	—	40.1	38.2	16.6	17.1	1.97	1.89
HPK_HGC3101_120um_com_5Vfb	-0.53	6.05	76.4	751.7	19.3	—	—	39.4	39.4	23.9	24.3	1.72	1.64
HPK_HGC3102_120um_com_2Vfb_STD0_5	3.57	2.43	76.8	748.1	9.0	—	—	38.5	38.3	24.9	25.0	1.97	1.88
HPK_HGC3103_120um_com_2Vfb	5.42	2.41	76.6	749.5	8.9	—	—	39.0	37.9	16.2	16.2	1.93	1.85
HPK_HGC3104_120um_com_5Vfb	-0.57	6.16	76.3	752.8	19.6	—	—	39.4	39.3	24.2	23.9	1.67	1.57
HPK_HGC3105_120um_com_2Vfb_STD0_5	3.59	2.43	76.7	748.8	9.0	—	—	38.6	38.2	25.4	25.2	1.97	1.87
HPK_HGC3106_120um_com_2Vfb_STD0_5	3.48	2.50	77.1	745.0	9.2	—	—	38.5	38.1	26.2	25.8	1.96	1.87
HPK_HGC3107_120um_com_2Vfb	5.43	2.44	77.4	741.8	9.1	—	—	38.5	38.2	16.0	16.1	1.97	1.87
HPK_HGC3108_120um_com_2Vfb	5.42	2.43	77.3	742.9	9.0	—	—	38.8	38.0	16.5	16.3	1.97	1.87
HPK_HGC3109_120um_com_2Vfb	5.41	2.42	77.2	743.7	9.0	—	—	38.9	37.6	16.3	16.3	1.98	1.89
HPK_HGC3110_120um_com_2Vfb	5.42	2.44	77.2	743.8	9.1	—	—	38.6	37.9	16.4	16.3	2.01	1.92
HPK_HGC3111_120um_com_2Vfb	5.42	2.43	77.1	744.9	9.0	—	—	38.7	38.0	16.3	16.4	1.98	1.90
HPK_HGC3112_120um_com_2Vfb	5.32	2.44	76.9	746.6	9.0	—	—	38.7	38.1	17.1	16.4	1.98	1.90
HPK_HGC3113_120um_com_2Vfb	5.32	2.49	77.6	740.3	9.3	—	—	38.3	38.6	16.5	16.5	2.04	1.95
HPK_HGC3114_120um_com_2Vfb	5.36	2.48	77.6	740.2	9.2	—	—	38.4	38.5	16.4	16.5	2.04	1.94
Median	3.87	2.44	77.5	741.3	9.0	0.00	0.00	38.7	38.3	17.3	17.2	1.97	1.87
Average	3.87	2.45	77.9	738.2	9.1	0.00	0.00	38.8	38.5	18.2	18.0	2.01	1.89
Std dev.	0.42	0.04	1.7	14.2	0.4	0.00	0.00	0.9	0.7	2.6	2.4	0.33	0.24
OK/Tot.	10/81	40/81	77/81	74/81	41/81	1/1	1/1	79/81	81/81	41/81	40/81	67/81	70/81
OK (rel)	0.12	0.49	0.95	0.91	0.51	1.00	1.00	0.98	1.00	0.51	0.49	0.83	0.86

Flute 2

	GCD		Poly-R	Line thickness			break-down
	i_surf	s0	me-and_poly	lw_n	lw_pstp1	lw_pstp2	v_bd
	pA	cm/s	MOhm	um	um	um	V
HPK_HGC1003_300um_ind_2Vfb	40.35	7.11	—	33.8	62.3	1.1	failed
HPK_HGC1004_300um_ind_5Vfb	37.79	6.66	—	35.6	83.1	3.7	200.0
HPK_HGC1005_300um_ind_5Vfb_STD2_5	37.42	6.60	—	35.8	failed	—	failed
HPK_HGC1006_300um_ind_5Vfb_STD5	37.86	6.68	—	35.5	49.7	—	failed
HPK_HGC1007_300um_ind_5Vfb_OxA	failed	failed	—	37.1	94.7	4.2	200.0
HPK_HGC1008_300um_ind_5Vfb_OxB	13.03	2.30	—	35.3	80.3	2.8	200.0
HPK_HGC1009_300um_ind_5Vfb_OxC	3.97	0.70	—	35.6	failed	failed	200.0
HPK_HGC1010_300um_ind_5Vfb_OxD	11.87	2.09	—	35.7	83.4	4.2	200.0
HPK_HGC1011_300um_ind_5Vfb_OxE	28.55	5.03	—	35.5	failed	4.0	failed
HPK_HGC1012_300um_ind_2Vfb	34.37	6.06	—	33.7	58.1	failed	failed
HPK_HGC1013_300um_ind_2Vfb	34.40	6.07	—	34.2	61.6	—	100.0
HPK_HGC1014_300um_ind_5Vfb_MCZ	42.47	7.49	—	35.3	73.0	3.9	200.0
HPK_HGC1101_300um_com_5Vfb	40.82	7.20	—	35.3	74.2	—	failed
HPK_HGC1102_300um_com_2Vfb	42.05	7.41	—	34.3	56.3	—	failed
HPK_HGC1103_300um_com_2Vfb	40.76	7.19	—	33.5	57.9	—	failed
HPK_HGC1104_300um_com_2Vfb	40.93	7.22	—	34.0	57.4	—	200.0
HPK_HGC1105_300um_com_5Vfb	38.52	6.79	—	35.4	88.4	—	200.0
HPK_HGC1106_300um_com_5Vfb_STD2_5	40.84	7.20	—	35.5	62.0	—	200.0
HPK_HGC1107_300um_com_5Vfb_STD5	40.84	7.20	—	35.6	failed	—	200.0
HPK_HGC1108_300um_com_5Vfb_OxA	failed	failed	—	37.1	96.6	—	200.0
HPK_HGC1109_300um_com_5Vfb_OxB	3.69	0.65	—	35.3	79.6	—	200.0
HPK_HGC1110_300um_com_5Vfb_OxC	13.46	2.37	—	35.5	83.6	3.3	200.0
HPK_HGC1111_300um_com_5Vfb_OxD	12.94	2.28	—	35.3	82.8	—	200.0
HPK_HGC1112_300um_com_5Vfb_OxE	31.20	5.50	—	35.5	82.3	—	130.0
HPK_HGC1113_300um_com_2Vfb	34.54	6.09	—	33.9	54.0	—	200.0
HPK_HGC2003_200um_ind_2Vfb	38.19	6.73	—	34.4	62.3	failed	failed
HPK_HGC2004_200um_ind_5Vfb	36.10	6.37	—	35.5	84.1	1.3	200.0
HPK_HGC2005_200um_ind_5Vfb_STD2_5	35.45	6.25	—	35.8	failed	—	200.0
HPK_HGC2006_200um_ind_5Vfb_STD5	36.89	6.51	—	35.5	50.1	0.3	150.0
HPK_HGC2007_200um_ind_5Vfb_OxA	failed	failed	—	37.0	92.4	—	200.0
HPK_HGC2008_200um_ind_5Vfb_OxB	11.93	2.10	—	35.3	78.4	1.4	failed
HPK_HGC2009_200um_ind_5Vfb_OxC	12.67	2.23	—	44.9	81.3	2.5	150.0
HPK_HGC2010_200um_ind_5Vfb_OxD	3.80	0.67	—	35.6	83.4	5.7	failed
HPK_HGC2011_200um_ind_5Vfb_OxE	29.59	5.22	—	35.6	82.1	4.4	failed
HPK_HGC2012_200um_ind_2Vfb	33.67	5.94	—	34.1	58.6	1.6	failed
HPK_HGC2013_200um_ind_2Vfb	33.56	5.92	—	33.8	56.3	2.5	failed
HPK_HGC2014_200um_ind_5Vfb_MCZ	39.20	6.91	—	38.0	79.4	3.7	150.0
HPK_HGC2101_200um_com_5Vfb	35.10	6.19	—	35.2	78.6	—	failed
HPK_HGC2102_200um_com_2Vfb	40.86	7.21	—	33.5	59.1	—	failed
HPK_HGC2103_200um_com_2Vfb	40.32	7.11	—	34.0	57.4	—	failed
HPK_HGC2104_200um_com_2Vfb	39.64	6.99	—	34.3	56.9	—	200.0
HPK_HGC2105_200um_com_5Vfb	failed	failed	—	failed	failed	—	165.0
HPK_HGC2106_200um_ind_5Vfb_STD2_5	39.75	7.01	—	35.7	57.6	—	200.0
HPK_HGC2107_200um_ind_5Vfb_STD5	39.57	6.98	—	35.4	53.5	—	200.0
HPK_HGC2108_200um_com_5Vfb_OxA	failed	failed	—	37.2	88.9	—	200.0
HPK_HGC2109_200um_com_5Vfb_OxB	3.79	0.67	—	35.4	84.4	—	200.0
HPK_HGC2110_200um_com_5Vfb_OxC	13.79	2.43	—	35.4	83.6	—	200.0
HPK_HGC2111_200um_com_5Vfb_OxD	12.89	2.27	—	35.3	86.1	—	200.0
HPK_HGC2112_200um_com_5Vfb_OxE	30.75	5.42	—	35.4	77.4	—	130.0
HPK_HGC2113_200um_com_2Vfb	34.05	6.00	—	33.7	55.4	—	200.0
HPK_HGC2114_200um_com_2Vfb	33.90	5.98	—	34.0	61.8	—	200.0
HPK_HGC3001_120um_ind_5Vfb	40.23	7.09	—	35.4	73.8	—	failed
HPK_HGC3002_120um_ind_2Vfb_STD0_5	40.06	7.06	—	34.6	77.8	—	200.0
HPK_HGC3003_120um_ind_2Vfb	39.29	6.93	—	34.1	52.9	—	failed
HPK_HGC3004_120um_ind_5Vfb	36.66	6.46	—	52.8	81.3	—	failed
HPK_HGC3005_120um_ind_2Vfb_STD0_5	38.15	6.73	—	35.8	70.5	—	failed
HPK_HGC3006_120um_ind_2Vfb_STD0_5	38.71	6.83	—	34.1	63.9	—	failed
HPK_HGC3007_120um_ind_2Vfb	38.24	6.74	—	34.1	68.4	—	failed
HPK_HGC3008_120um_ind_2Vfb	39.31	6.93	—	33.9	55.3	—	failed
HPK_HGC3009_120um_ind_2Vfb	39.56	6.98	—	34.0	55.8	—	failed
HPK_HGC3010_120um_ind_2Vfb	38.68	6.82	—	35.1	55.0	—	200.0
HPK_HGC3011_120um_ind_2Vfb	38.80	6.84	—	34.1	54.3	—	200.0
HPK_HGC3013_120um_ind_2Vfb	39.76	7.01	—	34.1	54.0	—	failed
HPK_HGC3014_120um_ind_2Vfb	39.30	6.93	—	36.1	55.5	—	failed
HPK_HGC3015_120um_ind_2Vfb	38.47	6.78	—	34.2	51.7	—	failed
HPK_HGC3016_120um_ind_2Vfb	39.86	7.03	—	34.1	55.1	—	200.0
HPK_HGC3023_120um_ind_2Vfb	39.11	6.90	—	35.3	56.0	—	200.0
HPK_HGC3101_120um_com_5Vfb	37.66	6.64	—	35.6	74.7	—	200.0
HPK_HGC3102_120um_com_2Vfb_STD0_5	39.04	6.88	—	34.0	46.5	—	failed
HPK_HGC3103_120um_com_2Vfb	38.63	6.81	—	34.2	50.9	—	100.0
HPK_HGC3104_120um_com_5Vfb	37.73	6.65	—	35.6	72.3	—	200.0
HPK_HGC3105_120um_com_2Vfb_STD0_5	40.33	7.11	—	34.2	57.0	—	failed
HPK_HGC3106_120um_com_2Vfb_STD0_5	41.98	7.40	—	34.1	58.4	—	failed
HPK_HGC3107_120um_com_2Vfb	40.71	7.18	—	33.9	53.5	—	failed
HPK_HGC3108_120um_com_2Vfb	38.17	6.73	—	34.1	54.0	—	200.0
HPK_HGC3109_120um_com_2Vfb	37.81	6.67	—	34.2	54.8	—	200.0
HPK_HGC3110_120um_com_2Vfb	37.14	6.55	—	34.1	52.1	—	200.0
HPK_HGC3111_120um_com_2Vfb	37.41	6.60	—	34.1	58.1	—	200.0
HPK_HGC3112_120um_com_2Vfb	40.15	7.08	—	34.1	54.6	—	200.0
HPK_HGC3113_120um_com_2Vfb	40.52	7.15	—	34.1	56.0	—	200.0
HPK_HGC3114_120um_com_2Vfb	40.05	7.06	—	34.2	53.6	—	200.0
Median	12.30	0.67	0.00	35.3	57.6	nan	200.0
Average	9.82	0.67	0.00	35.0	62.2	nan	193.1
Std dev.	4.28	0.02	0.00	1.5	10.3	nan	18.6
OK/Tot.	12/81	4/81	1/1	79/81	61/81	0/20	47/81
OK (rel)	0.15	0.05	1.00	0.98	0.75	0.00	0.58

Flute 3

	DiodeHalf					Metal VdP		p-edge			Bulk VdP		
	i600	v_fd	rho	d_conc	me-and_metal	vdp_metv	vdp_metp	vdp_cb	vdp_cb	tr_line_cb	vdp-Bulk	vdp-Bulk_r	vdp-Bulk_rho
	uA	V	kOhm cm	1E12cm^-3	Ohm	mOhm/sq	mOhm/sq	kOhm/sq	kOhm/sq	um	kOhm/sq	kOhm/sq	kOhm*cm (1.081)
HPK_HGC1003_300um_ind_2Vfb	73.3	261.2	3.48	3.99	226.7	27.3	28.4	1.37	1.35	34.5	69.5	68.8	3.31
HPK_HGC1004_300um_ind_5Vfb	failed	failed	failed	failed	226.2	27.3	27.2	1.42	1.42	34.6	63.3	64.5	3.06
HPK_HGC1005_300um_ind_5Vfb_STD2_5	failed	failed	failed	failed	238.8	28.5	26.5	1.42	1.39	34.8	63.8	66.4	3.11
HPK_HGC1006_300um_ind_5Vfb_STD5	failed	failed	failed	failed	227.8	26.8	26.9	1.40	1.40	34.4	63.6	63.6	3.04
HPK_HGC1007_300um_ind_5Vfb_OxA	failed	failed	failed	failed	225.9	27.7	27.1	1.44	1.45	34.2	68.8	68.5	3.28
HPK_HGC1008_300um_ind_5Vfb_OxB	failed	failed	failed	failed	229.1	26.9	26.8	1.36	1.42	32.9	66.4	67.1	3.19
HPK_HGC1009_300um_ind_5Vfb_OxC	failed	failed	failed	failed	226.1	26.6	26.9	1.39	1.39	34.3	66.8	67.0	3.20
HPK_HGC1010_300um_ind_5Vfb_OxD	failed	failed	failed	failed	226.6	26.4	26.8	1.43	1.41	34.6	67.1	66.5	3.20
HPK_HGC1011_300um_ind_5Vfb_OxE	failed	failed	failed	failed	226.9	27.3	27.5	1.36	1.35	34.6	71.5	73.7	3.47
HPK_HGC1012_300um_ind_2Vfb	83.1	257.2	3.71	3.75	228.3	27.9	27.8	1.38	1.43	34.4	69.7	69.2	3.32
HPK_HGC1013_300um_ind_2Vfb	—	—	—	—	233.4	20.6	20.8	1.37	1.38	34.2	68.9	69.2	3.30
HPK_HGC1014_300um_ind_5Vfb_MCZ	failed	failed	failed	failed	226.7	28.1	28.1	1.42	1.41	34.9	70.4	70.0	3.36
HPK_HGC1101_300um_com_5Vfb	—	—	—	—	225.2	20.5	20.9	1.43	1.41	34.5	78.5	77.6	3.73
HPK_HGC1102_300um_com_2Vfb	—	—	—	—	227.9	20.6	20.8	1.43	1.47	35.9	68.9	68.8	3.29
HPK_HGC1103_300um_com_2Vfb	—	—	—	—	234.8	20.5	20.8	1.38	1.37	34.6	69.7	69.0	3.32
HPK_HGC1104_300um_com_2Vfb	—	—	—	—	228.8	20.7	20.4	1.39	1.34	34.7	69.9	69.7	3.34
HPK_HGC1105_300um_com_5Vfb	—	—	—	—	231.6	20.6	20.5	1.40	1.41	34.3	64.9	65.1	3.11
HPK_HGC1106_300um_com_5Vfb_STD2_5	failed	failed	failed	failed	227.2	27.8	27.3	1.43	1.41	34.5	67.1	66.6	3.20
HPK_HGC1107_300um_com_5Vfb_STD5	failed	failed	failed	failed	245.6	28.3	28.1	1.39	1.42	33.7	65.3	66.2	3.15
HPK_HGC1108_300um_com_5Vfb_OxA	—	—	—	—	235.9	20.5	20.4	1.46	1.45	34.5	66.6	65.7	3.16
HPK_HGC1109_300um_com_5Vfb_OxB	—	—	—	—	242.0	20.9	20.4	1.39	1.41	34.1	67.0	67.3	3.21
HPK_HGC1110_300um_com_5Vfb_OxC	failed	failed	failed	failed	227.1	27.4	26.7	1.46	failed	35.5	67.1	63.5	3.12
HPK_HGC1111_300um_com_5Vfb_OxD	—	—	—	—	231.5	20.8	20.4	1.43	1.42	34.6	63.4	63.3	3.03
HPK_HGC1112_300um_com_5Vfb_OxE	—	—	—	—	237.7	21.0	20.5	1.36	1.33	34.9	64.8	64.2	3.09
HPK_HGC1113_300um_com_2Vfb	—	—	—	—	229.5	20.8	20.5	1.38	1.38	34.4	68.4	68.5	3.27
HPK_HGC2003_200um_ind_2Vfb	133.4	140.2	2.85	4.88	231.2	27.9	27.3	1.36	1.36	34.3	54.5	54.7	2.61
HPK_HGC2004_200um_ind_5Vfb	failed	failed	failed	failed	145.5	27.8	27.0	1.50	1.40	36.8	52.7	52.9	2.53
HPK_HGC2005_200um_ind_5Vfb_STD2_5	failed	failed	failed	failed	229.8	28.7	27.0	1.42	1.40	34.7	53.6	54.0	2.57
HPK_HGC2006_200um_ind_5Vfb_STD5	failed	failed	failed	failed	failed	28.0	26.7	1.42	1.40	34.9	54.2	53.9	2.59
HPK_HGC2007_200um_ind_5Vfb_OxA	failed	failed	failed	failed	426.9	27.9	26.4	1.44	1.43	34.4	58.9	58.6	2.81
HPK_HGC2008_200um_ind_5Vfb_OxB	failed	failed	failed	failed	226.8	27.9	26.6	1.42	1.41	34.4	55.7	55.3	2.65
HPK_HGC2009_200um_ind_5Vfb_OxC	failed	failed	failed	failed	238.0	27.7	27.9	1.40	1.40	34.0	56.2	73.2	3.09
HPK_HGC2010_200um_ind_5Vfb_OxD	failed	failed	failed	failed	206.7	28.4	26.7	1.40	1.40	34.3	57.4	57.0	2.74
HPK_HGC2011_200um_ind_5Vfb_OxE	failed	failed	failed	failed	227.8	28.3	27.2	1.33	1.33	34.3	52.9	52.7	2.53
HPK_HGC2012_200um_ind_2Vfb	103.6	131.3	3.03	4.58	failed	28.4	27.0	1.37	1.36	34.5	57.0	58.5	2.76
HPK_HGC2013_200um_ind_2Vfb	111.6	134.5	3.34	4.16	243.1	28.2	27.5	1.36	1.36	34.4	54.2	54.0	2.59
HPK_HGC2014_200um_ind_5Vfb_MCZ	failed	failed	failed	failed	failed	27.6	29.0	1.41	1.40	34.6	61.4	61.7	2.94
HPK_HGC2101_200um_com_5Vfb	—	—	—	—	227.6	20.6	20.9	1.42	1.43	34.3	62.6	62.2	2.99
HPK_HGC2102_200um_com_2Vfb	—	—	—	—	228.4	20.6	20.8	1.37	1.38	34.2	54.1	54.4	2.59
HPK_HGC2103_200um_com_2Vfb	—	—	—	—	236.3	20.5	20.7	1.37	1.37	34.6	53.3	53.7	2.56
HPK_HGC2104_200um_com_2Vfb	—	—	—	—	228.5	20.7	20.3	1.36	1.37	34.2	53.3	54.3	2.57
HPK_HGC2105_200um_com_5Vfb	—	—	—	—	failed	534404.	534381.	failed	failed	failed	failed	7211.4	failed
HPK_HGC2106_200um_ind_5Vfb_STD2_5	failed	failed	failed	failed	234.1	28.0	27.2	1.40	1.41	34.1	58.3	58.5	2.80
HPK_HGC2107_200um_ind_5Vfb_STD5	failed	failed	failed	failed	227.5	27.7	26.4	1.40	1.41	34.1	58.7	59.2	2.82
HPK_HGC2108_200um_com_5Vfb_OxA	—	—	—	—	227.4	20.7	20.5	1.44	1.45	34.3	56.0	55.4	2.66
HPK_HGC2109_200um_com_5Vfb_OxB	—	—	—	—	227.0	20.8	20.5	1.38	1.41	34.1	52.8	53.1	2.53
HPK_HGC2110_200um_com_5Vfb_OxC	—	—	—	—	227.2	20.7	20.4	1.41	1.41	34.4	53.9	54.0	2.58
HPK_HGC2111_200um_com_5Vfb_OxD	—	—	—	—	230.9	20.7	20.5	1.44	1.40	34.8	53.0	51.9	2.51
HPK_HGC2112_200um_com_5Vfb_OxE	—	—	—	—	227.8	20.8	20.6	1.31	1.36	33.6	54.4	55.2	2.62
HPK_HGC2113_200um_com_2Vfb	—	—	—	—	227.9	20.8	20.5	1.39	1.36	34.8	58.6	58.4	2.80
HPK_HGC2114_200um_com_2Vfb	—	—	—	—	227.9	20.8	20.5	1.37	1.38	34.2	58.2	58.7	2.80
HPK_HGC3001_120um_ind_5Vfb	—	—	—	—	241.8	21.2	21.4	1.41	1.41	34.9	26.2	26.3	1.26
HPK_HGC3002_120um_ind_2Vfb_STD0_5	—	—	—	—	231.5	20.9	21.2	1.35	1.37	33.9	27.4	27.9	1.32
HPK_HGC3003_120um_ind_2Vfb	—	—	—	—	231.3	20.9	21.2	1.31	1.29	34.8	29.5	37.5	1.60
HPK_HGC3004_120um_ind_5Vfb	failed	failed	failed	failed	231.9	28.3	27.8	1.38	1.37	34.4	30.1	45.1	1.80
HPK_HGC3005_120um_ind_2Vfb_STD0_5	failed	111.8	0.87	15.91	231.4	28.8	27.2	1.34	1.34	34.3	28.1	28.1	1.34
HPK_HGC3006_120um_ind_2Vfb_STD0_5	155.4	150.6	0.61	22.72	233.0	27.5	28.2	1.35	1.34	34.3	29.5	29.7	1.42
HPK_HGC3007_120um_ind_2Vfb	200.3	104.9	0.99	14.06	232.2	28.1	27.8	1.34	1.35	34.2	28.2	27.8	1.34
HPK_HGC3008_120um_ind_2Vfb	—	—	—	—	230.9	21.1	21.2	1.34	1.35	34.0	28.8	28.3	1.37
HPK_HGC3009_120um_ind_2Vfb	—	—	—	—	232.1	20.9	21.1	1.34	1.36	34.1	28.5	28.9	1.37
HPK_HGC3010_120um_ind_2Vfb	—	—	—	—	230.8	21.0	20.8	1.33	1.33	34.2	27.1	27.2	1.30
HPK_HGC3011_120um_ind_2Vfb	—	—	—	—	231.5	21.0	20.7	1.35	1.34	34.3	28.9	28.9	1.38
HPK_HGC3013_120um_ind_2Vfb	—	—	—	—	232.1	20.9	21.1	1.35	1.34	34.5	28.1	27.8	1.34
HPK_HGC3014_120um_ind_2Vfb	195.0	96.0	1.35	10.28	232.7	27.3	28.7	1.34	1.34	34.3	28.8	28.8	1.38
HPK_HGC3015_120um_ind_2Vfb	failed	172.8	0.67	20.65	231.5	27.8	27.3	1.35	1.34	34.3	failed	29.1	failed
HPK_HGC3016_120um_ind_2Vfb	—	—	—	—	232.4	21.2	20.8	1.33	1.35	33.9	29.0	28.7	1.38
HPK_HGC3023_120um_ind_2Vfb	—	—	—	—	232.3	21.0	20.9	1.36	1.33	34.7	29.5	29.1	1.40
HPK_HGC3101_120um_com_5Vfb	—	—	—	—	231.6	20.9	21.2	1.41	1.39	34.5	29.3	29.1	1.40
HPK_HGC3102_120um_com_2Vfb_STD0_5	—	—	—	—	231.3	20.9	21.2	1.34	1.34	34.2	27.8	27.5	1.32
HPK_HGC3103_120um_com_2Vfb	—	—	—	—	231.2	20.9	21.2	1.35	1.36	34.1	27.4	27.4	1.31
HPK_HGC3104_120um_com_5Vfb	failed	failed	failed	failed	233.5	28.7	27.3	1.38	1.38	34.0	28.4	28.7	1.37
HPK_HGC3105_120um_com_2Vfb_STD0_5	158.5	81.8	1.28	10.87	232.2	29.1	27.6	1.34	1.35	34.1	28.1	28.2	1.35
HPK_HGC3106_120um_com_2Vfb_STD0_5	158.2	110.6	1.01	13.75	233.2	29.0	28.3	1.34	1.34	34.1	28.8	28.7	1.37
HPK_HGC3107_120um_com_2Vfb	failed	116.0	0.87	15.99	232.3	28.2	28.4	1.34	1.34	34.3	28.2	28.1	1.35
HPK_HGC3108_120um_com_2Vfb	—	—	—	—	232.0	21.1	20.9	1.33	1.36	34.0	28.0	28.4	1.35
HPK_HGC3109_120um_com_2Vfb	—	—	—	—	231.5	21.1	21.2	1.35	1.35	34.4	29.3	28.7	1.39
HPK_HGC3110_120um_com_2Vfb	—	—	—	—	231.1	20.9	20.8	1.34	1.35	33.9	28.3	28.1	1.35
HPK_HGC3111_120um_com_2Vfb	—	—	—	—	failed	21.0	20.7	1.35	1.35	34.4	28.5	28.2	1.36
HPK_HGC3112_120um_com_2Vfb	—	—	—	—	232.7	21.1	21.0	1.35	1.34	34.4	31.3	36.0	1.61
HPK_HGC3113_120um_com_2Vfb	—	—	—	—	231.6	21.0	20.8	1.35	1.33	34.4	29.1	29.1	1.39
HPK_HGC3114_120um_com_2Vfb	—	—	—	—	232.3	21.0	21.1	1.33	1.35	34.0	29.4	29.6	1.41
Median	133.4	259.2	3.71	4.16	231.3	21.1	21.2	1.37	1.37	34.3	54.2	54.4	3.73
Average	130.3	259.2	3.71	4.27	229.7	24.2	23.9	1.38	1.38	34.4	49.6	49.9	3.73
Std dev.	37.9	2.0	0.00	0.41	11.0	3.6	3.3	0.04	0.04	0.5	16.8	16.8	0.00
OK/Tot.	9/38	2/38	1/38	5/38	75/81	80/81	80/81	80/81	79/81	80/81	79/81	80/81	1/81
OK (rel)	0.24	0.05	0.03	0.13	0.93	0.99	0.99	0.99	0.98	0.99	0.98	0.99	0.01

Flute 4

	GCD05		CBKR		Contact chain		
	i_surf05s0_gcd05		cont_poly		cont_p	cont_poly	cont_n
	pA	cm/s	kOhm	Ohm	kOhm	MOhm	kOhm
HPK_HGC1003_300um_ind_2Vfb	56.6	6.89	—	32.6	473.8	—	failed
HPK_HGC1004_300um_ind_5Vfb	50.8	6.18	—	32.6	582.9	—	86.2
HPK_HGC1005_300um_ind_5Vfb_STD2_5	54.4	6.62	—	33.2	493.0	—	failed
HPK_HGC1006_300um_ind_5Vfb_STD5	53.5	6.50	—	31.0	491.9	—	failed
HPK_HGC1007_300um_ind_5Vfb_OxA	failed	failed	—	31.3	790.3	—	44.7
HPK_HGC1008_300um_ind_5Vfb_OxB	18.3	2.23	—	32.2	525.4	—	failed
HPK_HGC1009_300um_ind_5Vfb_OxC	5.4	0.65	—	31.3	466.1	—	failed
HPK_HGC1010_300um_ind_5Vfb_OxD	16.6	2.01	—	32.4	670.6	—	failed
HPK_HGC1011_300um_ind_5Vfb_OxE	39.4	4.80	—	32.2	502.3	—	failed
HPK_HGC1012_300um_ind_2Vfb	47.4	5.77	—	31.2	551.3	—	failed
HPK_HGC1013_300um_ind_2Vfb	47.7	5.81	—	45.8	552.6	—	failed
HPK_HGC1014_300um_ind_5Vfb_MCZ	58.3	7.09	—	33.1	554.1	—	failed
HPK_HGC1101_300um_com_5Vfb	55.1	6.70	—	34.3	672.8	—	failed
HPK_HGC1102_300um_com_2Vfb	59.0	7.18	—	33.4	499.5	—	failed
HPK_HGC1103_300um_com_2Vfb	57.2	6.96	—	32.8	560.1	—	failed
HPK_HGC1104_300um_com_2Vfb	58.0	7.05	—	32.4	491.3	—	failed
HPK_HGC1105_300um_com_5Vfb	56.1	6.82	—	33.3	629.8	—	failed
HPK_HGC1106_300um_com_5Vfb_STD2_5	57.1	6.94	—	31.7	528.4	—	failed
HPK_HGC1107_300um_com_5Vfb_STD5	58.2	7.08	—	29.5	510.1	—	failed
HPK_HGC1108_300um_com_5Vfb_OxA	failed	failed	—	31.8	803.6	—	44.4
HPK_HGC1109_300um_com_5Vfb_OxB	5.2	0.64	—	32.3	502.2	—	failed
HPK_HGC1110_300um_com_5Vfb_OxC	20.3	2.47	—	32.0	498.2	—	failed
HPK_HGC1111_300um_com_5Vfb_OxD	17.5	2.13	—	32.6	548.8	—	failed
HPK_HGC1112_300um_com_5Vfb_OxE	42.8	5.21	—	35.5	486.8	—	failed
HPK_HGC1113_300um_com_2Vfb	48.2	5.86	—	33.2	601.2	—	failed
HPK_HGC2003_200um_ind_2Vfb	54.5	6.63	—	31.5	481.0	—	failed
HPK_HGC2004_200um_ind_5Vfb	failed	failed	—	34.1	580.5	—	75.3
HPK_HGC2005_200um_ind_5Vfb_STD2_5	49.4	6.01	—	31.3	507.0	—	failed
HPK_HGC2006_200um_ind_5Vfb_STD5	51.1	6.21	—	30.5	489.5	—	failed
HPK_HGC2007_200um_ind_5Vfb_OxA	failed	failed	—	31.3	834.1	—	44.4
HPK_HGC2008_200um_ind_5Vfb_OxB	16.5	2.01	—	32.0	512.3	—	failed
HPK_HGC2009_200um_ind_5Vfb_OxC	19.5	2.38	—	29.3	513.0	—	47.9
HPK_HGC2010_200um_ind_5Vfb_OxD	5.1	0.62	—	31.3	523.3	—	35.0
HPK_HGC2011_200um_ind_5Vfb_OxE	40.5	4.93	—	32.6	495.6	—	failed
HPK_HGC2012_200um_ind_2Vfb	46.9	5.71	—	33.2	511.2	—	failed
HPK_HGC2013_200um_ind_2Vfb	46.6	5.67	—	31.1	501.2	—	failed
HPK_HGC2014_200um_ind_5Vfb_MCZ	55.3	6.72	—	33.4	568.9	—	failed
HPK_HGC2101_200um_com_5Vfb	47.9	5.83	—	33.7	579.3	—	failed
HPK_HGC2102_200um_com_2Vfb	57.2	6.95	—	42.6	461.5	—	failed
HPK_HGC2103_200um_com_2Vfb	56.7	6.89	—	23.8	452.1	—	failed
HPK_HGC2104_200um_com_2Vfb	55.8	6.79	—	30.0	500.4	—	failed
HPK_HGC2105_200um_com_5Vfb	failed	failed	—	10.2	35.9	—	failed
HPK_HGC2106_200um_ind_5Vfb_STD2_5	55.0	6.69	—	26.5	548.2	—	failed
HPK_HGC2107_200um_ind_5Vfb_STD5	55.5	6.76	—	26.4	551.4	—	failed
HPK_HGC2108_200um_com_5Vfb_OxA	failed	failed	—	32.0	813.4	—	44.3
HPK_HGC2109_200um_com_5Vfb_OxB	5.5	0.67	—	32.3	487.9	—	failed
HPK_HGC2110_200um_com_5Vfb_OxC	18.9	2.31	—	32.9	500.4	—	failed
HPK_HGC2111_200um_com_5Vfb_OxD	17.1	2.08	—	32.6	536.2	—	failed
HPK_HGC2112_200um_com_5Vfb_OxE	41.7	5.07	—	33.1	505.5	—	failed
HPK_HGC2113_200um_com_2Vfb	47.3	5.76	—	31.1	518.9	—	failed
HPK_HGC2114_200um_com_2Vfb	46.9	5.71	—	31.4	551.9	—	failed
HPK_HGC3001_120um_ind_5Vfb	54.6	6.64	—	34.7	655.5	—	70.2
HPK_HGC3002_120um_ind_2Vfb_STD0_5	55.3	6.72	—	33.1	580.0	—	683.6
HPK_HGC3003_120um_ind_2Vfb	52.4	6.38	—	-0.9	463.8	—	failed
HPK_HGC3004_120um_ind_5Vfb	50.9	6.19	—	27.3	561.2	—	failed
HPK_HGC3005_120um_ind_2Vfb_STD0_5	51.9	6.31	—	-42.7	474.0	—	failed
HPK_HGC3006_120um_ind_2Vfb_STD0_5	54.2	6.60	—	32.7	494.3	—	failed
HPK_HGC3007_120um_ind_2Vfb	51.7	6.29	—	32.4	460.3	—	failed
HPK_HGC3008_120um_ind_2Vfb	53.9	6.56	—	32.2	445.7	—	failed
HPK_HGC3009_120um_ind_2Vfb	53.7	6.53	—	32.7	504.4	—	failed
HPK_HGC3010_120um_ind_2Vfb	53.5	6.50	—	32.1	475.2	—	failed
HPK_HGC3011_120um_ind_2Vfb	53.0	6.44	—	33.2	480.8	—	failed
HPK_HGC3013_120um_ind_2Vfb	55.1	6.70	—	32.0	505.8	—	failed
HPK_HGC3014_120um_ind_2Vfb	54.1	6.58	—	32.5	448.8	—	failed
HPK_HGC3015_120um_ind_2Vfb	53.3	6.49	—	33.9	457.5	—	failed
HPK_HGC3016_120um_ind_2Vfb	55.4	6.74	—	31.8	483.2	—	failed
HPK_HGC3023_120um_ind_2Vfb	54.4	6.62	—	31.8	490.7	—	failed
HPK_HGC3101_120um_com_5Vfb	52.5	6.38	—	34.8	633.6	—	72.0
HPK_HGC3102_120um_com_2Vfb_STD0_5	53.8	6.55	—	35.6	483.4	—	failed
HPK_HGC3103_120um_com_2Vfb	51.6	6.28	—	24.5	433.7	—	failed
HPK_HGC3104_120um_com_5Vfb	53.5	6.51	—	32.0	539.5	—	failed
HPK_HGC3105_120um_com_2Vfb_STD0_5	55.0	6.70	—	31.1	456.2	—	failed
HPK_HGC3106_120um_com_2Vfb_STD0_5	58.6	7.13	—	31.0	477.1	—	failed
HPK_HGC3107_120um_com_2Vfb	55.6	6.76	—	31.8	451.2	—	failed
HPK_HGC3108_120um_com_2Vfb	52.3	6.37	—	31.8	478.0	—	failed
HPK_HGC3109_120um_com_2Vfb	51.3	6.24	—	31.0	458.5	—	failed
HPK_HGC3110_120um_com_2Vfb	50.9	6.19	—	31.9	452.4	—	failed
HPK_HGC3111_120um_com_2Vfb	53.5	6.50	—	32.9	472.0	—	failed
HPK_HGC3112_120um_com_2Vfb	54.6	6.64	—	31.9	453.4	—	failed
HPK_HGC3113_120um_com_2Vfb	55.6	6.76	—	34.9	479.1	—	failed
HPK_HGC3114_120um_com_2Vfb	54.5	6.63	—	35.2	465.6	—	failed
Median	16.8	0.64	0.0	32.2	nan	0.0	47.9
Average	13.8	0.64	0.0	31.9	nan	0.0	58.8
Std dev.	6.1	0.02	0.0	2.1	nan	0.0	15.9
OK/Tot.	12/81	4/81	1/1	76/81	0/81	1/1	9/81
OK (rel)	0.15	0.05	1.00	0.94	0.00	1.00	0.11

A.2 New type C

Flute 1

	FET	MOS Quarter				Polysilicon VdP		n+ VdP		p-stop VdP		Capacitor	
	fet	v_fb	c_acc	t_ox	n_ox	vdp-Poly	vdp-Poly_r	vdpN	vdpN_r	vdpP-stp	vdpP-stp_r	cap_l	cap_r
	V	V	pF	nm	1E10cm-2	kOhm/sq	kOhm/sq	Ohm/sq	Ohm/sq	kOhm/sq	kOhm/sq	pF	pF
HPK_HGC538_10_200um_RL	2.59	2.50	79.2	725.3	9.5	—	—	41.4	41.1	21.8	21.6	0.51	2.14
HPK_HGC538_10_200um_UL	2.62	2.56	79.2	725.6	9.6	—	—	41.1	failed	21.7	21.8	0.21	0.20
HPK_HGC538_11_200um_RL	2.42	2.53	79.4	723.5	9.6	—	—	41.4	41.0	21.4	21.6	2.23	2.13
HPK_HGC538_11_200um_UL	2.64	2.58	79.3	724.7	9.7	—	—	41.3	41.5	21.2	21.4	2.40	0.42
HPK_HGC538_25_300um_RL	2.42	2.58	79.6	721.7	9.8	—	—	41.3	41.0	23.9	failed	2.19	1.95
HPK_HGC538_25_300um_UL	2.48	2.61	79.3	724.3	9.8	—	—	41.1	41.1	20.3	21.0	2.26	2.16
Median	nan	2.57	79.3	724.5	9.7	0.00	0.00	41.3	41.1	21.5	21.6	2.24	2.14
Average	nan	2.56	79.3	724.2	9.7	0.00	0.00	41.3	41.1	21.7	21.5	2.27	2.10
Std dev.	nan	0.04	0.1	1.3	0.1	0.00	0.00	0.1	0.2	1.1	0.3	0.08	0.09
OK/Tot.	0/6	6/6	6/6	6/6	6/6	1/1	1/1	6/6	5/6	6/6	5/6	4/6	4/6
OK (rel)	0.00	1.00	1.00	1.00	1.00	1.00	1.00	1.00	0.83	1.00	0.83	0.67	0.67

Flute 2

	GCD		Poly-R	Line thickness			break-down
	i_surf	s0	me-and_poly	lw_n	lw_pstp1	lw_pstp2	v_bd
	pA	cm/s	MOhm	um	um	um	V
HPK_HGC538_10_200um_RL	36.36	6.41	—	34.5	61.7	3.9	failed
HPK_HGC538_10_200um_UL	37.16	6.55	failed	failed	61.5	1.9	failed
HPK_HGC538_11_200um_RL	36.27	6.39	—	34.4	64.8	failed	failed
HPK_HGC538_11_200um_UL	37.76	6.66	—	34.4	62.4	2.5	failed
HPK_HGC538_25_300um_RL	37.54	6.62	—	34.4	70.0	3.7	failed
HPK_HGC538_25_300um_UL	39.54	6.97	—	34.3	58.2	1.7	failed
Median	nan	nan	0.00	34.4	62.0	nan	0.0
Average	nan	nan	0.00	34.4	63.1	nan	0.0
Std dev.	nan	nan	0.00	0.1	3.6	nan	0.0
OK/Tot.	0/6	0/6	1/1	5/6	6/6	0/6	1/1
OK (rel)	0.00	0.00	1.00	0.83	1.00	0.00	1.00

Flute 3

	DiodeHalf					Metal VdP		p-edge			Bulk VdP		
	i600	v_fd	rho	d_conc	me-and_metal	vdp_met	vdp_met_r	vdp_cb	vdp_cb_r	tr_line_cb	vdp-Bulk	vdp-Bulk_r	vdp-Bulk_rho
	uA	V	kOhm cm	1E12cm^-3	Ohm	mOhm/sq	kOhm/sq	kOhm/sq	kOhm/sq	um	kOhm/sq	kOhm/sq	kOhm*cm (1.081)
HPK_HGC538_10_200um_RL	137.8	117.0	3.86	3.60	224.4	27.3	26.2	1.42	1.42	34.5	58.8	58.6	2.81
HPK_HGC538_10_200um_UL	133.1	144.6	2.70	5.15	228.0	27.5	27.9	1.41	1.43	34.0	57.3	57.9	2.76
HPK_HGC538_11_200um_RL	139.9	140.8	3.02	4.59	223.7	28.1	25.8	1.41	1.42	34.3	55.3	55.7	2.65
HPK_HGC538_11_200um_UL	128.1	65.0	-41.91	-0.33	failed	26.6	27.9	1.42	1.40	34.5	55.9	55.9	2.67
HPK_HGC538_25_300um_RL	136.4	300.6	3.16	4.40	224.6	28.9	26.7	1.41	1.41	34.5	62.5	61.8	2.97
HPK_HGC538_25_300um_UL	119.6	297.4	2.92	4.75	231.1	26.9	27.4	1.42	1.42	34.5	62.7	62.3	2.99
Median	134.7	299.0	3.86	4.59	224.6	27.4	27.1	1.42	1.42	34.5	58.1	58.2	nan
Average	132.5	299.0	3.86	4.50	226.3	27.6	27.0	1.42	1.42	34.4	58.8	58.7	nan
Std dev.	6.9	1.6	0.00	0.51	2.8	0.8	0.8	0.00	0.01	0.2	2.9	2.6	nan
OK/Tot.	6/6	2/6	1/6	5/6	5/6	6/6	6/6	6/6	6/6	6/6	6/6	6/6	0/6
OK (rel)	1.00	0.33	0.17	0.83	0.83	1.00	1.00	1.00	1.00	1.00	1.00	1.00	0.00

Flute 4

	GCD05		CBKR		Contact chain		
	i_surf05	s0_gcd05	i_cont_poly	cont_n	cont_p	cont_poly	cont_n
	pA	cm/s	kOhm	Ohm	kOhm	MOhm	kOhm
HPK_HGC538_10_200um_RL	49.6	6.03	—	35.1	415.3	—	failed
HPK_HGC538_10_200um_UL	51.5	6.26	—	34.6	519.1	—	681.3
HPK_HGC538_11_200um_RL	47.9	5.83	—	35.7	454.6	—	659.6
HPK_HGC538_11_200um_UL	51.9	6.32	—	- 7611.2	494.4	—	689.5
HPK_HGC538_25_300um_RL	51.2	6.22	—	34.7	439.9	—	662.6
HPK_HGC538_25_300um_UL	53.5	6.50	—	- 22424.0	failed	—	failed
Median	nan	nan	0.0	34.9	nan	0.0	nan
Average	nan	nan	0.0	35.0	nan	0.0	nan
Std dev.	nan	nan	0.0	0.4	nan	0.0	nan
OK/Tot.	0/6	0/6	1/1	4/6	0/6	1/1	0/6
OK (rel)	0.00	0.00	1.00	0.67	0.00	1.00	0.00

A.3 VPX35496(PS-p)

Flute 1

	FET	MOS Quarter				Polysilicon VdP		n+ VdP		p-stop VdP		Capacitor	
	fet	v_fb	c_acc	t_ox	n_ox	vdp-Poly	vdp-Poly_r	vdpN	vdpN_r	vdpP-stp	vdpP-stp_r	cap_l	cap_r
	V	V	pF	nm	1E10cm^-2	kOhm/sq	kOhm/sq	Ohm/sq	Ohm/sq	kOhm/sq	kOhm/sq	pF	pF
HPK_VPX35496_001_PSP_HM_EL	2.23	5.22	88.2	651.2	19.6	—	—	35.3	35.1	18.6	18.6	3.46	3.31
HPK_VPX35496_001_PSP_HM_ER	2.57	4.73	86.9	661.1	17.7	—	—	35.1	35.3	18.5	18.5	3.36	3.22
HPK_VPX35496_001_PSP_HM_WL	2.59	4.72	87.0	660.4	17.7	—	—	35.5	35.3	18.5	18.5	3.39	3.24
HPK_VPX35496_001_PSP_HM_WR	2.19	5.39	87.7	655.1	20.0	—	—	35.3	35.4	18.7	18.7	3.43	3.29
HPK_VPX35496_002_PSP_HM_EL	failed	5.29	88.0	652.7	19.7	—	—	failed	failed	failed	failed	3.39	3.27
HPK_VPX35496_002_PSP_HM_ER	2.50	4.81	87.2	658.8	18.0	—	—	35.2	35.3	18.6	18.6	3.33	3.21
HPK_VPX35496_002_PSP_HM_WL	2.64	4.65	87.2	658.7	17.5	—	—	35.6	35.3	18.5	18.5	3.37	3.25
HPK_VPX35496_002_PSP_HM_WR	2.23	5.29	88.0	653.0	19.7	—	—	35.3	35.4	18.7	18.7	3.42	3.29
HPK_VPX35496_010_PSP_HM_EL	2.25	5.21	88.4	649.7	19.6	—	—	35.4	35.3	18.6	18.6	3.48	3.34
HPK_VPX35496_010_PSP_HM_ER	2.47	4.89	87.2	658.8	18.2	—	—	35.3	35.3	18.7	18.7	3.38	3.25
HPK_VPX35496_010_PSP_HM_WL	2.60	4.74	87.1	659.4	17.7	—	—	35.7	35.4	18.6	18.6	3.36	3.22
HPK_VPX35496_010_PSP_HM_WR	2.26	5.30	87.3	658.1	19.6	—	—	35.4	35.4	18.7	18.7	3.41	3.27
HPK_VPX35496_017_PSP_HM_EL	2.28	5.14	88.3	650.3	19.3	—	—	35.2	35.3	18.6	18.6	3.38	3.26
HPK_VPX35496_017_PSP_HM_ER	2.49	4.87	87.4	657.4	18.2	—	—	35.2	35.4	18.7	18.6	3.32	3.21
HPK_VPX35496_017_PSP_HM_WL	2.41	4.80	86.9	661.1	17.9	—	—	35.7	35.4	18.6	18.7	3.35	3.23
HPK_VPX35496_017_PSP_HM_WR	2.26	5.26	87.8	654.1	19.6	—	—	35.4	35.4	18.8	18.7	3.40	3.28
HPK_VPX35496_026_PSP_HM_EL	2.38	5.01	88.4	649.5	18.9	—	—	35.3	35.1	18.4	18.5	3.45	3.30
HPK_VPX35496_026_PSP_HM_ER	2.70	4.38	87.6	655.6	16.7	—	—	35.0	35.3	18.5	18.5	3.37	3.23
HPK_VPX35496_026_PSP_HM_WL	2.78	4.31	87.3	657.7	16.4	—	—	35.4	35.2	18.5	18.5	3.38	3.24
HPK_VPX35496_026_PSP_HM_WR	2.35	5.12	87.9	653.4	19.1	—	—	35.3	35.5	18.5	18.5	3.42	3.28
HPK_VPX35496_032_PSP_HM_EL	2.38	4.99	88.2	650.8	18.8	—	—	35.2	35.2	18.6	18.7	3.36	3.24
HPK_VPX35496_032_PSP_HM_ER	2.70	4.35	88.1	651.9	16.7	—	—	35.1	35.2	18.6	18.6	3.33	3.21
HPK_VPX35496_032_PSP_HM_WL	2.75	4.26	88.2	651.1	16.4	—	—	35.6	35.2	18.6	18.6	3.39	3.26
HPK_VPX35496_032_PSP_HM_WR	2.37	5.04	88.5	649.1	19.0	—	—	35.3	35.3	18.7	18.7	3.41	3.28
HPK_VPX35496_040_PSP_HM_EL	2.31	5.01	88.7	647.6	19.0	—	—	35.3	35.2	18.7	18.8	3.24	3.11
HPK_VPX35496_040_PSP_HM_ER	2.63	4.47	88.2	651.5	17.1	—	—	35.1	35.4	18.7	18.7	3.16	3.04
HPK_VPX35496_040_PSP_HM_WL	2.68	4.35	88.5	648.9	16.7	—	—	35.6	35.2	18.7	18.7	3.18	3.06
HPK_VPX35496_040_PSP_HM_WR	2.26	5.09	88.5	648.9	19.2	—	—	35.4	35.4	18.8	18.8	3.22	3.10
HPK_VPX35496_044_PSP_HM_EL	2.27	5.13	88.1	652.2	19.2	—	—	35.1	35.2	18.9	18.8	3.14	3.03
HPK_VPX35496_044_PSP_HM_ER	2.53	4.60	88.1	651.8	17.5	—	—	35.1	35.3	18.9	18.9	3.12	3.02
HPK_VPX35496_044_PSP_HM_WL	2.63	4.48	88.7	647.4	17.2	—	—	35.7	35.4	18.9	18.9	3.19	3.09
HPK_VPX35496_044_PSP_HM_WR	2.20	5.17	89.1	645.0	19.6	—	—	35.5	35.5	18.9	18.9	3.23	3.12
Median	nan	nan	88.0	652.4	nan	0.00	0.00	35.3	35.3	18.6	18.7	3.37	3.24
Average	nan	nan	87.9	653.5	nan	0.00	0.00	35.4	35.3	18.7	18.7	3.34	3.21
Std dev.	nan	nan	0.6	4.4	nan	0.00	0.00	0.2	0.1	0.1	0.1	0.10	0.09
OK/Tot.	0/32	0/32	32/32	32/32	0/32	1/1	1/1	31/32	31/32	31/32	31/32	32/32	32/32
OK (rel)	0.00	0.00	1.00	1.00	0.00	1.00	1.00	0.97	0.97	0.97	0.97	1.00	1.00

Flute 2

	GCD		Poly-R	Line thickness			break-down
	i_surf	s0	me-and_poly	lw_n	lw_pstp1	lw_pstp2	v_bd
	pA	cm/s	MOhm	um	um	um	V
HPK_VPX35496_001_PSP_HM_EL	13.38	2.36	—	35.0	60.8	37.2	160.0
HPK_VPX35496_001_PSP_HM_ER	11.52	2.03	—	34.3	58.6	36.8	166.0
HPK_VPX35496_001_PSP_HM_WL	10.43	1.84	—	35.0	57.5	36.5	162.0
HPK_VPX35496_001_PSP_HM_WR	failed	failed	—	35.1	61.6	37.5	158.0
HPK_VPX35496_002_PSP_HM_EL	14.28	2.52	—	failed	failed	failed	failed
HPK_VPX35496_002_PSP_HM_ER	12.46	2.20	—	34.8	59.0	36.9	160.0
HPK_VPX35496_002_PSP_HM_WL	12.92	2.28	—	34.9	57.9	36.6	160.0
HPK_VPX35496_002_PSP_HM_WR	13.75	2.42	—	35.1	61.2	37.2	161.0
HPK_VPX35496_010_PSP_HM_EL	14.34	2.53	—	34.9	61.0	37.1	164.0
HPK_VPX35496_010_PSP_HM_ER	13.11	2.31	—	34.6	58.8	36.8	160.0
HPK_VPX35496_010_PSP_HM_WL	12.55	2.21	—	35.0	57.4	36.4	172.0
HPK_VPX35496_010_PSP_HM_WR	14.21	2.50	—	35.0	61.0	37.3	162.0
HPK_VPX35496_017_PSP_HM_EL	14.23	2.51	—	34.8	60.6	37.0	160.0
HPK_VPX35496_017_PSP_HM_ER	13.33	2.35	—	34.7	58.8	37.0	161.0
HPK_VPX35496_017_PSP_HM_WL	13.02	2.30	—	34.9	58.3	36.6	162.0
HPK_VPX35496_017_PSP_HM_WR	14.27	2.52	—	35.0	61.1	37.3	164.0
HPK_VPX35496_026_PSP_HM_EL	14.41	2.54	—	35.0	60.3	36.9	160.0
HPK_VPX35496_026_PSP_HM_ER	11.20	1.98	—	34.6	58.0	36.7	failed
HPK_VPX35496_026_PSP_HM_WL	11.23	1.98	—	34.8	57.2	36.8	150.0
HPK_VPX35496_026_PSP_HM_WR	13.73	2.42	—	35.0	60.2	37.0	159.0
HPK_VPX35496_032_PSP_HM_EL	14.30	2.52	—	34.7	60.2	36.9	160.0
HPK_VPX35496_032_PSP_HM_ER	11.33	2.00	—	34.5	57.7	36.3	150.0
HPK_VPX35496_032_PSP_HM_WL	11.60	2.05	—	34.7	57.0	36.0	150.0
HPK_VPX35496_032_PSP_HM_WR	14.54	2.56	—	34.9	60.6	37.1	160.0
HPK_VPX35496_040_PSP_HM_EL	15.62	2.75	—	34.8	60.0	37.0	170.0
HPK_VPX35496_040_PSP_HM_ER	12.82	2.26	—	34.5	58.3	36.4	170.0
HPK_VPX35496_040_PSP_HM_WL	12.49	2.20	—	35.0	57.1	36.5	165.0
HPK_VPX35496_040_PSP_HM_WR	15.03	2.65	—	34.9	62.2	38.4	155.0
HPK_VPX35496_044_PSP_HM_EL	15.65	2.76	—	34.7	61.0	37.1	165.0
HPK_VPX35496_044_PSP_HM_ER	12.99	2.29	—	34.6	58.7	36.5	165.0
HPK_VPX35496_044_PSP_HM_WL	12.83	2.26	—	34.8	58.0	36.7	160.0
HPK_VPX35496_044_PSP_HM_WR	14.95	2.64	—	34.9	60.9	36.8	155.0
Median	13.33	1.98	0.00	34.9	59.0	36.9	160.0
Average	13.31	1.95	0.00	34.8	59.4	36.9	160.9
Std dev.	1.33	0.06	0.00	0.2	1.5	0.4	5.3
OK/Tot.	31/32	4/32	1/1	31/32	31/32	31/32	30/32
OK (rel)	0.97	0.12	1.00	0.97	0.97	0.97	0.94

Flute 3

	DiodeHalf					Metal VdP		p-edge			Bulk VdP		
	i600	v_fd	rho	d_conc	me-and_metal	vdp_metal	vdp_metal	vdp_cb	vdp_cb	tr_line_cb	vdp-Bulk	vdp-Bulk_r	vdp-Bulk_rho
	uA	V	kOhm cm	1E12cm^-3	Ohm	mOhm/sq	mOhm/sq	kOhm/sq	kOhm/sq	um	kOhm/sq	kOhm/sq	kOhm*cm (1.081)
HPK_VPX35496_001_PSP_HM_EL	failed	failed	failed	failed	243.1	27.0	26.3	1.23	1.23	33.5	61.7	61.8	2.95
HPK_VPX35496_001_PSP_HM_ER	failed	failed	failed	failed	242.7	26.9	26.2	1.23	1.23	33.9	61.2	61.2	2.93
HPK_VPX35496_001_PSP_HM_WL	failed	290.0	2.12	6.54	241.5	26.2	24.7	1.19	1.19	33.3	61.4	61.2	2.93
HPK_VPX35496_001_PSP_HM_WR	failed	failed	failed	failed	239.6	26.0	26.0	1.19	1.19	33.4	61.6	61.2	2.94
HPK_VPX35496_002_PSP_HM_EL	failed	failed	failed	failed	240.7	27.2	26.8	1.25	1.25	33.4	60.7	60.7	2.90
HPK_VPX35496_002_PSP_HM_ER	failed	failed	failed	failed	240.0	25.6	26.3	1.24	1.24	33.7	60.4	60.4	2.89
HPK_VPX35496_002_PSP_HM_WL	failed	279.8	2.08	6.69	238.5	26.8	26.3	1.21	1.20	33.4	60.3	60.6	2.89
HPK_VPX35496_002_PSP_HM_WR	failed	failed	failed	failed	237.1	26.8	26.2	1.20	1.20	33.5	60.7	60.9	2.91
HPK_VPX35496_010_PSP_HM_EL	failed	failed	failed	failed	238.6	26.8	26.1	1.24	1.24	33.5	60.6	60.8	2.90
HPK_VPX35496_010_PSP_HM_ER	failed	332.5	2.19	6.33	238.3	26.8	26.3	1.23	1.23	33.9	60.7	60.5	2.90
HPK_VPX35496_010_PSP_HM_WL	390.1	failed	failed	failed	236.1	26.5	25.7	1.19	1.19	33.0	60.5	60.5	2.89
HPK_VPX35496_010_PSP_HM_WR	failed	failed	failed	failed	234.8	26.4	26.2	1.19	1.19	33.3	60.3	60.6	2.89
HPK_VPX35496_017_PSP_HM_EL	failed	failed	failed	failed	235.8	26.5	26.4	1.25	1.25	33.6	60.9	60.8	2.91
HPK_VPX35496_017_PSP_HM_ER	failed	343.9	2.11	6.58	235.0	27.1	25.8	1.24	1.24	33.6	61.0	60.9	2.92
HPK_VPX35496_017_PSP_HM_WL	495.3	failed	failed	failed	234.3	26.6	26.2	1.20	1.20	33.7	60.9	60.9	2.92
HPK_VPX35496_017_PSP_HM_WR	failed	failed	failed	failed	232.5	26.2	26.4	1.20	1.20	33.5	60.5	60.6	2.90
HPK_VPX35496_026_PSP_HM_EL	failed	352.7	1.86	7.48	240.0	26.6	25.7	1.24	1.24	33.2	60.9	61.1	2.92
HPK_VPX35496_026_PSP_HM_ER	failed	291.5	2.01	6.90	239.4	25.9	25.9	1.25	1.24	33.6	60.9	60.9	2.91
HPK_VPX35496_026_PSP_HM_WL	327.5	293.4	2.02	6.87	237.8	26.9	26.0	1.20	1.20	33.5	61.4	61.1	2.93
HPK_VPX35496_026_PSP_HM_WR	failed	failed	failed	failed	236.9	25.7	25.8	1.19	1.20	33.8	60.7	60.3	2.89
HPK_VPX35496_032_PSP_HM_EL	—	—	—	—	240.3	22.4	22.5	1.23	1.24	32.8	62.2	61.8	2.97
HPK_VPX35496_032_PSP_HM_ER	—	—	—	—	239.6	22.2	22.2	1.24	1.24	33.5	61.9	61.8	2.96
HPK_VPX35496_032_PSP_HM_WL	—	—	—	—	237.7	22.1	22.0	1.19	1.18	33.9	62.2	61.8	2.97
HPK_VPX35496_032_PSP_HM_WR	—	—	—	—	236.1	21.9	22.1	1.19	1.19	33.1	61.4	61.6	2.94
HPK_VPX35496_040_PSP_HM_EL	—	—	—	—	237.3	20.3	20.1	1.24	1.24	33.2	61.9	61.5	2.95
HPK_VPX35496_040_PSP_HM_ER	—	—	—	—	236.4	20.1	19.9	1.25	1.24	33.7	62.1	62.2	2.97
HPK_VPX35496_040_PSP_HM_WL	—	—	—	—	236.0	20.2	20.0	1.20	1.19	33.6	60.7	60.7	2.90
HPK_VPX35496_040_PSP_HM_WR	—	—	—	—	234.7	20.0	19.9	1.20	1.20	33.7	61.7	61.7	2.95
HPK_VPX35496_044_PSP_HM_EL	—	—	—	—	233.2	20.4	20.1	1.24	1.25	33.3	61.7	61.6	2.95
HPK_VPX35496_044_PSP_HM_ER	—	—	—	—	231.9	20.2	20.0	1.24	1.24	33.5	61.6	61.7	2.95
HPK_VPX35496_044_PSP_HM_WL	—	—	—	—	231.3	20.1	20.1	1.20	1.19	32.8	61.5	61.4	2.94
HPK_VPX35496_044_PSP_HM_WR	—	—	—	—	229.7	19.9	19.9	1.19	1.19	33.3	61.1	61.1	2.92
Median	nan	292.5	nan	nan	237.2	26.1	25.8	1.22	1.22	33.5	61.1	61.1	nan
Average	nan	305.2	nan	nan	237.1	24.4	24.1	1.22	1.22	33.5	61.2	61.1	nan
Std dev.	nan	24.0	nan	nan	3.2	2.8	2.7	0.02	0.02	0.3	0.6	0.5	nan
OK/Tot.	0/20	6/20	0/20	0/20	32/32	32/32	32/32	32/32	32/32	32/32	32/32	32/32	0/32
OK (rel)	0.00	0.30	0.00	0.00	1.00	1.00	1.00	1.00	1.00	1.00	1.00	1.00	0.00

Flute 4

	GCD05		CBKR		Contact chain		
	i_surf05	s0_gcd05	cont_poly	cont_n	cont_p	cont_poly	cont_n
	pA	cm/s	kOhm	Ohm	kOhm	MOhm	kOhm
HPK_VPX35496_001_PSP_HM_EL	19.3	2.35	—	27.8	71.5	—	96.8
HPK_VPX35496_001_PSP_HM_ER	16.0	1.95	—	28.2	71.5	—	94.1
HPK_VPX35496_001_PSP_HM_WL	17.7	2.15	—	27.9	69.3	—	90.7
HPK_VPX35496_001_PSP_HM_WR	19.4	2.36	—	28.0	70.6	—	94.5
HPK_VPX35496_002_PSP_HM_EL	19.4	2.36	—	failed	71.5	—	92.2
HPK_VPX35496_002_PSP_HM_ER	16.6	2.02	—	28.1	72.2	—	96.7
HPK_VPX35496_002_PSP_HM_WL	18.2	2.22	—	28.0	70.1	—	89.3
HPK_VPX35496_002_PSP_HM_WR	20.7	2.51	—	28.1	71.5	—	93.4
HPK_VPX35496_010_PSP_HM_EL	20.4	2.48	—	27.9	71.3	—	90.8
HPK_VPX35496_010_PSP_HM_ER	18.0	2.19	—	28.2	71.3	—	93.7
HPK_VPX35496_010_PSP_HM_WL	18.1	2.21	—	27.9	69.6	—	87.6
HPK_VPX35496_010_PSP_HM_WR	20.3	2.46	—	28.6	71.0	—	89.2
HPK_VPX35496_017_PSP_HM_EL	20.2	2.46	—	27.7	71.9	—	88.6
HPK_VPX35496_017_PSP_HM_ER	18.4	2.24	—	28.0	71.9	—	95.6
HPK_VPX35496_017_PSP_HM_WL	19.1	2.32	—	28.0	70.1	—	88.1
HPK_VPX35496_017_PSP_HM_WR	20.5	2.49	—	28.4	71.2	—	90.9
HPK_VPX35496_026_PSP_HM_EL	20.3	2.46	—	27.7	73.4	—	83.0
HPK_VPX35496_026_PSP_HM_ER	15.8	1.92	—	27.8	73.8	—	86.0
HPK_VPX35496_026_PSP_HM_WL	16.6	2.01	—	28.0	71.3	—	80.1
HPK_VPX35496_026_PSP_HM_WR	20.7	2.52	—	28.2	72.6	—	82.1
HPK_VPX35496_032_PSP_HM_EL	20.1	2.44	—	27.9	72.5	—	89.7
HPK_VPX35496_032_PSP_HM_ER	15.7	1.91	—	27.8	73.2	—	89.5
HPK_VPX35496_032_PSP_HM_WL	17.3	2.10	—	27.9	71.4	—	85.8
HPK_VPX35496_032_PSP_HM_WR	21.0	2.56	—	28.5	72.8	—	88.8
HPK_VPX35496_040_PSP_HM_EL	22.1	2.69	—	28.0	72.5	—	90.4
HPK_VPX35496_040_PSP_HM_ER	17.7	2.16	—	28.4	73.4	—	92.2
HPK_VPX35496_040_PSP_HM_WL	18.7	2.28	—	27.8	71.5	—	86.4
HPK_VPX35496_040_PSP_HM_WR	22.2	2.70	—	28.3	72.3	—	92.0
HPK_VPX35496_044_PSP_HM_EL	21.9	2.67	—	28.1	73.0	—	84.6
HPK_VPX35496_044_PSP_HM_ER	17.9	2.18	—	28.4	72.2	—	90.3
HPK_VPX35496_044_PSP_HM_WL	19.4	2.36	—	27.7	70.9	—	82.2
HPK_VPX35496_044_PSP_HM_WR	22.4	2.72	—	28.2	72.7	—	88.5
Median	19.4	1.92	0.0	28.0	71.5	0.0	89.6
Average	19.1	1.92	0.0	28.1	71.7	0.0	89.5
Std dev.	1.9	0.02	0.0	0.2	1.1	0.0	4.2
OK/Tot.	32/32	3/32	1/1	31/32	32/32	1/1	32/32
OK (rel)	1.00	0.09	1.00	0.97	1.00	1.00	1.00

A.4 VPX35499(PS-p)

Flute 1

	FET	MOS Quarter				Polysilicon VdP		n+ VdP		p-stop VdP		Capacitor	
	fet	v_fb	c_acc	t_ox	n_ox	vdp-Poly	vdp-Poly_r	vdpN	vdpN_r	vdpP-stp	vdpP-stp_r	cap_l	cap_r
	V	V	pF	nm	1E10cm-2	kOhm/sq	kOhm/sq	Ohm/sq	Ohm/sq	kOhm/sq	kOhm/sq	pF	pF
HPK_VPX35499_001_PSP_HM_EL	2.27	5.01	88.3	650.8	18.9	—	—	35.6	35.3	19.3	19.3	3.13	3.00
HPK_VPX35499_001_PSP_HM_ER	2.59	4.63	87.1	659.8	17.4	—	—	35.3	35.5	19.2	19.3	3.02	2.91
HPK_VPX35499_001_PSP_HM_WL	2.72	4.44	87.6	655.4	16.9	—	—	35.6	35.5	19.3	19.3	3.06	2.94
HPK_VPX35499_001_PSP_HM_WR	2.27	5.12	87.6	655.4	19.1	—	—	35.6	35.5	19.4	19.4	3.09	2.97
HPK_VPX35499_002_PSP_HM_EL	2.28	5.03	88.7	647.9	19.0	—	—	35.5	35.6	19.4	19.4	3.06	2.97
HPK_VPX35499_002_PSP_HM_ER	2.60	4.64	87.4	657.4	17.5	—	—	35.4	35.5	19.3	19.3	2.98	2.88
HPK_VPX35499_002_PSP_HM_WL	2.76	4.42	87.5	656.3	16.8	—	—	35.7	35.4	19.3	19.3	3.03	2.92
HPK_VPX35499_002_PSP_HM_WR	2.29	5.07	88.2	651.0	19.1	—	—	35.6	35.6	19.6	19.5	3.08	2.96
HPK_VPX35499_011_PSP_HM_EL	2.31	5.07	88.5	648.7	19.1	—	—	35.6	35.4	19.3	19.4	3.14	3.01
HPK_VPX35499_011_PSP_HM_ER	2.56	4.72	87.4	657.1	17.7	—	—	35.4	35.6	19.4	19.4	3.03	2.90
HPK_VPX35499_011_PSP_HM_WL	2.71	4.49	88.0	652.9	17.1	—	—	35.8	35.4	19.4	19.4	3.03	2.91
HPK_VPX35499_011_PSP_HM_WR	2.25	5.18	88.0	652.3	19.4	—	—	35.5	35.6	19.5	19.5	3.08	2.95
HPK_VPX35499_015_PSP_HM_EL	2.24	5.18	88.1	651.9	19.4	—	—	35.5	35.3	19.4	19.4	3.10	2.98
HPK_VPX35499_015_PSP_HM_ER	2.40	4.90	87.7	654.6	18.4	—	—	35.5	35.7	19.5	19.5	3.05	2.93
HPK_VPX35499_015_PSP_HM_WL	2.56	4.72	87.8	653.9	17.8	—	—	35.8	35.4	19.5	19.4	3.03	2.90
HPK_VPX35499_015_PSP_HM_WR	2.20	5.29	87.9	653.6	19.7	—	—	35.5	35.5	19.6	19.5	3.07	2.95
HPK_VPX35499_021_PSP_HM_EL	2.27	5.11	88.3	650.1	19.2	—	—	35.4	35.5	19.5	19.5	3.06	2.95
HPK_VPX35499_021_PSP_HM_ER	2.42	4.89	87.8	654.2	18.4	—	—	35.4	35.6	19.5	19.4	2.99	2.89
HPK_VPX35499_021_PSP_HM_WL	2.54	4.76	87.9	653.4	18.0	—	—	35.7	35.5	19.5	19.5	3.04	2.92
HPK_VPX35499_021_PSP_HM_WR	2.24	5.24	88.2	651.3	19.6	—	—	35.5	35.5	19.5	19.5	3.08	2.96
HPK_VPX35499_027_PSP_HM_EL	2.25	5.15	88.0	652.4	19.3	—	—	35.5	35.3	19.3	19.3	3.08	2.95
HPK_VPX35499_027_PSP_HM_ER	2.65	4.53	88.0	652.4	17.2	—	—	35.4	35.7	19.3	19.3	3.04	2.92
HPK_VPX35499_027_PSP_HM_WL	2.78	4.29	88.8	647.1	16.6	—	—	35.8	35.5	19.1	19.1	3.09	2.97
HPK_VPX35499_027_PSP_HM_WR	2.23	5.16	88.5	648.7	19.4	—	—	35.6	35.6	19.5	19.5	3.10	2.98
HPK_VPX35499_035_PSP_HM_EL	2.30	5.05	88.8	646.5	19.1	—	—	35.5	35.4	19.1	19.1	3.14	3.01
HPK_VPX35499_035_PSP_HM_ER	2.69	4.55	88.0	652.7	17.3	—	—	35.3	35.5	19.0	19.1	3.04	2.92
HPK_VPX35499_035_PSP_HM_WL	2.81	4.31	88.6	648.5	16.6	—	—	35.5	35.5	19.0	19.0	3.05	2.93
HPK_VPX35499_035_PSP_HM_WR	2.30	5.14	88.3	650.2	19.3	—	—	35.8	35.4	19.3	19.2	3.09	2.96
HPK_VPX35499_039_PSP_HM_EL	2.27	5.12	88.6	648.5	19.3	—	—	35.4	35.5	19.2	19.2	3.06	2.96
HPK_VPX35499_039_PSP_HM_ER	2.56	4.69	88.2	651.0	17.8	—	—	35.4	35.5	19.0	19.0	3.00	2.90
HPK_VPX35499_039_PSP_HM_WL	2.79	4.38	88.5	649.4	16.8	—	—	35.7	35.4	19.0	19.0	3.02	2.92
HPK_VPX35499_039_PSP_HM_WR	2.26	5.18	88.4	649.9	19.5	—	—	35.6	35.6	19.2	19.1	3.07	2.96
HPK_VPX35499_043_PSP_HM_EL	2.32	5.06	88.1	652.3	19.0	—	—	35.4	35.2	19.2	19.2	3.06	2.94
HPK_VPX35499_043_PSP_HM_ER	2.63	4.60	87.9	653.4	17.4	—	—	35.4	35.4	19.2	19.2	3.04	2.92
HPK_VPX35499_043_PSP_HM_WL	2.80	4.35	88.6	648.1	16.8	—	—	35.8	35.4	19.0	19.0	3.08	2.95
HPK_VPX35499_043_PSP_HM_WR	2.32	5.10	88.3	650.7	19.2	—	—	35.6	35.6	19.3	19.3	3.09	2.97
HPK_VPX35499_049_PSP_HM_EL	2.31	5.05	88.6	648.6	19.1	—	—	35.3	35.4	19.1	19.1	3.06	2.96
HPK_VPX35499_049_PSP_HM_ER	2.61	4.63	87.8	654.2	17.5	—	—	35.5	35.5	19.0	19.0	3.01	2.91
HPK_VPX35499_049_PSP_HM_WL	2.80	4.43	88.0	653.0	16.9	—	—	35.7	35.3	19.0	18.9	3.00	2.90
HPK_VPX35499_049_PSP_HM_WR	2.33	5.11	88.2	651.1	19.2	—	—	35.6	35.4	19.2	19.2	3.07	2.96
Median	nan	nan	88.1	652.1	nan	0.00	0.00	35.5	35.5	19.3	19.3	3.06	2.95
Average	nan	nan	88.1	651.9	nan	0.00	0.00	35.5	35.5	19.3	19.3	3.06	2.94
Std dev.	nan	nan	0.4	3.0	nan	0.00	0.00	0.1	0.1	0.2	0.2	0.04	0.03
OK/Tot.	0/40	0/40	40/40	40/40	0/40	1/1	1/1	40/40	40/40	40/40	40/40	40/40	40/40
OK (rel)	0.00	0.00	1.00	1.00	0.00	1.00	1.00	1.00	1.00	1.00	1.00	1.00	1.00

Flute 2

	GCD		Poly-R	Line thickness			break-down
	i_surf	s0	me-and_poly	lw_n	lw_pstp1	lw_pstp2	v_bd
	pA	cm/s	MOhm	um	um	um	V
HPK_VPX35499_001_PSP_HM_EL	18.25	3.22	—	34.9	60.0	37.1	165.0
HPK_VPX35499_001_PSP_HM_ER	16.22	2.86	—	34.7	58.0	36.9	175.0
HPK_VPX35499_001_PSP_HM_WL	15.21	2.68	—	34.5	57.0	36.7	175.0
HPK_VPX35499_001_PSP_HM_WR	17.57	3.10	—	34.9	60.8	37.7	170.0
HPK_VPX35499_002_PSP_HM_EL	17.79	3.14	—	34.9	60.5	37.5	170.0
HPK_VPX35499_002_PSP_HM_ER	16.14	2.85	—	34.7	58.4	36.8	175.0
HPK_VPX35499_002_PSP_HM_WL	15.45	2.73	—	34.8	57.2	36.9	175.0
HPK_VPX35499_002_PSP_HM_WR	18.10	3.19	—	34.6	60.9	37.5	170.0
HPK_VPX35499_011_PSP_HM_EL	17.75	3.13	—	34.8	59.8	36.9	170.0
HPK_VPX35499_011_PSP_HM_ER	16.22	2.86	—	34.6	58.4	36.9	175.0
HPK_VPX35499_011_PSP_HM_WL	15.48	2.73	—	34.9	57.1	36.7	175.0
HPK_VPX35499_011_PSP_HM_WR	17.31	3.05	—	34.8	60.7	37.3	175.0
HPK_VPX35499_015_PSP_HM_EL	17.61	3.11	—	34.9	60.3	37.0	175.0
HPK_VPX35499_015_PSP_HM_ER	16.94	2.99	—	34.7	58.9	36.8	175.0
HPK_VPX35499_015_PSP_HM_WL	15.76	2.78	—	34.7	57.6	36.5	180.0
HPK_VPX35499_015_PSP_HM_WR	17.05	3.01	—	34.8	61.1	37.5	170.0
HPK_VPX35499_021_PSP_HM_EL	17.20	3.03	—	34.8	60.1	37.1	170.0
HPK_VPX35499_021_PSP_HM_ER	16.98	2.99	—	34.7	58.6	36.7	170.0
HPK_VPX35499_021_PSP_HM_WL	16.03	2.83	—	34.8	57.9	37.2	175.0
HPK_VPX35499_021_PSP_HM_WR	17.22	3.04	—	34.8	60.7	37.1	170.0
HPK_VPX35499_027_PSP_HM_EL	16.62	2.93	—	34.9	60.1	36.9	175.0
HPK_VPX35499_027_PSP_HM_ER	13.65	2.41	—	34.7	58.0	37.0	175.0
HPK_VPX35499_027_PSP_HM_WL	13.40	2.36	—	34.6	56.0	35.9	170.0
HPK_VPX35499_027_PSP_HM_WR	failed	failed	—	34.6	60.9	37.0	170.0
HPK_VPX35499_035_PSP_HM_EL	16.16	2.85	—	34.9	59.3	36.5	175.0
HPK_VPX35499_035_PSP_HM_ER	13.36	2.36	—	34.7	57.6	36.3	175.0
HPK_VPX35499_035_PSP_HM_WL	13.01	2.29	—	34.7	56.1	36.1	175.0
HPK_VPX35499_035_PSP_HM_WR	15.76	2.78	—	35.1	60.1	37.0	175.0
HPK_VPX35499_039_PSP_HM_EL	16.57	2.92	—	34.7	59.9	37.0	175.0
HPK_VPX35499_039_PSP_HM_ER	14.28	2.52	—	34.7	57.3	36.4	175.0
HPK_VPX35499_039_PSP_HM_WL	13.59	2.40	—	34.8	56.5	36.7	175.0
HPK_VPX35499_039_PSP_HM_WR	failed	failed	—	34.9	59.9	37.2	175.0
HPK_VPX35499_043_PSP_HM_EL	17.01	3.00	—	34.9	59.7	36.7	175.0
HPK_VPX35499_043_PSP_HM_ER	14.83	2.61	—	34.6	58.0	36.2	175.0
HPK_VPX35499_043_PSP_HM_WL	14.13	2.49	—	34.7	56.2	36.6	175.0
HPK_VPX35499_043_PSP_HM_WR	16.80	2.96	—	34.9	60.2	36.9	175.0
HPK_VPX35499_049_PSP_HM_EL	16.87	2.97	—	34.6	59.5	36.9	170.0
HPK_VPX35499_049_PSP_HM_ER	14.93	2.63	—	34.7	57.8	37.0	175.0
HPK_VPX35499_049_PSP_HM_WL	14.14	2.49	—	34.7	56.1	36.8	175.0
HPK_VPX35499_049_PSP_HM_WR	16.67	2.94	—	35.0	60.0	37.6	170.0
Median	14.28	nan	0.00	34.8	59.1	36.9	175.0
Average	14.47	nan	0.00	34.8	58.8	36.9	173.4
Std dev.	0.91	nan	0.00	0.1	1.6	0.4	2.8
OK/Tot.	15/40	0/40	1/1	40/40	40/40	40/40	40/40
OK (rel)	0.38	0.00	1.00	1.00	1.00	1.00	1.00

Flute 3

	DiodeHalf					Metal VdP		p-edge			Bulk VdP		
	i600	v_fd	rho	d_conc	me-and_metal	vdp_metal	vdp_metal	vdp_cb	vdp_cb	tr_line_cb	vdp-Bulk	vdp-Bulk_r	vdp-Bulk_rho
	uA	V	kOhm cm	1E12cm^-3	Ohm	mOhm/sq	mOhm/sq	kOhm/sq	kOhm/sq	um	kOhm/sq	kOhm/sq	kOhm*cm (1.081)
HPK_VPX35499_001_PSP_HM_EL	—	—	—	—	245.8	19.8	20.1	1.20	1.20	33.1	66.9	66.4	3.19
HPK_VPX35499_001_PSP_HM_ER	—	—	—	—	243.6	19.5	19.5	1.20	1.20	33.1	66.4	66.3	3.18
HPK_VPX35499_001_PSP_HM_WL	—	—	—	—	242.1	19.6	19.5	1.19	1.18	33.4	66.2	66.1	3.17
HPK_VPX35499_001_PSP_HM_WR	—	—	—	—	244.2	19.7	19.6	1.19	1.19	33.5	66.3	66.3	3.17
HPK_VPX35499_002_PSP_HM_EL	—	—	—	—	250.0	20.0	19.8	1.21	1.21	33.6	65.9	66.1	3.16
HPK_VPX35499_002_PSP_HM_ER	—	—	—	—	249.9	19.8	19.6	1.21	1.21	33.9	66.7	66.8	3.19
HPK_VPX35499_002_PSP_HM_WL	—	—	—	—	248.3	19.9	19.9	1.20	1.19	33.7	66.3	66.1	3.17
HPK_VPX35499_002_PSP_HM_WR	—	—	—	—	248.1	19.8	19.6	1.20	1.20	33.6	66.7	66.6	3.19
HPK_VPX35499_011_PSP_HM_EL	—	—	—	—	248.1	19.9	19.7	1.21	1.21	32.8	66.6	66.8	3.19
HPK_VPX35499_011_PSP_HM_ER	—	—	—	—	246.4	19.8	19.5	1.21	1.21	33.1	66.8	66.7	3.19
HPK_VPX35499_011_PSP_HM_WL	—	—	—	—	245.2	19.8	19.6	1.20	1.19	32.8	66.7	66.6	3.19
HPK_VPX35499_011_PSP_HM_WR	—	—	—	—	246.2	19.8	19.7	1.20	1.20	33.1	66.6	66.6	3.19
HPK_VPX35499_015_PSP_HM_EL	—	—	—	—	246.6	20.2	19.9	1.21	1.21	33.2	66.3	66.2	3.17
HPK_VPX35499_015_PSP_HM_ER	—	—	—	—	244.4	19.8	19.6	1.21	1.20	33.5	66.6	66.4	3.18
HPK_VPX35499_015_PSP_HM_WL	—	—	—	—	244.2	19.7	19.7	1.19	1.19	32.3	66.5	66.1	3.17
HPK_VPX35499_015_PSP_HM_WR	—	—	—	—	244.6	19.8	19.6	1.20	1.20	33.1	66.6	66.3	3.18
HPK_VPX35499_021_PSP_HM_EL	—	—	—	—	242.0	19.9	19.8	1.21	1.21	33.5	66.9	66.8	3.20
HPK_VPX35499_021_PSP_HM_ER	—	—	—	—	240.1	19.9	19.6	1.21	1.21	33.2	67.0	66.9	3.20
HPK_VPX35499_021_PSP_HM_WL	—	—	—	—	239.9	19.9	19.4	1.20	1.20	33.4	67.0	66.7	3.20
HPK_VPX35499_021_PSP_HM_WR	—	—	—	—	240.3	19.8	19.6	1.20	1.20	33.1	66.9	67.0	3.20
HPK_VPX35499_027_PSP_HM_EL	—	—	—	—	249.0	20.0	19.8	1.21	1.21	33.3	66.1	66.2	3.17
HPK_VPX35499_027_PSP_HM_ER	—	—	—	—	246.1	19.6	19.5	1.21	1.20	33.1	66.9	66.8	3.20
HPK_VPX35499_027_PSP_HM_WL	—	—	—	—	245.7	19.8	19.4	1.20	1.19	33.1	66.4	66.3	3.18
HPK_VPX35499_027_PSP_HM_WR	—	—	—	—	247.2	19.7	19.5	1.20	1.20	33.5	66.4	66.4	3.18
HPK_VPX35499_035_PSP_HM_EL	—	—	—	—	244.0	19.8	19.6	1.21	1.21	32.9	66.3	66.1	3.17
HPK_VPX35499_035_PSP_HM_ER	—	—	—	—	241.5	19.6	19.3	1.21	1.20	33.7	66.5	66.2	3.17
HPK_VPX35499_035_PSP_HM_WL	—	—	—	—	241.2	19.5	19.4	1.20	1.19	33.1	66.2	66.0	3.16
HPK_VPX35499_035_PSP_HM_WR	—	—	—	—	242.9	19.6	19.4	1.20	1.20	32.9	66.4	66.6	3.18
HPK_VPX35499_039_PSP_HM_EL	—	—	—	—	247.4	19.8	19.6	1.21	1.21	33.3	66.5	66.5	3.18
HPK_VPX35499_039_PSP_HM_ER	—	—	—	—	245.4	19.7	19.5	1.20	1.20	33.3	66.4	66.0	3.17
HPK_VPX35499_039_PSP_HM_WL	—	—	—	—	243.9	19.1	19.0	1.20	1.19	33.3	66.2	66.5	3.17
HPK_VPX35499_039_PSP_HM_WR	—	—	—	—	245.7	19.6	19.6	1.20	1.20	33.2	65.9	66.0	3.15
HPK_VPX35499_043_PSP_HM_EL	—	—	—	—	246.9	19.8	19.6	1.21	1.21	33.1	65.9	66.3	3.16
HPK_VPX35499_043_PSP_HM_ER	—	—	—	—	243.9	19.6	19.5	1.20	1.20	32.7	66.4	66.1	3.17
HPK_VPX35499_043_PSP_HM_WL	—	—	—	—	243.2	19.7	19.4	1.20	1.19	33.7	66.5	66.4	3.18
HPK_VPX35499_043_PSP_HM_WR	—	—	—	—	245.0	19.8	19.5	1.20	1.20	33.2	66.2	66.1	3.17
HPK_VPX35499_049_PSP_HM_EL	—	—	—	—	242.8	19.8	19.7	1.20	1.20	33.0	66.7	66.6	3.19
HPK_VPX35499_049_PSP_HM_ER	—	—	—	—	240.6	19.7	19.3	1.20	1.20	33.3	66.9	66.9	3.20
HPK_VPX35499_049_PSP_HM_WL	—	—	—	—	240.0	19.7	19.4	1.19	1.19	33.3	66.9	66.8	3.20
HPK_VPX35499_049_PSP_HM_WR	—	—	—	—	241.6	19.8	19.5	1.20	1.20	33.6	66.6	66.6	3.19
Median	0.0	0.0	0.00	0.00	244.5	19.8	19.6	1.20	1.20	33.2	66.5	66.4	nan
Average	0.0	0.0	0.00	0.00	244.6	19.8	19.6	1.20	1.20	33.2	66.5	66.4	nan
Std dev.	0.0	0.0	0.00	0.00	2.8	0.2	0.2	0.01	0.01	0.3	0.3	0.3	nan
OK/Tot.	1/1	1/1	1/1	1/1	40/40	40/40	40/40	40/40	40/40	40/40	40/40	40/40	0/40
OK (rel)	1.00	1.00	1.00	1.00	1.00	1.00	1.00	1.00	1.00	1.00	1.00	1.00	0.00

Flute 4

	GCD05		CBKR		Contact chain		
	i_surf05s0_gcd05		s_cont_poly	cont_poly	cont_p	cont_poly	cont_n
	pA	cm/s	kOhm	Ohm	kOhm	MOhm	kOhm
HPK_VPX35499_001_PSP_HM_EL	25.4	3.10	—	27.8	73.7	—	75.4
HPK_VPX35499_001_PSP_HM_ER	21.9	2.66	—	28.1	73.2	—	77.3
HPK_VPX35499_001_PSP_HM_WL	22.3	2.71	—	28.4	71.3	—	71.3
HPK_VPX35499_001_PSP_HM_WR	25.6	3.12	—	28.6	74.2	—	79.4
HPK_VPX35499_002_PSP_HM_EL	25.1	3.06	—	28.1	73.9	—	75.6
HPK_VPX35499_002_PSP_HM_ER	21.9	2.66	—	28.3	74.5	—	81.1
HPK_VPX35499_002_PSP_HM_WL	22.6	2.75	—	28.4	72.4	—	73.8
HPK_VPX35499_002_PSP_HM_WR	26.3	3.20	—	28.6	74.1	—	80.2
HPK_VPX35499_011_PSP_HM_EL	25.1	3.05	—	28.0	73.6	—	71.7
HPK_VPX35499_011_PSP_HM_ER	22.1	2.69	—	28.2	74.2	—	73.5
HPK_VPX35499_011_PSP_HM_WL	22.7	2.76	—	28.1	72.1	—	68.9
HPK_VPX35499_011_PSP_HM_WR	25.0	3.05	—	28.5	74.2	—	77.1
HPK_VPX35499_015_PSP_HM_EL	25.0	3.05	—	28.0	73.5	—	72.5
HPK_VPX35499_015_PSP_HM_ER	23.5	2.86	—	28.3	74.0	—	76.7
HPK_VPX35499_015_PSP_HM_WL	23.0	2.80	—	28.4	71.7	—	69.0
HPK_VPX35499_015_PSP_HM_WR	25.1	3.06	—	28.5	73.9	—	77.0
HPK_VPX35499_021_PSP_HM_EL	24.5	2.98	—	28.1	73.6	—	68.7
HPK_VPX35499_021_PSP_HM_ER	23.6	2.88	—	28.4	74.7	—	73.4
HPK_VPX35499_021_PSP_HM_WL	23.0	2.79	—	28.5	72.2	—	65.8
HPK_VPX35499_021_PSP_HM_WR	25.0	3.04	—	28.4	74.5	—	75.4
HPK_VPX35499_027_PSP_HM_EL	22.8	2.77	—	27.9	73.7	—	67.3
HPK_VPX35499_027_PSP_HM_ER	19.2	2.34	—	28.1	74.9	—	68.6
HPK_VPX35499_027_PSP_HM_WL	19.8	2.40	—	28.4	72.3	—	69.7
HPK_VPX35499_027_PSP_HM_WR	24.4	2.97	—	28.4	75.2	—	74.5
HPK_VPX35499_035_PSP_HM_EL	22.1	2.69	—	28.2	74.9	—	72.1
HPK_VPX35499_035_PSP_HM_ER	18.3	2.23	—	28.4	74.8	—	72.1
HPK_VPX35499_035_PSP_HM_WL	19.1	2.32	—	28.2	73.3	—	77.6
HPK_VPX35499_035_PSP_HM_WR	23.1	2.81	—	28.4	74.9	—	79.6
HPK_VPX35499_039_PSP_HM_EL	22.5	2.74	—	28.0	74.8	—	75.8
HPK_VPX35499_039_PSP_HM_ER	19.1	2.32	—	28.2	74.6	—	75.7
HPK_VPX35499_039_PSP_HM_WL	19.7	2.39	—	28.4	72.6	—	79.3
HPK_VPX35499_039_PSP_HM_WR	24.1	2.93	—	28.5	75.4	—	81.1
HPK_VPX35499_043_PSP_HM_EL	23.9	2.90	—	28.0	75.5	—	75.5
HPK_VPX35499_043_PSP_HM_ER	20.1	2.44	—	28.4	74.3	—	73.5
HPK_VPX35499_043_PSP_HM_WL	20.7	2.52	—	28.7	73.0	—	78.9
HPK_VPX35499_043_PSP_HM_WR	24.5	2.98	—	28.2	75.0	—	81.6
HPK_VPX35499_049_PSP_HM_EL	23.7	2.88	—	28.1	74.0	—	80.4
HPK_VPX35499_049_PSP_HM_ER	20.8	2.53	—	28.4	75.1	—	91.6
HPK_VPX35499_049_PSP_HM_WL	21.0	2.56	—	28.3	72.8	—	86.6
HPK_VPX35499_049_PSP_HM_WR	24.7	3.01	—	28.6	75.2	—	86.5
Median	22.6	nan	0.0	28.3	74.0	0.0	75.5
Average	22.2	nan	0.0	28.3	73.9	0.0	75.8
Std dev.	1.9	nan	0.0	0.2	1.1	0.0	5.4
OK/Tot.	32/40	0/40	1/1	40/40	40/40	1/1	40/40
OK (rel)	0.80	0.00	1.00	1.00	1.00	1.00	1.00

A.5 VPX35953(2-S)

Flute 1

	FET	MOS Quarter				Polysilicon VdP		n+ VdP		p-stop VdP		Capacitor	
	fet	v_fb	c_acc	t_ox	n_ox	vdp-Poly	vdp-Poly_r	vdpN	vdpN_r	vdpP-stp	vdpP-stp_r	cap_l	cap_r
	V	V	pF	nm	1E10cm-2	kOhm/sq	kOhm/sq	kOhm/sq	kOhm/sq	kOhm/sq	kOhm/sq	pF	pF
HPK_VPX35953_001_2-S_HM_WL	3.10	2.86	84.5	679.5	11.3	1.88	1.88	34.7	34.5	20.0	20.3	2.60	2.48
HPK_VPX35953_001_2-S_HM_WR	3.92	2.93	85.4	672.3	11.6	failed	1.88	34.6	35.1	18.6	18.6	2.62	2.50
HPK_VPX35953_002_2-S_HM_EL	3.89	2.91	85.8	669.5	11.6	1.88	1.88	34.9	34.8	18.5	18.6	2.64	2.52
HPK_VPX35953_002_2-S_HM_ER	3.28	2.94	84.7	678.0	11.5	1.91	1.85	34.5	34.7	24.7	20.2	2.59	2.48
HPK_VPX35953_002_2-S_HM_WL	3.12	2.91	84.7	677.9	11.4	1.88	1.89	34.6	34.7	20.3	20.3	2.61	2.49
HPK_VPX35953_002_2-S_HM_WR	3.86	2.96	85.6	671.3	11.7	1.88	1.90	34.8	35.0	23.5	23.3	2.62	2.50
HPK_VPX35953_012_2-S_HM_WL	3.19	3.01	84.0	683.9	11.7	1.87	1.87	34.7	34.7	20.6	20.6	2.58	2.47
HPK_VPX35953_012_2-S_HM_WR	3.89	2.99	85.5	671.7	11.8	1.88	1.87	34.7	34.8	18.8	18.8	2.64	2.52
HPK_VPX35953_013_2-S_HM_WL	3.65	2.95	85.0	675.7	11.6	1.87	1.88	34.9	34.9	19.6	19.6	2.63	2.51
HPK_VPX35953_013_2-S_HM_WR	3.90	3.00	85.8	669.8	11.9	1.82	1.86	34.7	35.0	18.9	18.8	2.63	2.50
HPK_VPX35953_017_2-S_HM_EL	3.83	2.98	86.2	666.6	11.9	1.89	1.87	34.8	34.7	18.9	18.9	2.64	2.52
HPK_VPX35953_017_2-S_HM_ER	3.84	2.96	85.1	674.6	11.7	1.85	1.85	34.6	34.9	19.3	19.2	2.62	2.49
HPK_VPX35953_017_2-S_HM_WL	3.66	2.85	84.8	677.2	11.3	1.88	1.88	35.0	34.9	19.4	19.4	2.61	2.47
HPK_VPX35953_017_2-S_HM_WR	3.84	3.03	85.4	672.6	11.9	1.88	1.88	34.6	35.1	19.0	19.0	2.63	2.52
HPK_VPX35953_024_2-S_HM_EL	3.83	3.01	86.3	665.5	12.0	1.89	1.88	35.0	34.7	18.9	18.9	2.62	2.52
HPK_VPX35953_024_2-S_HM_ER	3.74	3.05	85.2	674.5	12.0	1.86	1.88	34.6	34.8	19.2	19.2	2.57	2.47
HPK_VPX35953_024_2-S_HM_WL	3.74	2.96	84.9	676.3	11.6	1.89	1.89	35.0	34.9	19.2	19.2	2.60	2.50
HPK_VPX35953_024_2-S_HM_WR	3.83	3.06	85.9	669.0	12.1	1.90	1.89	34.6	34.9	18.9	18.9	2.63	2.52
HPK_VPX35953_035_2-S_HM_EL	3.99	2.80	86.1	667.1	11.3	1.91	1.91	34.9	34.9	18.8	18.9	2.65	2.53
HPK_VPX35953_035_2-S_HM_ER	2.57	2.89	85.4	672.2	11.5	1.93	1.89	34.4	34.6	22.3	22.2	2.66	2.51
HPK_VPX35953_035_2-S_HM_WL	2.62	2.89	85.5	671.5	11.5	1.90	1.90	34.7	34.6	21.9	21.9	2.64	2.52
HPK_VPX35953_035_2-S_HM_WR	3.96	2.88	85.8	669.7	11.5	1.92	1.92	34.7	35.0	18.9	19.2	0.22	failed
HPK_VPX35953_040_2-S_HM_EL	4.34	2.83	86.3	665.2	11.4	1.87	failed	34.9	34.8	18.8	18.8	2.67	2.54
HPK_VPX35953_040_2-S_HM_ER	3.08	2.88	85.6	671.1	11.5	1.86	1.86	34.4	34.8	20.8	20.8	2.62	2.49
HPK_VPX35953_040_2-S_HM_WL	2.93	2.87	85.5	671.8	11.4	1.88	1.87	34.6	34.6	21.1	21.2	0.22	0.20
HPK_VPX35953_040_2-S_HM_WR	3.99	2.88	85.8	669.5	11.5	1.88	1.89	34.8	35.1	18.7	18.8	2.64	2.50
HPK_VPX35953_043_2-S_HM_EL	3.92	2.87	86.2	666.0	11.5	1.90	1.90	34.6	34.9	18.7	18.7	2.59	2.49
HPK_VPX35953_043_2-S_HM_ER	2.86	2.95	85.5	672.0	11.7	1.84	1.85	34.6	34.4	21.1	21.2	2.57	2.48
HPK_VPX35953_043_2-S_HM_WL	3.01	2.97	85.7	669.8	11.8	1.89	failed	36.5	35.8	25.0	25.3	2.82	2.65
HPK_VPX35953_043_2-S_HM_WR	3.87	2.93	86.3	665.5	11.7	1.90	1.93	39.4	38.7	19.2	18.8	0.31	2.55
Median	3.84	2.93	85.5	671.6	11.6	1.88	1.88	34.7	34.8	19.2	19.2	2.62	2.50
Average	3.70	2.93	85.5	671.9	11.6	1.88	1.88	34.9	35.0	19.9	19.7	2.63	2.51
Std dev.	0.34	0.07	0.6	4.5	0.2	0.02	0.02	0.9	0.7	1.5	1.2	0.04	0.03
OK/Tot.	26/30	30/30	30/30	30/30	30/30	29/30	28/30	30/30	30/30	29/30	29/30	27/30	28/30
OK (rel)	0.87	1.00	1.00	1.00	1.00	0.97	0.93	1.00	1.00	0.97	0.97	0.90	0.93

Flute 2

	GCD		Poly-R	Line thickness			break-down
	i_surf	s0	me-and_poly	lw_n	lw_pstp1	lw_pstp2	v_bd
	pA	cm/s	MOhm	um	um	um	V
HPK_VPX35953_001_2-S_HM_WL	4.76	0.84	1.37	34.4	49.5	32.3	failed
HPK_VPX35953_001_2-S_HM_WR	4.95	0.87	failed	33.9	48.4	34.9	failed
HPK_VPX35953_002_2-S_HM_EL	5.21	0.92	1.38	34.1	48.2	10.3	failed
HPK_VPX35953_002_2-S_HM_ER	5.98	1.05	failed	34.3	59.0	40.8	failed
HPK_VPX35953_002_2-S_HM_WL	4.77	0.84	1.36	34.0	49.6	32.5	failed
HPK_VPX35953_002_2-S_HM_WR	4.70	0.83	1.38	34.2	60.9	44.6	failed
HPK_VPX35953_012_2-S_HM_WL	5.53	0.98	1.36	34.3	50.3	36.7	failed
HPK_VPX35953_012_2-S_HM_WR	5.52	0.97	1.38	34.2	48.3	35.0	failed
HPK_VPX35953_013_2-S_HM_WL	4.95	0.87	1.37	34.3	48.8	31.6	failed
HPK_VPX35953_013_2-S_HM_WR	5.02	0.88	failed	34.1	48.3	17.7	failed
HPK_VPX35953_017_2-S_HM_EL	5.19	0.92	1.40	34.4	48.5	35.1	failed
HPK_VPX35953_017_2-S_HM_ER	5.15	0.91	1.37	33.9	48.3	31.3	failed
HPK_VPX35953_017_2-S_HM_WL	5.25	0.93	1.37	34.3	49.2	34.1	failed
HPK_VPX35953_017_2-S_HM_WR	5.15	0.91	1.37	34.0	48.5	30.7	failed
HPK_VPX35953_024_2-S_HM_EL	5.55	0.98	1.43	34.5	48.4	26.4	failed
HPK_VPX35953_024_2-S_HM_ER	5.65	1.00	1.39	34.2	48.3	24.1	failed
HPK_VPX35953_024_2-S_HM_WL	5.20	0.92	1.40	34.3	49.3	30.5	failed
HPK_VPX35953_024_2-S_HM_WR	5.54	0.98	1.42	34.3	48.4	12.1	failed
HPK_VPX35953_035_2-S_HM_EL	4.66	0.82	1.44	34.5	48.0	8.8	failed
HPK_VPX35953_035_2-S_HM_ER	4.51	0.80	1.38	34.1	50.8	32.5	failed
HPK_VPX35953_035_2-S_HM_WL	failed	failed	1.38	34.5	50.3	24.5	failed
HPK_VPX35953_035_2-S_HM_WR	4.51	0.79	1.39	34.3	47.9	33.6	failed
HPK_VPX35953_040_2-S_HM_EL	4.71	0.83	1.48	34.6	48.3	32.2	failed
HPK_VPX35953_040_2-S_HM_ER	4.76	0.84	1.41	34.2	48.7	5.5	failed
HPK_VPX35953_040_2-S_HM_WL	4.64	0.82	373.24	34.1	50.1	9.9	failed
HPK_VPX35953_040_2-S_HM_WR	5.08	0.90	69.24	34.3	49.2	5.1	failed
HPK_VPX35953_043_2-S_HM_EL	4.88	0.86	1.41	34.0	58.5	26.7	failed
HPK_VPX35953_043_2-S_HM_ER	5.33	0.94	1.37	34.5	50.0	15.2	failed
HPK_VPX35953_043_2-S_HM_WL	4.81	0.85	1.37	36.0	60.8	20.3	failed
HPK_VPX35953_043_2-S_HM_WR	5.10	0.90	1.38	38.6	50.0	9.6	failed
Median	5.08	0.90	1.38	34.3	49.0	32.3	0.0
Average	5.07	0.89	1.39	34.4	50.4	31.9	0.0
Std dev.	0.36	0.06	0.03	0.8	3.8	5.4	0.0
OK/Tot.	29/30	29/30	25/30	30/30	30/30	21/30	1/1
OK (rel)	0.97	0.97	0.83	1.00	1.00	0.70	1.00

Flute 3

	DiodeHalf					Metal VdP		p-edge			Bulk VdP		
	i600	v_fd	rho	d_conc	me-and_metal	vdp_met	vdp_met_r	vdp_cb	vdp_cb_r	tr_line_cb	vdp-Bulk	vdp-Bulk_r	vdp-Bulk_rho
	uA	V	kOhm cm	1E12cm-3	Ohm	mOhm/sq	mOhm/sq	kOhm/sq	kOhm/sq	um	kOhm/sq	kOhm/sq	kOhm*cm (1.081)
HPK_VPX35953_001_2-S_HM_WL	42.5	249.1	3.76	3.69	252.2	26.9	26.9	1.24	1.24	33.3	68.3	68.3	3.27
HPK_VPX35953_001_2-S_HM_WR	52.2	249.1	4.09	3.40	260.9	27.3	26.2	1.23	1.24	33.4	68.8	68.5	3.28
HPK_VPX35953_002_2-S_HM_EL	—	—	—	—	—	—	—	—	—	—	67.0	68.7	3.24
HPK_VPX35953_002_2-S_HM_ER	39.0	246.9	4.05	3.43	254.5	26.0	26.0	1.26	1.26	32.6	68.7	68.7	3.28
HPK_VPX35953_002_2-S_HM_WL	21.5	248.1	3.51	3.96	254.9	27.3	27.3	1.24	1.24	33.4	67.1	69.2	3.26
HPK_VPX35953_002_2-S_HM_WR	44.2	249.9	4.10	3.39	256.4	28.1	26.9	1.24	1.24	33.4	68.4	68.5	3.28
HPK_VPX35953_012_2-S_HM_WL	33.9	238.1	3.68	3.78	247.0	27.3	26.8	1.23	1.24	33.3	70.4	70.6	3.37
HPK_VPX35953_012_2-S_HM_WR	46.3	241.8	4.17	3.33	247.3	27.5	26.8	1.24	1.25	33.5	71.0	71.1	3.40
HPK_VPX35953_013_2-S_HM_WL	51.1	240.4	3.54	3.92	failed	27.6	26.3	1.24	1.24	33.6	71.4	70.7	3.40
HPK_VPX35953_013_2-S_HM_WR	54.2	235.8	4.16	3.34	249.2	26.9	26.6	1.24	1.24	33.3	71.3	72.0	3.43
HPK_VPX35953_017_2-S_HM_EL	38.5	238.0	3.30	4.21	243.3	27.4	26.4	1.26	1.26	33.3	71.8	71.6	3.43
HPK_VPX35953_017_2-S_HM_ER	51.0	242.6	3.94	3.52	240.3	27.5	26.5	1.25	1.26	32.8	71.6	71.4	3.42
HPK_VPX35953_017_2-S_HM_WL	47.4	241.9	3.49	3.98	242.9	27.0	26.8	1.24	1.24	32.6	71.8	71.9	3.44
HPK_VPX35953_017_2-S_HM_WR	67.0	246.9	3.97	3.50	244.3	26.6	26.5	1.25	1.24	32.9	71.9	71.5	3.43
HPK_VPX35953_024_2-S_HM_EL	38.3	235.1	3.77	3.68	238.4	27.4	27.1	1.26	1.26	34.4	72.5	72.0	3.46
HPK_VPX35953_024_2-S_HM_ER	42.2	235.1	4.17	3.33	235.8	27.1	26.3	1.25	1.25	33.7	73.0	72.7	3.48
HPK_VPX35953_024_2-S_HM_WL	57.1	233.8	3.58	3.88	237.0	27.3	26.4	1.24	1.24	34.3	73.0	72.4	3.48
HPK_VPX35953_024_2-S_HM_WR	67.3	242.1	4.01	3.46	238.5	25.8	26.5	1.25	1.25	33.9	72.7	73.0	3.49
HPK_VPX35953_035_2-S_HM_EL	39.9	231.0	3.57	3.90	242.6	27.0	25.8	1.25	1.25	32.7	76.9	73.0	3.59
HPK_VPX35953_035_2-S_HM_ER	45.1	233.7	4.02	3.45	227.1	27.1	25.8	1.26	1.26	33.3	failed	73.2	failed
HPK_VPX35953_035_2-S_HM_WL	27.4	failed	failed	failed	240.9	failed	failed	1.24	1.24	32.1	failed	failed	failed
HPK_VPX35953_035_2-S_HM_WR	55.1	244.5	3.87	3.59	failed	26.8	27.5	1.23	1.24	33.8	71.3	73.0	3.45
HPK_VPX35953_040_2-S_HM_EL	41.6	32.4	756.74	-0.02	failed	27.0	26.8	1.25	1.25	33.3	70.5	70.5	3.37
HPK_VPX35953_040_2-S_HM_ER	51.0	238.3	4.05	3.43	238.2	26.9	25.7	1.26	1.26	33.1	71.0	71.1	3.40
HPK_VPX35953_040_2-S_HM_WL	42.3	238.8	3.59	3.87	239.9	27.6	25.9	1.24	1.24	32.9	70.7	70.7	3.38
HPK_VPX35953_040_2-S_HM_WR	56.5	243.9	4.04	3.44	failed	25.1	26.2	1.24	1.24	33.3	failed	4241.3	failed
HPK_VPX35953_043_2-S_HM_EL	41.6	252.8	3.34	4.16	235.4	27.8	27.0	1.25	1.25	33.8	67.4	67.1	3.22
HPK_VPX35953_043_2-S_HM_ER	59.1	254.3	3.74	3.71	233.0	27.8	26.7	1.26	1.26	33.0	67.5	67.1	3.22
HPK_VPX35953_043_2-S_HM_WL	42.6	248.4	3.33	4.17	232.8	26.8	26.3	1.23	1.23	32.7	67.2	67.0	3.21
HPK_VPX35953_043_2-S_HM_WR	51.3	255.6	3.76	3.69	234.1	27.0	27.1	1.23	1.24	34.1	67.6	70.0	3.29
Median	45.1	242.1	3.94	3.68	240.9	27.1	26.5	1.24	1.24	33.3	71.0	70.9	3.59
Average	46.4	242.8	3.88	3.67	242.7	27.1	26.5	1.24	1.25	33.3	70.4	70.6	3.59
Std dev.	10.1	6.6	0.22	0.27	8.2	0.6	0.5	0.01	0.01	0.5	2.3	1.9	0.00
OK/Tot.	29/29	27/29	23/29	27/29	25/29	28/29	28/29	29/29	29/29	29/29	27/30	28/30	1/30
OK (rel)	1.00	0.93	0.79	0.93	0.86	0.97	0.97	1.00	1.00	1.00	0.90	0.93	0.03

Flute 4

	GCD05		CBKR		Contact chain		
	i_surf05s0_gcd05		5_cont_poly_n	cont_n	cont_p	cont_poly_p	cont_n
	pA	cm/s	kOhm	Ohm	kOhm	MOhm	kOhm
HPK_VPX35953_001_2-S_HM_WL	7.1	0.87	56.7	27.6	73.3	16.5	49.5
HPK_VPX35953_001_2-S_HM_WR	7.4	0.90	failed	28.3	73.5	19.7	54.3
HPK_VPX35953_002_2-S_HM_EL	—	—	—	—	—	—	—
HPK_VPX35953_002_2-S_HM_ER	7.3	0.88	62.4	27.7	77.3	16.4	51.5
HPK_VPX35953_002_2-S_HM_WL	6.9	0.84	56.9	29.9	74.3	16.0	46.4
HPK_VPX35953_002_2-S_HM_WR	7.3	0.89	75.5	28.1	73.1	19.7	54.5
HPK_VPX35953_012_2-S_HM_WL	7.8	0.94	72.8	28.1	74.8	17.1	52.3
HPK_VPX35953_012_2-S_HM_WR	7.7	0.94	71.1	27.8	73.6	19.3	56.8
HPK_VPX35953_013_2-S_HM_WL	7.7	0.94	63.9	28.2	74.8	16.6	49.3
HPK_VPX35953_013_2-S_HM_WR	8.2	0.99	67.4	28.2	73.4	20.0	56.1
HPK_VPX35953_017_2-S_HM_EL	7.6	0.92	53.1	27.5	74.2	16.8	54.0
HPK_VPX35953_017_2-S_HM_ER	7.6	0.92	65.5	28.2	75.2	16.3	54.2
HPK_VPX35953_017_2-S_HM_WL	7.7	0.93	65.8	27.9	75.9	16.1	49.3
HPK_VPX35953_017_2-S_HM_WR	7.8	0.95	79.2	28.1	74.2	19.5	56.5
HPK_VPX35953_024_2-S_HM_EL	8.0	0.97	72.2	28.0	73.0	18.5	55.7
HPK_VPX35953_024_2-S_HM_ER	7.8	0.95	56.7	28.0	75.0	16.4	53.5
HPK_VPX35953_024_2-S_HM_WL	7.6	0.93	64.2	27.8	74.0	17.5	52.6
HPK_VPX35953_024_2-S_HM_WR	8.1	0.99	74.7	27.9	73.4	21.5	54.0
HPK_VPX35953_035_2-S_HM_EL	—	—	—	—	—	—	—
HPK_VPX35953_035_2-S_HM_ER	6.4	0.77	69.2	29.4	80.8	16.6	49.1
HPK_VPX35953_035_2-S_HM_WL	6.4	0.77	70.8	28.2	76.9	16.2	48.2
HPK_VPX35953_035_2-S_HM_WR	7.0	0.85	58.9	28.4	74.8	19.6	55.9
HPK_VPX35953_040_2-S_HM_EL	failed	failed	62.9	- 17364.7	failed	17.6	failed
HPK_VPX35953_040_2-S_HM_ER	7.0	0.85	71.9	472.9	77.8	17.3	54.1
HPK_VPX35953_040_2-S_HM_WL	6.7	0.82	68.2	27.4	74.4	17.5	52.2
HPK_VPX35953_040_2-S_HM_WR	7.0	0.85	74.7	14112.6	failed	18.8	failed
HPK_VPX35953_043_2-S_HM_EL	7.3	0.89	77.3	28.0	74.0	18.6	52.2
HPK_VPX35953_043_2-S_HM_ER	7.2	0.88	65.5	28.4	77.7	17.5	46.9
HPK_VPX35953_043_2-S_HM_WL	7.1	0.87	61.7	27.4	73.2	16.3	48.0
HPK_VPX35953_043_2-S_HM_WR	7.9	0.96	76.7	26.7	72.4	19.6	52.0
Median	7.4	0.90	67.4	28.0	74.3	17.5	52.5
Average	7.4	0.90	67.3	28.0	74.8	17.8	52.3
Std dev.	0.5	0.06	7.0	0.6	1.9	1.5	3.0
OK/Tot.	27/28	27/28	27/28	25/28	26/28	28/28	26/28
OK (rel)	0.96	0.96	0.96	0.89	0.93	1.00	0.93

A.6 VPX35957(2-S)

Flute 1

	FET	MOS Quarter				Polysilicon VdP		n+ VdP		p-stop VdP		Capacitor	
	fet	v_fb	c_acc	t_ox	n_ox	vdp-Poly	vdp-Poly_r	vdpN	vdpN_r	vdpP-stp	vdpP-stp_r	cap_l	cap_r
	V	V	pF	nm	1E10cm^-2	kOhm/sq	kOhm/sq	kOhm/sq	Ohm/sq	kOhm/sq	kOhm/sq	pF	pF
HPK_VPX35957_001_2-S_HM_EL	3.93	2.88	85.7	670.4	11.5	1.87	1.88	34.8	34.8	18.8	18.8	—	—
HPK_VPX35957_001_2-S_HM_ER	3.88	2.93	84.6	678.9	11.5	1.87	1.86	34.7	35.0	18.7	18.7	2.36	2.26
HPK_VPX35957_001_2-S_HM_WL	3.90	2.91	84.5	679.9	11.4	1.91	1.92	35.1	35.0	18.9	18.8	—	—
HPK_VPX35957_001_2-S_HM_WR	3.92	2.94	85.5	672.0	11.6	1.92	1.92	34.9	34.9	18.7	18.8	2.40	2.29
HPK_VPX35957_005_2-S_HM_EL	3.93	2.88	85.6	670.8	11.5	1.87	1.86	35.0	34.6	18.8	18.9	—	—
HPK_VPX35957_005_2-S_HM_ER	3.91	2.90	84.8	677.4	11.4	1.86	1.87	34.6	35.0	18.9	18.8	2.33	2.24
HPK_VPX35957_005_2-S_HM_WL	3.91	2.90	84.7	678.4	11.4	1.90	1.90	35.2	34.9	19.0	18.9	—	—
HPK_VPX35957_005_2-S_HM_WR	3.94	2.93	85.3	673.6	11.6	1.91	1.90	34.8	35.1	18.9	18.9	2.39	2.29
HPK_VPX35957_011_2-S_HM_EL	3.98	2.86	85.9	668.7	11.5	1.87	1.87	34.8	34.8	18.8	18.8	2.45	2.34
HPK_VPX35957_011_2-S_HM_ER	3.98	2.88	84.5	680.1	11.3	1.86	1.86	34.7	35.0	18.9	18.8	2.36	2.25
HPK_VPX35957_011_2-S_HM_WL	3.93	2.88	85.0	675.4	11.4	1.90	1.90	34.9	35.0	18.9	18.9	2.38	2.28
HPK_VPX35957_011_2-S_HM_WR	3.97	2.93	85.6	671.3	11.6	1.91	1.90	34.7	35.0	18.8	18.8	2.42	2.31
HPK_VPX35957_019_2-S_HM_EL	3.93	2.91	86.0	667.8	11.6	1.88	1.87	34.9	34.6	19.3	19.4	2.40	2.32
HPK_VPX35957_019_2-S_HM_ER	3.92	2.94	84.7	677.9	11.5	1.85	1.85	34.7	34.8	19.4	19.3	2.34	2.25
HPK_VPX35957_019_2-S_HM_WL	3.88	2.95	84.7	677.9	11.6	1.88	1.89	35.1	34.9	19.5	19.4	2.36	2.27
HPK_VPX35957_019_2-S_HM_WR	3.93	2.96	85.7	669.8	11.7	1.90	1.89	34.7	35.1	19.4	19.4	2.41	2.30
HPK_VPX35957_028_2-S_HM_EL	4.06	2.80	85.7	670.1	11.2	1.84	1.84	35.0	34.8	19.3	19.3	—	—
HPK_VPX35957_028_2-S_HM_ER	4.02	2.81	85.4	672.8	11.2	1.84	1.83	34.9	35.1	19.3	19.3	2.38	2.27
HPK_VPX35957_028_2-S_HM_WL	4.02	2.81	84.7	677.9	11.1	1.86	1.86	35.1	35.0	19.5	19.4	—	—
HPK_VPX35957_028_2-S_HM_WR	4.04	2.87	85.7	669.9	11.4	1.87	1.88	34.9	35.0	19.3	19.2	2.41	2.29
HPK_VPX35957_035_2-S_HM_EL	4.04	2.81	86.0	667.9	11.3	1.85	1.85	35.0	34.7	19.3	19.4	—	—
HPK_VPX35957_035_2-S_HM_ER	4.01	2.82	85.0	675.4	11.2	1.84	1.85	34.6	35.2	19.3	19.3	2.34	2.25
HPK_VPX35957_035_2-S_HM_WL	3.98	6.05	65.2	881.5	16.5	1.88	1.88	35.2	35.1	19.4	19.3	—	—
HPK_VPX35957_035_2-S_HM_WR	4.03	failed	59.4	failed	failed	1.89	1.89	35.0	34.9	19.3	19.3	2.40	2.30
HPK_VPX35957_042_2-S_HM_EL	3.96	2.86	86.0	667.9	11.5	1.85	1.85	34.9	34.8	19.5	19.5	2.44	2.33
HPK_VPX35957_042_2-S_HM_ER	3.94	2.88	85.4	672.4	11.4	1.85	1.85	34.8	35.0	19.5	19.5	2.39	2.28
HPK_VPX35957_042_2-S_HM_WL	3.95	2.89	84.9	676.4	11.4	1.89	1.90	34.9	34.9	19.5	19.4	2.37	2.26
HPK_VPX35957_042_2-S_HM_WR	3.94	2.92	86.2	666.4	11.7	1.90	1.89	34.8	35.0	19.5	19.5	2.43	2.32
HPK_VPX35957_045_2-S_HM_EL	3.95	2.86	86.2	666.4	11.5	1.85	1.86	35.0	34.9	19.6	19.6	2.46	2.34
HPK_VPX35957_045_2-S_HM_ER	3.94	2.87	85.7	670.1	11.4	1.85	1.85	34.7	35.0	19.6	19.5	2.40	2.29
HPK_VPX35957_045_2-S_HM_WL	3.93	2.88	85.6	671.3	11.5	1.90	1.90	35.1	35.1	19.5	19.5	2.41	2.30
HPK_VPX35957_045_2-S_HM_WR	3.96	2.93	85.8	669.7	11.6	1.89	1.90	34.7	35.0	19.5	19.5	2.43	2.31
Median	3.94	2.88	85.5	672.0	11.5	1.87	1.87	34.9	35.0	19.3	19.3	2.40	2.29
Average	3.96	2.89	85.4	679.6	11.5	1.88	1.88	34.9	34.9	19.2	19.2	2.39	2.29
Std dev.	0.05	0.04	0.5	37.1	0.1	0.02	0.02	0.2	0.1	0.3	0.3	0.03	0.03
OK/Tot.	32/32	30/32	30/32	31/32	30/32	32/32	32/32	32/32	32/32	32/32	32/32	24/24	24/24
OK (rel)	1.00	0.94	0.94	0.97	0.94	1.00	1.00	1.00	1.00	1.00	1.00	1.00	1.00

Flute 2

	GCD		Poly-R	Line thickness			break-down
	i_surf	s0	me-and_poly	lw_n	lw_pstp1	lw_pstp2	v_bd
	pA	cm/s	MOhm	um	um	um	V
HPK_VPX35957_001_2-S_HM_EL	—	—	—	—	—	—	—
HPK_VPX35957_001_2-S_HM_ER	5.92	1.04	1.27	34.2	51.8	36.2	200.0
HPK_VPX35957_001_2-S_HM_WL	—	—	—	—	—	—	—
HPK_VPX35957_001_2-S_HM_WR	5.96	1.05	1.35	34.4	52.8	36.3	200.0
HPK_VPX35957_005_2-S_HM_EL	—	—	—	—	—	—	—
HPK_VPX35957_005_2-S_HM_ER	6.09	1.07	1.27	34.2	51.5	36.0	200.0
HPK_VPX35957_005_2-S_HM_WL	—	—	—	—	—	—	—
HPK_VPX35957_005_2-S_HM_WR	5.82	1.03	1.35	34.4	52.8	36.6	200.0
HPK_VPX35957_011_2-S_HM_EL	6.47	1.14	1.31	34.3	49.6	35.9	200.0
HPK_VPX35957_011_2-S_HM_ER	6.04	1.06	1.28	34.4	50.9	36.4	200.0
HPK_VPX35957_011_2-S_HM_WL	6.02	1.06	1.33	34.5	49.3	36.1	200.0
HPK_VPX35957_011_2-S_HM_WR	6.04	1.06	1.35	34.4	51.0	36.4	failed
HPK_VPX35957_019_2-S_HM_EL	6.59	1.16	1.32	34.3	49.2	36.2	200.0
HPK_VPX35957_019_2-S_HM_ER	6.34	1.12	1.28	34.1	51.6	36.9	200.0
HPK_VPX35957_019_2-S_HM_WL	6.34	1.12	1.32	34.3	48.9	3.6	200.0
HPK_VPX35957_019_2-S_HM_WR	6.65	1.17	1.34	34.4	52.2	34.6	200.0
HPK_VPX35957_028_2-S_HM_EL	—	—	—	—	—	—	—
HPK_VPX35957_028_2-S_HM_ER	5.52	0.97	1.27	34.0	50.2	36.2	200.0
HPK_VPX35957_028_2-S_HM_WL	—	—	—	—	—	—	—
HPK_VPX35957_028_2-S_HM_WR	5.60	0.99	1.33	34.4	51.7	36.9	200.0
HPK_VPX35957_035_2-S_HM_EL	—	—	—	—	—	—	—
HPK_VPX35957_035_2-S_HM_ER	5.57	0.98	1.28	34.1	50.2	35.4	200.0
HPK_VPX35957_035_2-S_HM_WL	—	—	—	—	—	—	—
HPK_VPX35957_035_2-S_HM_WR	5.59	0.99	1.34	34.4	52.0	36.8	200.0
HPK_VPX35957_042_2-S_HM_EL	6.20	1.09	1.30	34.5	48.4	36.0	200.0
HPK_VPX35957_042_2-S_HM_ER	5.78	1.02	1.28	34.3	50.1	36.7	200.0
HPK_VPX35957_042_2-S_HM_WL	5.71	1.01	1.32	34.4	49.0	36.3	200.0
HPK_VPX35957_042_2-S_HM_WR	5.89	1.04	1.34	34.1	51.6	37.0	200.0
HPK_VPX35957_045_2-S_HM_EL	6.28	1.11	1.31	34.6	50.5	36.8	200.0
HPK_VPX35957_045_2-S_HM_ER	5.74	1.01	1.27	34.0	49.4	36.6	200.0
HPK_VPX35957_045_2-S_HM_WL	5.82	1.03	1.33	34.4	48.6	36.5	200.0
HPK_VPX35957_045_2-S_HM_WR	6.07	1.07	1.36	34.1	52.2	37.2	200.0
Median	5.99	1.06	1.32	34.3	50.7	36.4	200.0
Average	6.00	1.06	1.31	34.3	50.6	36.4	200.0
Std dev.	0.31	0.06	0.03	0.2	1.3	0.6	0.0
OK/Tot.	24/24	24/24	24/24	24/24	24/24	23/24	23/24
OK (rel)	1.00	1.00	1.00	1.00	1.00	0.96	0.96

Flute 3

	DiodeHalf					Metal VdP		p-edge			Bulk VdP		
	i600	v_fd	rho	d_conc	me-and_metal	vdp_metal	vdp_metal	vdp_cb	vdp_cb	tr_line_cb	vdp-Bulk	vdp-Bulk_r	vdp-Bulk_rho
	uA	V	kOhm cm	1E12cm^-3	Ohm	mOhm/sq	kOhm/sq	kOhm/sq	kOhm/sq	um	kOhm/sq	kOhm/sq	kOhm*cm (1.081)
HPK_VPX35957_001_2-S_HM_EL	—	—	—	—	—	—	—	—	—	—	67.5	67.8	3.24
HPK_VPX35957_001_2-S_HM_ER	47.2	279.6	3.13	4.43	266.2	19.7	19.4	1.23	1.23	33.1	67.2	66.8	3.20
HPK_VPX35957_001_2-S_HM_WL	—	—	—	—	—	—	—	—	—	—	67.7	67.7	3.24
HPK_VPX35957_001_2-S_HM_WR	failed	270.9	2.49	5.57	269.2	19.9	19.6	1.23	1.23	33.3	67.9	67.3	3.23
HPK_VPX35957_005_2-S_HM_EL	—	—	—	—	—	—	—	—	—	—	68.1	67.7	3.25
HPK_VPX35957_005_2-S_HM_ER	41.2	282.5	3.15	4.41	261.4	19.5	19.4	1.24	1.24	33.3	67.8	67.2	3.23
HPK_VPX35957_005_2-S_HM_WL	—	—	—	—	—	—	—	—	—	—	68.3	68.1	3.26
HPK_VPX35957_005_2-S_HM_WR	failed	268.9	2.53	5.49	264.7	19.9	19.5	1.25	1.25	33.5	68.3	67.9	3.26
HPK_VPX35957_011_2-S_HM_EL	47.8	272.0	2.81	4.95	255.7	19.3	19.4	1.25	1.26	33.2	67.7	67.9	3.24
HPK_VPX35957_011_2-S_HM_ER	51.9	277.4	3.13	4.44	255.6	19.5	19.4	1.24	1.24	33.4	67.3	66.9	3.21
HPK_VPX35957_011_2-S_HM_WL	44.7	264.7	3.14	4.42	263.5	19.8	20.2	1.24	1.24	33.5	67.4	67.7	3.23
HPK_VPX35957_011_2-S_HM_WR	160.2	329.1	1.97	7.04	259.5	19.8	19.4	1.25	1.25	33.3	67.8	67.7	3.24
HPK_VPX35957_019_2-S_HM_EL	49.6	283.3	2.61	5.32	245.4	19.5	19.5	1.25	1.25	33.4	74.4	74.6	3.56
HPK_VPX35957_019_2-S_HM_ER	46.7	264.0	3.38	4.10	246.5	19.6	19.4	1.24	1.24	33.6	74.8	74.0	3.56
HPK_VPX35957_019_2-S_HM_WL	42.8	253.2	3.11	4.47	253.6	20.4	19.8	1.25	1.25	32.9	75.0	75.0	3.59
HPK_VPX35957_019_2-S_HM_WR	failed	248.6	2.49	5.58	251.9	19.9	19.6	1.26	1.26	33.4	75.5	75.2	3.60
HPK_VPX35957_028_2-S_HM_EL	—	—	—	—	—	—	—	—	—	—	76.1	75.6	3.63
HPK_VPX35957_028_2-S_HM_ER	28.4	233.7	4.00	3.47	254.0	19.6	19.4	1.24	1.24	33.3	75.9	75.8	3.63
HPK_VPX35957_028_2-S_HM_WL	—	—	—	—	—	—	—	—	—	—	76.1	75.8	3.63
HPK_VPX35957_028_2-S_HM_WR	failed	311.7	2.08	6.69	257.3	19.8	19.4	1.26	1.26	32.8	75.5	75.8	3.62
HPK_VPX35957_035_2-S_HM_EL	—	—	—	—	—	—	—	—	—	—	74.2	74.1	3.55
HPK_VPX35957_035_2-S_HM_ER	27.3	260.9	3.54	3.92	249.2	19.7	19.4	1.24	1.24	33.3	74.6	74.7	3.57
HPK_VPX35957_035_2-S_HM_WL	—	—	—	—	—	—	—	—	—	—	74.5	74.5	3.56
HPK_VPX35957_035_2-S_HM_WR	failed	259.2	2.62	5.31	253.0	19.8	19.5	1.25	1.26	33.3	74.5	74.1	3.56
HPK_VPX35957_042_2-S_HM_EL	37.4	255.0	2.91	4.78	242.6	19.9	19.6	1.25	1.26	33.2	77.2	77.1	3.69
HPK_VPX35957_042_2-S_HM_ER	37.8	247.3	3.61	3.85	242.3	20.0	19.3	1.24	1.25	33.4	76.4	76.7	3.66
HPK_VPX35957_042_2-S_HM_WL	42.0	238.2	3.42	4.06	247.4	20.0	19.8	1.25	1.25	33.4	76.6	77.0	3.67
HPK_VPX35957_042_2-S_HM_WR	failed	309.1	2.08	6.69	244.4	19.8	19.5	1.26	1.26	33.5	76.6	76.6	3.66
HPK_VPX35957_045_2-S_HM_EL	49.7	265.0	2.64	5.27	240.2	19.7	19.4	1.25	1.26	33.2	77.2	76.6	3.68
HPK_VPX35957_045_2-S_HM_ER	42.7	251.0	3.47	4.00	238.6	19.7	19.4	1.24	1.25	33.5	77.9	77.6	3.72
HPK_VPX35957_045_2-S_HM_WL	43.4	242.1	3.24	4.28	245.4	19.9	19.6	1.25	1.25	33.1	77.1	77.6	3.70
HPK_VPX35957_045_2-S_HM_WR	failed	257.9	2.51	5.53	243.3	19.7	20.1	1.25	1.25	33.2	77.9	77.9	3.73
Median	43.4	264.3	3.61	4.34	252.5	19.8	19.4	1.25	1.25	33.3	74.6	74.5	3.63
Average	49.5	267.7	3.72	4.26	252.1	19.8	19.5	1.25	1.25	33.3	72.8	72.7	3.63
Std dev.	28.5	22.8	0.20	0.37	8.6	0.2	0.2	0.01	0.01	0.2	4.1	4.1	0.06
OK/Tot.	17/24	24/24	3/24	14/24	24/24	24/24	24/24	24/24	24/24	24/24	32/32	32/32	20/32
OK (rel)	0.71	1.00	0.12	0.58	1.00	1.00	1.00	1.00	1.00	1.00	1.00	1.00	0.62

Flute 4

	GCD05		CBKR		Contact chain		
	i_surf05	s0_gcd05	cont_poly	cont_n	cont_p	cont_poly	cont_n
	pA	cm/s	kOhm	Ohm	kOhm	MOhm	kOhm
HPK_VPX35957_001_2-S_HM_EL	—	—	—	—	—	—	—
HPK_VPX35957_001_2-S_HM_ER	8.5	1.04	82.6	29.8	70.4	23.8	68.6
HPK_VPX35957_001_2-S_HM_WL	—	—	—	—	—	—	—
HPK_VPX35957_001_2-S_HM_WR	8.6	1.05	100.9	28.9	70.8	26.8	70.7
HPK_VPX35957_005_2-S_HM_EL	—	—	—	—	—	—	—
HPK_VPX35957_005_2-S_HM_ER	8.5	1.04	90.7	28.7	70.3	23.3	69.8
HPK_VPX35957_005_2-S_HM_WL	—	—	—	—	—	—	—
HPK_VPX35957_005_2-S_HM_WR	9.0	1.10	98.6	29.0	70.6	24.8	68.2
HPK_VPX35957_011_2-S_HM_EL	9.2	1.12	77.0	28.0	69.3	21.3	66.4
HPK_VPX35957_011_2-S_HM_ER	9.1	1.11	91.2	28.3	69.5	23.5	69.8
HPK_VPX35957_011_2-S_HM_WL	8.8	1.07	81.9	28.0	68.9	20.4	66.6
HPK_VPX35957_011_2-S_HM_WR	9.2	1.12	94.1	28.0	69.6	27.3	70.6
HPK_VPX35957_019_2-S_HM_EL	9.4	1.14	60.7	28.1	71.7	20.8	65.3
HPK_VPX35957_019_2-S_HM_ER	9.4	1.14	86.3	28.3	72.4	21.6	69.2
HPK_VPX35957_019_2-S_HM_WL	9.3	1.13	78.6	27.7	71.7	19.7	64.8
HPK_VPX35957_019_2-S_HM_WR	9.8	1.19	100.8	28.4	73.3	25.4	68.1
HPK_VPX35957_028_2-S_HM_EL	—	—	—	—	—	—	—
HPK_VPX35957_028_2-S_HM_ER	7.9	0.96	66.9	28.9	74.8	19.5	56.1
HPK_VPX35957_028_2-S_HM_WL	—	—	—	—	—	—	—
HPK_VPX35957_028_2-S_HM_WR	8.3	1.01	70.6	29.3	75.8	22.0	58.4
HPK_VPX35957_035_2-S_HM_EL	—	—	—	—	—	—	—
HPK_VPX35957_035_2-S_HM_ER	8.3	1.01	72.4	28.7	72.3	19.3	57.4
HPK_VPX35957_035_2-S_HM_WL	—	—	—	—	—	—	—
HPK_VPX35957_035_2-S_HM_WR	8.3	1.01	75.8	28.7	73.7	22.7	60.7
HPK_VPX35957_042_2-S_HM_EL	8.9	1.08	59.7	27.9	73.4	17.7	57.9
HPK_VPX35957_042_2-S_HM_ER	8.5	1.03	70.2	28.4	72.7	19.8	61.5
HPK_VPX35957_042_2-S_HM_WL	8.4	1.03	63.0	28.0	73.3	17.1	54.8
HPK_VPX35957_042_2-S_HM_WR	8.8	1.07	86.8	28.5	73.8	23.9	61.8
HPK_VPX35957_045_2-S_HM_EL	9.0	1.09	57.4	28.2	73.2	17.0	58.5
HPK_VPX35957_045_2-S_HM_ER	8.6	1.04	77.2	27.9	72.7	20.0	64.8
HPK_VPX35957_045_2-S_HM_WL	8.7	1.06	68.3	27.8	73.0	17.1	57.2
HPK_VPX35957_045_2-S_HM_WR	9.0	1.09	83.7	28.7	74.4	24.5	63.1
Median	8.8	1.07	77.9	28.3	72.5	21.5	64.8
Average	8.8	1.07	79.0	28.4	72.1	21.6	63.8
Std dev.	0.4	0.05	12.8	0.5	1.8	3.0	5.1
OK/Tot.	24/24	24/24	24/24	24/24	24/24	24/24	24/24
OK (rel)	1.00	1.00	1.00	1.00	1.00	1.00	1.00

Appendix B

Usage of the Python analysis script

The python analysis script is required to extract the parameters from the measurements. It can output multiple different table formats. The available templates are located in:

```
analysis-pqc/scripts/templates/.
```

To enable individual formats, symbolic links to:

```
analysis-pqc/scripts/templates-enabled/
```

can be created for the particular file to enable it.

The script can be called with:

```
python3 scripts/full_line.py <opt-args> <path>
```

Whith <path> is the path to the directory of the raw measurement data for a whole batch. Optional parameters can be used to enable different features:

```
-h, --help   show this help message and exit
-o outdir    override output directory location to outdir
-l           lazy evaluation: skip if the measurement folder is
             older than the analysis folder
-H           create histograms
-P           create plots (for each single measurement analyzed)
-f           force evaluating all directories (normally, only
             directroies with at least one VdP measurement are
             evaluated to prevent blank lines in the tables if
             the is a wrong file or so)
```

The HTML tables are mainly intended for exploratory analysis of the tables, the LaTeX output format is intended for presentation. The tables form appendix A are automatically created using the script.

A portion of the HTML table output is shown in figure B.1. The Serial numbers are link, that open a new window to see the plots of the individual measurements. This is show in figure B.2.

PQC Batch VPX35953:

Flute 1:

# #	fet V	v_fb V	c_acc pF	t_ox nm	n_ox 1E10cm^-2	vdpPoly kOhm/sq	vdpPoly_r kOhm/sq	vdpN Ohm/sq	vdpN_r Ohm/sq	vdpPstp kOhm/sq	vdpPstp_r kOhm/sq	cap_l pF	cap_r pF
HPK_VPX35953_001_2-S_HM_WL	3.10	2.86	84.5	679.5	11.3	1.88	1.88	34.7	34.5	20.0	20.3	2.60	2.48
HPK_VPX35953_001_2-S_HM_WR	3.92	2.93	85.4	672.3	11.6	failed	1.88	34.6	35.1	18.6	18.6	2.62	2.50
HPK_VPX35953_002_2-S_HM_EL	3.89	2.91	85.8	669.5	11.6	1.88	1.88	34.9	34.8	18.5	18.6	2.64	2.52
HPK_VPX35953_002_2-S_HM_ER	3.28	2.94	84.7	678.0	11.5	1.91	1.85	34.5	34.7	24.7	20.2	2.59	2.48
HPK_VPX35953_002_2-S_HM_WL	3.12	2.91	84.7	677.9	11.4	1.88	1.89	34.6	34.7	20.3	20.3	2.61	2.49
HPK_VPX35953_002_2-S_HM_WR	3.86	2.96	85.6	671.3	11.7	1.88	1.90	34.8	35.0	23.5	23.3	2.62	2.50
HPK_VPX35953_012_2-S_HM_WL	3.19	3.01	84.0	683.9	11.7	1.87	1.87	34.7	34.7	20.6	20.6	2.58	2.47
HPK_VPX35953_012_2-S_HM_WR	3.89	2.99	85.5	671.7	11.8	1.88	1.87	34.7	34.8	18.8	18.8	2.64	2.52
HPK_VPX35953_013_2-S_HM_WL	3.65	2.95	85.0	675.7	11.6	1.87	1.88	34.9	34.9	19.6	19.6	2.63	2.51
HPK_VPX35953_013_2-S_HM_WR	3.90	3.00	85.8	669.8	11.9	1.82	1.86	34.7	35.0	18.9	18.8	2.63	2.50
HPK_VPX35953_017_2-S_HM_EL	3.83	2.98	86.2	666.6	11.9	1.89	1.87	34.8	34.7	18.9	18.9	2.64	2.52
HPK_VPX35953_017_2-S_HM_ER	3.84	2.96	85.1	674.6	11.7	1.85	1.85	34.6	34.9	19.3	19.2	2.62	2.49
HPK_VPX35953_017_2-S_HM_WL	3.66	2.85	84.8	677.2	11.3	1.88	1.88	35.0	34.9	19.4	19.4	2.61	2.47
HPK_VPX35953_017_2-S_HM_WR	3.84	3.03	85.4	672.6	11.9	1.88	1.88	34.6	35.1	19.0	19.0	2.63	2.52
HPK_VPX35953_024_2-S_HM_EL	3.83	3.01	86.3	665.5	12.0	1.89	1.88	35.0	34.7	18.9	18.9	2.62	2.52
HPK_VPX35953_024_2-S_HM_ER	3.74	3.05	85.2	674.5	12.0	1.86	1.88	34.6	34.8	19.2	19.2	2.57	2.47
HPK_VPX35953_024_2-S_HM_WL	3.74	2.96	84.9	676.3	11.6	1.89	1.89	35.0	34.9	19.2	19.2	2.60	2.50
HPK_VPX35953_024_2-S_HM_WR	3.83	3.06	85.9	669.0	12.1	1.90	1.89	34.6	34.9	18.9	18.9	2.63	2.52
HPK_VPX35953_035_2-S_HM_EL	3.99	2.80	86.1	667.1	11.3	1.91	1.91	34.9	34.9	18.8	18.9	2.65	2.53
HPK_VPX35953_035_2-S_HM_ER	2.57	2.89	85.4	672.2	11.5	1.93	1.89	34.4	34.6	22.3	22.2	2.66	2.51
HPK_VPX35953_035_2-S_HM_WL	2.62	2.89	85.5	671.5	11.5	1.90	1.90	34.7	34.6	21.9	21.9	2.64	2.52
HPK_VPX35953_035_2-S_HM_WR	3.96	2.88	85.8	669.7	11.5	1.92	1.92	34.7	35.0	18.9	19.2	0.22	failed
HPK_VPX35953_040_2-S_HM_EL	4.34	2.83	86.3	665.2	11.4	1.87	failed	34.9	34.8	18.8	18.8	2.67	2.54
HPK_VPX35953_040_2-S_HM_ER	3.08	2.88	85.6	671.1	11.5	1.86	1.86	34.4	34.8	20.8	20.8	2.62	2.49
HPK_VPX35953_040_2-S_HM_WL	2.93	2.87	85.5	671.8	11.4	1.88	1.87	34.6	34.6	21.1	21.2	0.22	0.20
HPK_VPX35953_040_2-S_HM_WR	3.99	2.88	85.8	669.5	11.5	1.88	1.89	34.8	35.1	18.7	18.8	2.64	2.50
HPK_VPX35953_043_2-S_HM_EL	3.92	2.87	86.2	666.0	11.5	1.90	1.90	34.6	34.9	18.7	18.7	2.59	2.49
HPK_VPX35953_043_2-S_HM_ER	2.86	2.95	85.5	672.0	11.7	1.84	1.85	34.6	34.4	21.1	21.2	2.57	2.48
HPK_VPX35953_043_2-S_HM_WL	3.01	2.97	85.7	669.8	11.8	1.89	failed	36.5	35.8	25.0	25.3	2.82	2.65
HPK_VPX35953_043_2-S_HM_WR	3.87	2.93	86.3	665.5	11.7	1.90	1.93	39.4	38.7	19.2	18.8	0.31	2.55
Median	3.84	2.93	85.5	671.6	11.6	1.88	1.88	34.7	34.8	19.2	19.2	2.62	2.50
Average	3.70	2.93	85.5	671.9	11.6	1.88	1.88	34.9	35.0	19.9	19.7	2.63	2.51
Std dev.	0.34	0.07	0.6	4.5	0.2	0.02	0.02	0.9	0.7	1.5	1.2	0.04	0.03

Figure B.1: HTML table created with the analysis script. The color coding indicates values that deviate from the expected value. Red means that the measurement curve was not suited to reliably extract the resulting parameter.

PQC Plots:
HPK_VPX35953_002_2-S_HM_ER

Close window

Flute 1

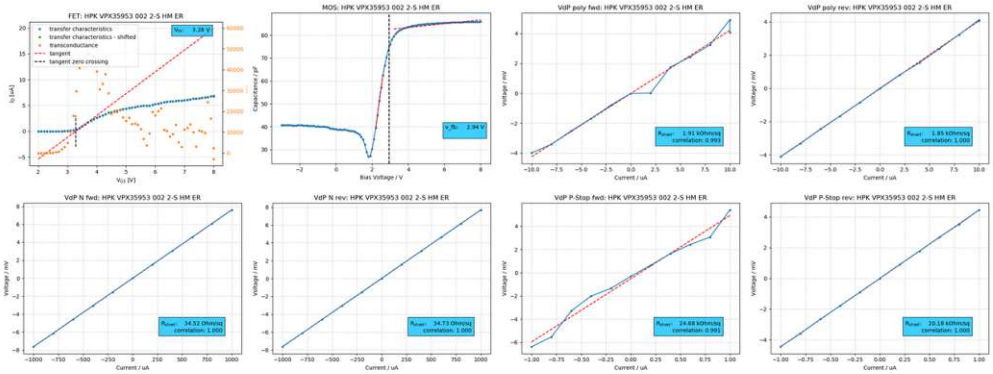

Flute 2

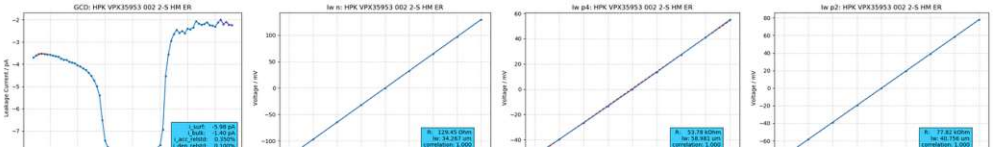

Figure B.2: HTML plot-window for a particular sample for inspection of suspicious measurements

Appendix C

Example R code for statistical analysis

This is an example code snippet, similar code has been used for the statistical plots.

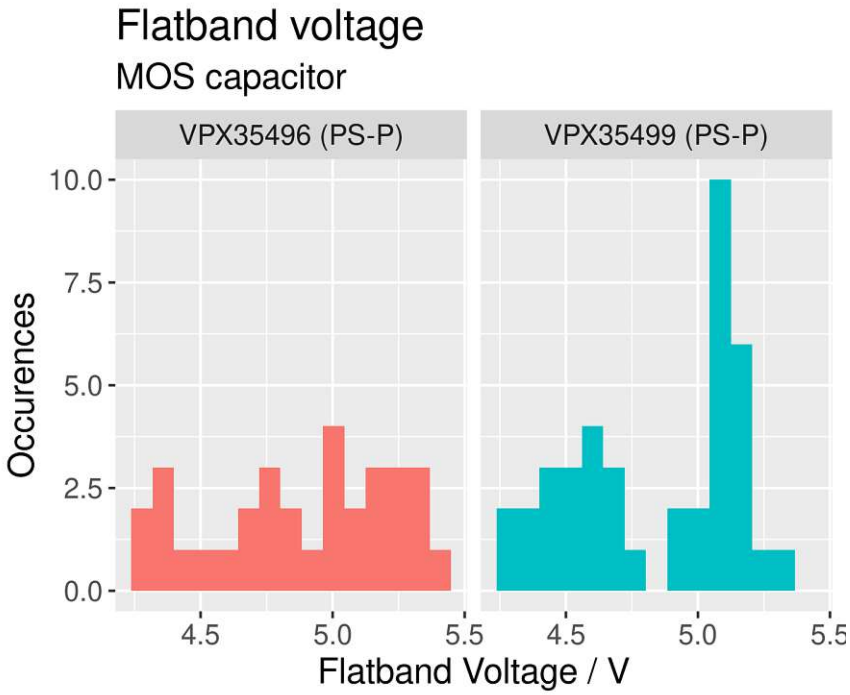

Figure C.1: Plot created with the following snippet

```
library(ggplot2)
library(plyr)
library(dplyr)


read_txt <- function(batch, name=0) {
    if(name == 0)
        name <- batch

    # all.txt is a space-seperated data file created with the corresponding
    # templates and with header in the first line
    path <- paste("analysis_", batch, "/all.txt", sep="")
```

```
    ret <- read.table(path, header=TRUE)

    # add batch ID
    ret$batch <- rep(name, nrow(ret))

    # positions on the Tracker wafers
    ret <- ret %>%
        mutate(pos = "n/a") %>%
        mutate(pos = ifelse(grepl("WR$", sample), "WR", pos)) %>%
        mutate(pos = ifelse(grepl("WL$", sample), "WL", pos)) %>%
        mutate(pos = ifelse(grepl("ER$", sample), "ER", pos)) %>%
        mutate(pos = ifelse(grepl("EL$", sample), "EL", pos)) %>%
        mutate(pos = factor(pos, levels=c("n/a", "ER","EL","WR","WL")))

    # if position is n/a, we assume that it is from HGCal
    ret <- ret %>%
        mutate(project = ifelse(pos=="n/a", "HGC", "Tracker")) %>%
        mutate(project = factor(project, levels=c("HGC", "Tracker")))

    return(ret)
}

# change directory to data directory, there the analysis_<batch> folders
# should be located
setwd('data')

vpx35496_psp <- read_txt("VPX35496", "VPX35496 (PS-P)")
vpx35499_psp <- read_txt("VPX35499", "VPX35499 (PS-P)")

pqcData <- vpx35496_psp
pqcData <- rbind.fill(pqcData, vpx35499_psp)

setwd('../plots')

hist_baseplot <- list(
        guides(fill = FALSE),
        theme(text = element_text(size = 14)),
        facet_wrap(~batch, ncol = 2),
        labs(y="Occurences")
)

ggplot(pqcData, aes(v_fb, fill=batch)) +
        hist_baseplot +
        geom_histogram(bins = 15) +  # we want 15 bins, needs to be
                # adjusted for particular dataset
        scale_x_continuous(n.breaks = 4) + # optional: allows fine-tuning
                # the axis-labels if they look ugly, usually default is good
        labs(x="Flatband Voltage / V",
                title="Flatband voltage",
                subtitle="MOS capacitor")+
        ggsave("hist_mos_vfb_example.png", width=12, height=10, units="cm")

setwd('../')
```